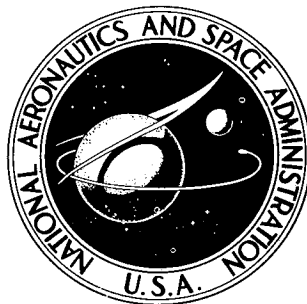


NASA TECHNICAL NOTE



NASA TN D-7713

NASA TN D-7713

CASE FILE  
COPY

# NUMERICAL METHODS FOR THE DESIGN AND ANALYSIS OF WINGS AT SUPERSONIC SPEEDS

*by Harry W. Carlson and David S. Miller*

*Langley Research Center*

*Hampton, Va. 23665*



1. Report No. NASA TN D-7713	2. Government Accession No.	3. Recipient's Catalog No.	
4. Title and Subtitle NUMERICAL METHODS FOR THE DESIGN AND ANALYSIS OF WINGS AT SUPERSONIC SPEEDS		5. Report Date December 1974	6. Performing Organization Code
		8. Performing Organization Report No. L-9542	10. Work Unit No. 760-65-11-02
7. Author(s) Harry W. Carlson and David S. Miller		11. Contract or Grant No.	13. Type of Report and Period Covered Technical Note
9. Performing Organization Name and Address NASA Langley Research Center Hampton, Va. 23665		14. Sponsoring Agency Code	
		12. Sponsoring Agency Name and Address National Aeronautics and Space Administration Washington, D.C. 20546	
15. Supplementary Notes			
16. Abstract  <p style="text-align: center;">In rather extensive employment of numerical methods for the design and analysis of arbitrary-planform wings at supersonic speeds, certain deficiencies have been revealed, particularly in application to wings with slightly subsonic leading edges. Recently devised numerical techniques which overcome the major part of these deficiencies have now been incorporated into the methods. In order to provide a self-contained description of the revised methods, the original development as well as the more recent revisions have been subjected to a thorough review in this report.</p>			
17. Key Words (Suggested by Author(s)) Supersonic wing analysis Supersonic wing design Wing twist and camber Drag minimization		18. Distribution Statement Unclassified - Unlimited  STAR Category 01	
19. Security Classif. (of this report) Unclassified	20. Security Classif. (of this page) Unclassified	21. No. of Pages 74	22. Price* \$ 4.25

# NUMERICAL METHODS FOR THE DESIGN AND ANALYSIS OF WINGS AT SUPERSONIC SPEEDS

By Harry W. Carlson and David S. Miller  
Langley Research Center

## SUMMARY

In rather extensive employment of numerical methods for the design and analysis of arbitrary-planform wings at supersonic speeds, certain deficiencies have been revealed, particularly in application to wings with slightly subsonic leading edges. Recently devised numerical techniques which overcome the major part of these deficiencies have now been incorporated into the methods. In order to provide a self-contained description of the revised methods, the original development as well as the more recent revisions have been subjected to a thorough review in this report.

Revisions to the wing-design method have virtually eliminated irregularities that often arose in the definition of the camber surface in the immediate vicinity of the wing leading edge. An aft-element sensing technique has been incorporated in the analysis method to suppress pressure oscillations which formerly required application of a powerful nine-point smoothing formula. These improvements, in combination with more compatible summation methods in the design and analysis mode, have reduced small but disturbing discrepancies which sometimes arose between wing loadings and forces determined for an optimized wing and loadings and forces calculated for that same shape upon submittal to the evaluation program.

## INTRODUCTION

Because of its simplicity and versatility, linearized theory has been employed rather extensively in the design and analysis of supersonic aircraft. Descriptions of design and analysis methods based on linearized theory and examples of results obtained in application to typical problems are given in references 1 to 4.

One important application of linearized-theory methods is in the design of wing lifting surfaces for drag minimization and in the analysis of pressure loadings and overall forces on wings of specified shape. Although exact linearized-theory solutions are available for certain problems, for example, definition of minimum-drag surfaces for delta or arrow planforms and evaluation of loadings and forces on flat-plate wings of simple planform, these solutions are not directly applicable to the complex wing planforms

and surface shapes often employed in real aircraft. Such limitations, however, have been removed by the introduction of numerical methods for implementation of linearized theory on high-speed digital computers.

Widely used computer-implemented numerical methods for the design and analysis of wings with arbitrary planform which employ a rectangular grid system for representation of the wing lifting surface and simplified numerical techniques for evaluation of linearized-theory integrals are presented in references 5, 6, and 7. These methods can accommodate large numbers of wing elements (in the thousands) for the description of rather complex planforms and the handling of intricate surface shapes. Reference 5 described a method for the design of wing camber surfaces to minimize drag at a given lift coefficient through employment of an optimum combination of component loadings. This was followed by a method (ref. 6) which employed the same basic formulations for the evaluation of lifting pressures on flat-plate wings. The evaluation method was later extended to cover the case of wings with arbitrary-surface shape as described in reference 7.

Although the wing-design and analysis methods have for the most part been used quite successfully for a number of years, certain deficiencies are known to exist. Most notable is the tendency for solutions to be poorly behaved for wings whose leading edges are only slightly subsonic. Recently, means of overcoming the major part of these deficiencies have been devised and the results of the study are presented herein. In order to provide a self-contained description of the revised methods, the original development as well as the more recent revisions have been subjected to a thorough review.

In the design of wings with slightly subsonic leading edges, sporadic irregularities were found in the definition of the camber surface in the immediate vicinity of the leading edge. These irregularities could be removed by a manual alteration, but in fact were more often ignored. A numerical procedure (programable for use on high-speed digital computers) which approximates the strategy employed in manual elimination of irregularities has recently been devised and is now incorporated in the design method.

For the analysis method, especially in application to flat wings with near-sonic leading edges, large oscillations in local pressure coefficients were known to exist from the inception of the method. In the original method these oscillations were largely eliminated by introduction of a powerful nine-point smoothing formula which operated after an initial definition of unsmoothed pressure coefficients for all the wing elements. The smoothing operation necessitated an extension of the wing grid system for four elements behind the actual wing trailing edge, and thus it effectively limited application of the method to wings with supersonic trailing edges. For the particular case of a flat wing with an exact sonic leading edge the oscillations became so severe that the only recourse was to avoid that condition by considering either a slightly subsonic or slightly supersonic

leading edge. An aft-element sensing technique which will be described has now been incorporated in the program to permit an integral smoothing and thus eliminate the necessity for a separate terminal smoothing routine. This provision also extends applicability of the method to wings with subsonic trailing edges.

There has also been a small but disturbing discrepancy between wing loadings and forces determined for an optimized wing shape in the design mode and the loadings and forces calculated for that same shape in the analysis mode. A part of that discrepancy is resolved by employment of the previously discussed modifications. Other means of providing more accurate results in both modes so as to insure the proper correspondence are to be discussed.

### SYMBOLS

$A(L,N)$	leading-edge-element weighting factor for influence summations
$A(L^*,N^*)$	leading-edge-element weighting factor for force and moment summations
$A_i$	load strength factor for $i$ th loading
$B(L,N)$	trailing-edge-element weighting factor for influence summations
$B(L^*,N^*)$	trailing-edge-element weighting factor for force and moment summations
$b$	wing span
$C(L,N)$	wing center-line element or wing-tip-element weighting factor for influence summations
$C(L^*,N^*)$	wing center-line element or wing-tip-element weighting factor for force and moment summations
$C_D$	drag coefficient
$C_{D,ij}$	interference-drag coefficient between $i$ th and $j$ th specified loadings (eq. (25))
$C_L$	lift coefficient
$C_{L,d}$	design lift coefficient

$C_m$	pitching-moment coefficient
$\Delta C_p$	lifting-pressure coefficient
$c$	local wing chord
$\bar{c}$	mean aerodynamic chord
$c_d$	section drag coefficient (eq. (16))
$c_l$	section lift coefficient (eq. (15))
$c_m$	section pitching-moment coefficient (eq. (17))
$L, N$	designation of influencing elements
$L^*, N^*$	designation of field-point elements
$l$	wing overall length
$M$	Mach number
$R$	influence function (eq. (3))
$\bar{R}$	average value of influence function within a grid element (eqs. (6), (7), and (8))
$S$	reference wing area
$x, y, z$	distances measured in a Cartesian coordinate system (see fig. 1)
$x'$	distance from wing leading edge measured in x-direction
$x_a$	longitudinal distance from leading edge of specified area loading (see fig. 8)
$z_c$	camber-surface z-ordinate
$z_{c,s}$	smoothed camber-surface z-ordinate

- $z_r$  camber-surface z-ordinate at wing-root trailing edge
- $\alpha$  angle of attack, deg
- $\beta = \sqrt{M^2 - 1}$
- $\Lambda$  wing leading-edge sweepback angle, deg
- $\lambda_L, \lambda_m, \lambda_z$  Lagrange multipliers for lift, moment, and camber-surface ordinates, respectively
- $\xi, \eta$  dummy variables of integration for x and y, respectively
- $\tau$  designation of a region of integration bound by the wing planform and the fore Mach cone from the point (x,y)

Subscripts:

- a,b step indices
- ac aerodynamic center
- C,F,T aerodynamic coefficients for the cambered wing, the corresponding flat wing, and the totaled combination of cambered and flat wing, respectively
- i,j ith and jth specified loading
- le leading edge
- max maximum
- min minimum
- n number of specified loadings
- te trailing edge

## NUMERICAL-CALCULATION METHODS

### Camber Surface for a Given Loading

A typical wing planform described by a rectangular Cartesian coordinate system is illustrated in figure 1. For a wing of zero thickness lying essentially in the  $z = 0$  plane, linearized theory for supersonic flow defines the wing-surface slopes necessary to support a specified lift distribution by the equation

$$\frac{\partial z_c}{\partial x}(x,y) = \frac{-\beta}{4} \Delta C_p(x,y) + \frac{1}{4\pi} \iint_{\tau} \frac{(x - \xi) \Delta C_p(\xi, \eta) d\eta d\xi}{(y - \eta)^2 \sqrt{(x - \xi)^2 - \beta^2(y - \eta)^2}} \quad (1)$$

which is a slightly modified form of equation (77a) of reference 8. The integral represents the influence of a continuous distribution of horseshoe vortices originating from wing elements with vanishingly small chords and spans. The region of integration  $\tau$  extends over the wing planform within the fore Mach cone from the field point  $(x,y)$  as shown by the shaded area in figure 1. The integral gives the appearance of being improper and divergent because of the singularity at  $\eta = y$  within the region of integration. This integrand is, however, the limiting form in the  $z = 0$  plane of a more general integrand that arises from lifting-surface theory and does not have a singularity at  $\eta = y$  when  $z \neq 0$ . Consequently, the integral can be treated according to the concept of the generalization of the Cauchy principal value, which is discussed and explained in section 3 of reference 9 and also in reference 8. The integral is thus generally found to be convergent at points  $(x,y)$  on a wing surface, although regions of nonconvergence exist if there are values of  $y$  for which the spanwise derivative of the chordwise integral

$$\frac{\partial}{\partial \eta} \int_{\xi_{1e}}^{x-\beta|y-\eta|} \frac{(x - \xi) \Delta C_p(\xi, \eta)}{\sqrt{(x - \xi)^2 - \beta^2(y - \eta)^2}} d\xi$$

is not single valued at  $\eta = y$ . Such conditions can arise along a streamwise line directly behind a discontinuity in the wing leading-edge sweep (for example, at the wing apex) and can occur at spanwise stations for which discontinuities appear in spanwise derivatives of the loading distribution. These regions of nonconvergence, however, do not invalidate results over the remainder of the wing surface.

For the purposes of this study, equation (1) will be rewritten in the form

$$\frac{\partial z_c}{\partial x}(x,y) = \frac{-\beta}{4} \Delta C_p(x,y) + \frac{\beta}{4\pi} \iint_{\tau} R(x-\xi, y-\eta) \Delta C_p(\xi, \eta) d\beta\eta d\xi \quad (2)$$

where the function  $R$  is defined as

$$R(x-\xi, y-\eta) = \frac{x - \xi}{\beta^2(y - \eta)^2 \sqrt{(x - \xi)^2 - \beta^2(y - \eta)^2}} \quad (3)$$

and may be thought of as an influence function relating the local loading at point  $(\xi, \eta)$  to its influence in determining the necessary slope at downstream point  $(x, y)$ . A graphical representation of the influence function  $R$  is shown in figure 2. The singularity at  $\eta = y$  has been expanded to illustrate its peculiar character. The physical significance of the function may be better understood when it is applied in the definition of the upwash field produced by a small elemental lifting surface. If in equation (2)  $\Delta C_p(x, y)$  is set equal to zero, the resultant slope  $\frac{\partial z_c}{\partial x}(x, y)$  will define the local upwash angularity. The nature of this upwash distribution is illustrated in figure 3. The negative singularity of the influence function at  $\eta = y$  makes its presence felt in a strong downwash field extending downstream from the lifting element. The remainder of the flow field, outboard of streamwise lines from the element tips, is composed entirely of upwash. The abrupt change from negative to positive infinities corresponds to the trailing tip vortices. A positive singularity is noted to exist also at the Mach cone limits.

It is this upwash field, and particularly the large values of upwash near the Mach cone limits, that makes twisted and cambered arrow wings with subsonic leading edges attractive from the standpoint of aerodynamic efficiency. Because of the upwash created by forward elements of the wing, the wing surface at and near the leading edge may be shaped so as to create an appreciable amount of lift on a forwardly inclined surface and produce a local thrust rather than a drag. The theory predicts that drag reductions approaching these levels can also be achieved for flat wings if the full benefits of leading-edge suction can be realized; however, little evidence of any appreciable amount of leading-edge suction has been seen for supersonic speeds. Unfortunately, this same upwash field, with the large values of upwash near the Mach cone limits, is also largely responsible for the difficulties in representing supersonic-flow phenomena by means of finite-element numerical techniques.

In order to replace the indicated integration in equation (2) by a numerical summation, it is first necessary to introduce a grid system superimposed over the Cartesian coordinate system used in describing the wing planform as shown in figure 4. (This sketch is illustrative only; in application many more grid elements would be employed.) The numbers assigned to  $L$  and  $N$  identify the spaces in the grid which replace the element of integration  $(d\xi, d\beta\eta)$ . The starred values of  $L$  and  $N$  identify the space or element associated with and immediately ahead of the field point  $(x, y)$ ;  $L^*$  is numerically equal to  $x$  and  $N^*$  is numerically equal to  $\beta y$ , where  $x$  and  $\beta y$  take on only

integer values. The region of integration, originally bound by the wing leading edge and the Mach lines, now consists of a set of grid elements approximating that region as shown by the shaded area in the example of figure 4. Inclusion of partial as well as full grid elements provides a better definition of the wing leading edge and tends to reduce any irregularities that may arise in local surface slopes for elements in the vicinity of the leading edge.

The contribution of each element of the wing (L,N) to the local slope at (x,βy) may be written as

$$\frac{\partial z_c}{\partial x}(x,y) = \frac{\beta}{4\pi} \bar{R}(L^*-L, N^*-N) A(L,N) B(L,N) C(L,N) \Delta C_p(L,N) \quad (4)$$

Terms in this equation and methods used in their evaluation will be described in some detail in the following paragraphs.

The  $\bar{R}$  term represents an average value within the element of the function  $R(x-\xi, y-\eta)$ . The value of this factor may be found from the integral

$$\bar{R}(L^*-L, N^*-N) = \frac{1}{\Delta \xi \Delta \beta \eta} \int_{\xi_1}^{\xi_2} d\xi \int_{\beta \eta_1}^{\beta \eta_2} \frac{(x - \xi)}{\beta^2 (y - \eta)^2 \sqrt{(x - \xi)^2 - \beta^2 (y - \eta)^2}} d\beta \eta \quad (5)$$

in which the integration extends over one grid element. Since, by numerical evaluation of the integrand, the  $\bar{R}$  factor has been determined to be relatively insensitive to variations in  $\xi$ , as an approximation the  $\bar{R}$  factor may be written as

$$\bar{R}(L^*-L, N^*-N) = \frac{1}{\Delta \beta \eta} \int_{\beta \eta_1}^{\beta \eta_2} \frac{(L^* - L + 0.5)}{\beta^2 (y - \eta)^2 \sqrt{(L^* - L + 0.5)^2 - \beta^2 (y - \eta)^2}} d\beta \eta \quad (6)$$

with  $(L^* - L + 0.5)$  representing the value of  $x - \xi$  at the midpoint of the element. On integration the expression takes the form

$$\bar{R}(L^*-L, N^*-N) = \frac{(L^* - L + 0.5) \sqrt{(L^* - L + 0.5)^2 - \beta^2 (y - \eta)^2}}{(L^* - L + 0.5)^2 \beta (y - \eta)} \Big|_{\beta \eta_1}^{\beta \eta_2} \quad (7)$$

and with  $\beta y = N^*$ ,  $\beta \eta_1 = N - 0.5$ , and  $\beta \eta_2 = N + 0.5$  (see fig. 4), the influence factor  $\bar{R}$  becomes

$$\bar{R}(L^*-L, N^*-N) = \frac{\sqrt{(L^* - L + 0.5)^2 - (N^* - N - 0.5)^2}}{(L^* - L + 0.5)(N^* - N - 0.5)} - \frac{\sqrt{(L^* - L + 0.5)^2 - (N^* - N + 0.5)^2}}{(L^* - L + 0.5)(N^* - N + 0.5)} \quad (8)$$

A graphical representation of this factor is shown in figure 5. Note the rather small variations of the factor in the x- or L-direction contrasted with the drastic variations in the y- or N-direction. For a given  $L^* - L$  set of elements, the spanwise summation of the  $\bar{R}$  values is found to be zero, due to the single negative value at  $N^* - N = 0$  balancing all the others. This insures that a lifting element, or a complete wing, will produce a flow field which consists of equal amounts of upwash and downwash and thus introduces no net vertical displacements of the medium in which it is moving. At  $L^* - L = 0$  where there is only one element in the spanwise summation, the  $\bar{R}$  value of that element is zero. This fact, which insures that an element will have no influence on itself, will be useful in a later section of the report dealing with the inverse problem, that of defining loadings for a specified surface.

The  $A(L,N)$  term in equation (4) is a weighting factor which allows consideration of partial elements in the summation process and permits a better definition of the wing leading-edge shape. The factor  $A(L,N)$  takes on values from 0 to 1 given by

$$\left. \begin{aligned} A(L,N) &= 0 & (L - x_{1e} \leq 0) \\ A(L,N) &= L - x_{1e} & (0 < L - x_{1e} < 1) \\ A(L,N) &= 1 & (L - x_{1e} \geq 1) \end{aligned} \right\} \quad (9)$$

The  $B(L,N)$  term is a trailing-edge influencing-element weighting factor which also takes on values from 0 to 1 given by

$$\left. \begin{aligned} B(L,N) &= 0 & (L - x_{te} \geq 1) \\ B(L,N) &= 1 - (L - x_{te}) & (0 < L - x_{te} < 1) \\ B(L,N) &= 1 & (L - x_{te} \leq 0) \end{aligned} \right\} \quad (10)$$

The  $C(L,N)$  term is a wing-tip influencing-element weighting factor which takes on values of 0.5 or 1 given by

$$\left. \begin{aligned} C(L,N) &= 0.5 && (N = N_{\max}) \\ C(L,N) &= 1.0 && (N \neq N_{\max}) \end{aligned} \right\} \quad (11)$$

Desired values of lifting-pressure coefficient  $\Delta C_p(L,N)$  assigned to each space or element of the grid are obtained from loading formulas evaluated at the centroid of the element. The pressure may vary from element to element but is assumed to be constant within a given element.

The control point  $(x,y)$  of an element is fixed at the midspan of the element trailing edge by the mathematical modeling of the supersonic horseshoe vortex system. The wing-surface slope at that point may be found by a summation of the contributions of each of the elements within the influencing region and is expressed as

$$\begin{aligned} \frac{\partial z}{\partial x} c(L^*,N^*) &= \frac{-\beta}{4} \Delta C_p(L^*,N^*) + \frac{\beta}{4\pi} \sum_{N=N_{\min}}^{N=N_{\max}} \sum_{L=L^* - |N^* - N|}^{L=1 + [x_{1e}]} \bar{R}(L^* - L, N^* - L) \\ &\times A(L,N) B(L,N) C(L,N) \Delta C_p(L,N) \end{aligned} \quad (12)$$

The vertical lines as used in  $|N^* - N|$  designate the absolute value of the enclosed quantity, and the brackets in  $[x_{1e}]$  designate the whole-number part of the quantity. The initial summation with respect to  $L$  is made only when

$$L^* - |N^* - N| \geq 1 + [x_{1e}]$$

In the original method (ref. 5) values of the surface slope as given by equation (12) were used directly. However, experience has shown that irregularities in the definition of the camber surface in the immediate vicinity of the wing leading edge often arise. By observation of design-program calculated slopes and comparisons with analytic solutions, it was noted that errors which occur for the leading-edge elements (especially notable when the weighting factor  $A$  is small) were followed by a smaller error in the opposite direction for the next element. Errors were found to decrease rapidly for successive downstream elements. A smoothing process based on this observation is depicted in figure 6. Values of the surface slopes from equation (12) and their assumed distribution are shown, respectively, as small solid circular symbols and as a dashed line in the upper portion of the figure. As noted previously, the slope calculated for a given field-point element  $(L^*,N^*)$  is applicable to the rear midpoint of that element. That slope is assumed to extend over the rear half of the  $(L^*,N^*)$  element and over the front half of the  $(L^*+1,N^*)$  element. As shown, a forward extrapolation of  $\partial z/\partial x$  values from the second and third element to the first produces a  $\partial z/\partial x$  value in marked contrast to the original

value. A simple averaging of these two values is found to yield a much more reasonable value of the first element slope. With the process carried out for successive downstream elements a smoothed slope distribution as shown in the lower portion of figure 6 is obtained. In equation form the smoothing procedure is expressed as

$$\frac{\partial z_{c,s}}{\partial x}(L^*,N^*) = \frac{1}{2} \frac{\partial z_c}{\partial x}(L^*,N^*) + \frac{\partial z_c}{\partial x}(L^* + 1,N^*) - \frac{1}{2} \frac{\partial z_c}{\partial x}(L^* + 2,N^*) \quad (13)$$

The z-ordinates of the wing surface at station  $x = L^* + 0.5$  for a given semispan station  $y = N^*/\beta$  may be found by a chordwise summation of the local slopes

$$z_{c,s}(x,y) = \sum_{L^*=1+[x_{1e}]}^{L^*=1+[x_{te}]} \frac{\partial z_{c,s}}{\partial x}(L^*,N^*) A(L^*,N^*) \quad (14)$$

Wing-section ordinates as a function of the chord fraction  $x'/c$  may be found by linear interpolation.

Section lift, drag, and pitching-moment coefficients at any selected semispan station  $y = N^*/\beta$  (see the appendix) may be evaluated by the following summations:

$$c_l = \frac{1}{c} \sum_{L^*=1+[x_{1e}]}^{L^*=1+[x_{te}]} \Delta C_p(L^*,N^*) A(L^*,N^*) B(L^*,N^*) \quad (15)$$

$$c_d = \frac{-1}{c} \sum_{L^*=1+[x_{1e}]}^{L^*=1+[x_{te}]} \frac{\partial z}{\partial x}(L^*,N^*) \Delta C_p(L^*,N^*) A(L^*,N^*) B(L^*,N^*) \quad (16)$$

$$c_m = \frac{1}{c^2} \sum_{L^*=1+[x_{1e}]}^{L^*=1+[x_{te}]} (L^*) \Delta C_p(L^*,N^*) A(L^*,N^*) B(L^*,N^*) \quad (17)$$

The  $A(L^*,N^*)$  term in equations (14) to (17) is a leading-edge field-point-element weighting factor which takes on values from 0 to 1.5 given by

$$\left. \begin{aligned} A(L^*,N^*) &= 0 & (L^* - x_{1e} \leq 0) \\ A(L^*,N^*) &= L^* - x_{1e} + 0.5 & (0 < L^* - x_{1e} < 1) \\ A(L^*,N^*) &= 1 & (L^* - x_{1e} \geq 1) \end{aligned} \right\} \quad (18)$$

The  $B(L^*, N^*)$  term in equations (15), (16), and (17) is a trailing-edge field-point-element weighting factor which takes on values from 0 to 1.5 given by

$$\left. \begin{aligned} B(L^*, N^*) &= 0 & (L^* - x_{te} \cong 0) \\ B(L^*, N^*) &= 0.5 - (L^* - x_{te}) & (0 > L^* - x_{te} > -1) \\ B(L^*, N^*) &= 1 & (L^* - x_{te} \cong -1) \end{aligned} \right\} \quad (19)$$

The lifting-pressure coefficient for the field-point elements  $\Delta C_p(L^*, N^*)$  is obtained from the loading formulas evaluated at the midspan of the trailing edge of the element so as to correspond to the surface slope  $\partial z_{c,s} / \partial x$  defined at that point. Figure 7 illustrates the element representation employed in camber-surface definition and in force and moment determination.

Wing lift, drag, and pitching-moment coefficients, respectively, are obtained from spanwise integrations of the section data as follows:

$$C_L = \frac{2}{\beta S} \int_0^{b/2} c_l c \, dy \quad (20)$$

$$C_D = \frac{2}{\beta S} \int_0^{b/2} c_d c \, dy \quad (21)$$

$$C_m = \frac{2}{\beta S l} \int_0^{b/2} c_m c^2 \, dy \quad (22)$$

The integrals are evaluated by means of standard numerical techniques applied to a selected set of spanwise stations corresponding to integer values of  $N^*$ .

The wing area used in the expressions for the aerodynamic coefficients may be found through a summation

$$S = \frac{2}{\beta} \sum_{N^*=0}^{N^*=N_{\max}} \sum_{L^*=1+[x_{le}]}^{L^*=1+[x_{te}]} A(L^*, N^*) B(L^*, N^*) C(L^*, N^*) \quad (23)$$

The leading-edge and trailing-edge grid-element fractions are determined as previously described, and the center-line or wing-tip grid-element width is defined by

$$\left. \begin{aligned}
C(L^*, N^*) &= 0.5 && (N^* = 0) \\
C(L^*, N^*) &= 1 && (0 < N^* < N_{\max}) \\
C(L^*, N^*) &= 0.5 && (N^* = N_{\max})
\end{aligned} \right\} \quad (24)$$

### Optimum Combination of Loadings

In reference 10 Lagrange's method of undetermined multipliers has been applied to the problem of selecting a combination of component loadings yielding a minimum drag for arrow and delta wings producing a given lift. The method may be used for wings of any planform, provided that the interference-drag coefficients are first determined. By using the nomenclature of the present report, the drag coefficient of the interference between any two loadings  $i, j$  may be expressed as

$$\begin{aligned}
C_{D,ij} = C_{D,ji} &= \frac{-2}{\beta S} \sum_{N^*=0}^{N^*=N_{\max}} \sum_{L^*=1+[x_{1e}]}^{L^*=1+[x_{te}]} \Delta C_{p,i}(L^*, N^*) \left( \frac{\partial z}{\partial x} \right)_j (L^*, N^*) A(L^*, N^*) B(L^*, N^*) C(L^*, N^*) \\
&\quad - \frac{2}{\beta S} \sum_{N^*=0}^{N^*=N_{\max}} \sum_{L^*=1+[x_{1e}]}^{L^*=1+[x_{te}]} \Delta C_{p,j}(L^*, N^*) \left( \frac{\partial z}{\partial x} \right)_i (L^*, N^*) A(L^*, N^*) B(L^*, N^*) C(L^*, N^*) \quad (25)
\end{aligned}$$

and may be evaluated by numerical means.

In reference 5 Lagrange's method of undetermined multipliers was applied to the problem of selecting a combination of loadings on arbitrary planform wings to yield a minimum drag subject only to a restraint on lift coefficient. In reference 11 the numerical methods were extended to permit additional constraints on pitching moment and the z-ordinate at the wing-root trailing edge.

The total lift coefficient resulting from  $n$  wing-loading distributions is given by

$$C_L = \sum_{i=1}^{i=n} C_{L,i} A_i \quad (26)$$

where  $C_{L,i}$  denotes the lift coefficient of the  $i$ th loading and  $A_i$  is the load strength factor of the  $i$ th loading. The total pitching-moment coefficient resulting from  $n$  wing-loading distributions is given by

$$C_m = \sum_{i=1}^{i=n} C_{m,i} A_i \quad (27)$$

where  $C_{m,i}$  denotes the pitching-moment coefficient of the  $i$ th loading and  $A_i$  is the load strength factor for the  $i$ th loading. Similarly, the  $z$ -ordinate at the wing-root trailing edge resulting from  $n$  wing-loading distributions is given by

$$z_r = \sum_{i=1}^{i=n} z_{r,i} A_i \quad (28)$$

where  $z_{r,i}$  denotes the  $z$ -ordinate at the wing-root trailing edge on the camber surface required to support the  $i$ th loading.

If, in addition to a given lift, the constraints of zero pitching moment ( $C_m = 0$ ) and given  $z_r$  are imposed on the drag-minimization problem, the method of Lagrange multipliers yields the following set of equations which establishes the relative strength of each loading:

$$\left. \begin{aligned} \lambda_L C_{L,1} + \lambda_m C_{m,1} + \lambda_z z_{r,1} + \sum_{i=1}^{i=n} C_{D,1i} A_i &= 0 \\ \lambda_L C_{L,2} + \lambda_m C_{m,2} + \lambda_z z_{r,2} + \sum_{i=1}^{i=n} C_{D,2i} A_i &= 0 \\ \cdot & \cdot \\ \cdot & \cdot \\ \lambda_L C_{L,n} + \lambda_m C_{m,n} + \lambda_z z_{r,n} + \sum_{i=1}^{i=n} C_{D,ni} A_i &= 0 \\ \sum_{i=1}^{i=n} C_{L,i} A_i &= C_{L,d} \\ \sum_{i=1}^{i=n} C_{m,i} A_i &= 0 \\ \sum_{i=1}^{i=n} z_{r,i} A_i &= z_r \end{aligned} \right\} \quad (29)$$

Machine-computing techniques allow the evaluation of the weighting factors  $A_i$ , and, thus, the camber surface for an optimum combination of preselected loadings may be determined as

$$z_c(x,y) = \sum_{i=1}^{i=n} z_{c,i}(x,y) A_i \quad (30)$$

The corresponding drag coefficient is

$$C_D = \frac{1}{2} \sum_{i=1}^{i=n} \sum_{j=1}^{j=n} C_{D,ij} A_i A_j \quad (31)$$

The numerical method for the design of camber surfaces for wings with arbitrary planforms as first presented in reference 5 was implemented for three specified wing-loading distributions: uniform, linear chordwise, and linear spanwise. In the present method, which incorporates improvements introduced in reference 11, five additional wing-loading distributions are provided so that the drag-minimization procedure will have more versatility in computing the optimum combination of loadings. This is particularly important because of the more stringent requirement of satisfying three constraints rather than just one. The eight specified wing-loading distributions presently available are illustrated in figure 8.

#### Loading for a Given Camber Surface

In the numerical solution for the camber surface required to support a specified loading it is found that the field-point element has no influence on itself (e.g.,  $\bar{R}(L^*-L=0, N^*-N=0) = 0$ ). Thus, equation (12) can be rewritten as

$$\Delta C_p(L^*, N^*) = -\frac{4}{\beta} \frac{\partial z_c}{\partial x}(L^*, N^*) + \frac{1}{\pi} \sum_{N_{\min}}^{N_{\max}} \sum_{L_{le}}^{L^* - |N^* - N|} \bar{R}(L^* - L, N^* - N) A(L, N) \times B(L, N) C(L, N) \Delta C_p(L, N) \quad (32)$$

and the lifting-pressure distribution  $\Delta C_p$  can be determined for a wing of arbitrary-surface shape provided the calculations are performed in the proper sequence. The order of calculating  $\Delta C_p(L^*, N^*)$  is from the apex rearward (i.e., increasing values of  $L^*$ ); thus, all pressure coefficients within the fore Mach cone from any element will have been previously obtained and no unknown pressure coefficients arise in the summation. Since the value of  $\bar{R}$  for  $L^* = L$  and  $N^* = N$  is zero,  $\Delta C_p(L=L^*, N=N^*)$  is not required for the summation. The influencing-element weighting factors  $A(L, N)$ ,  $B(L, N)$ , and  $C(L, N)$  are as defined as in the solution for a camber surface for a given loading.

Theoretically,  $\Delta C_p(L^*, N^*)$  defined by equation (32) is the pressure coefficient at the midspan of the trailing edge of the  $L^*, N^*$  element. In the numerical method presented in reference 6 provision was made for determination of an average value of  $\Delta C_p$

over the element. In spite of this averaging, however, there remained large oscillations in pressure coefficient from element to element which were subdued by inclusion of a powerful nine-point terminal smoothing formula. The terminal smoothing procedure took place after an initial definition of unsmoothed pressures for the entire wing and necessitated an extension of the wing grid system for four elements behind the actual wing trailing edge. This effectively limited application of the method to wings with supersonic trailing edges. An aft-element sensing technique which permits an integral smoothing has now been incorporated in the numerical method to eliminate the need for both averaging and the terminal smoothing steps.

The aft-element sensing technique involves the determination of preliminary  $\Delta C_p$  results for a given field-point element and for the element immediately following, combined with a subsequent fairing or smoothing of these preliminary results. The fairing is applied to the velocity potential (i.e., the integral of the pressure) rather than to the pressure itself because of the noticeably better behavior of the velocity potential in regard to the absence of discontinuities. The procedure outlined in the following steps may be clarified by reference to figure 9 which shows application of the technique to a typical element:

(a) Calculate and retain temporarily preliminary  $\Delta C_p$  values for a given row with  $L^* = \text{Constant}$ . Designate as  $\Delta C_{p,a}(L^*, N^*)$ .

(b) Calculate and retain temporarily preliminary  $\Delta C_p$  values for the following row with  $L^* = \text{Constant} + 1$  by using  $\Delta C_{p,a}$  values obtained in the previous step for contributions from the row with  $L^* = \text{Constant}$ . Designate as  $\Delta C_{p,b}(L^*, N^*)$ .

(c) Calculate a final  $\Delta C_p$  value from a fairing of integrated preliminary  $\Delta C_p$  results.

For leading-edge elements, defined as  $L^* - x_{1e}(N^*) \leq 1$ ,

$$\begin{aligned} \Delta C_p(L^*, N^*) = & \frac{1}{2} \left[ 1 + \frac{A(L^*, N^*)}{1 + A(L^*, N^*)} \right] \Delta C_{p,a}(L^*, N^*) \\ & + \frac{1}{2} \left[ \frac{A(L^*, N^*)}{1 + A(L^*, N^*)} \right] \Delta C_{p,b}(L^*, N^*) \end{aligned} \quad (33)$$

For all other elements, defined as  $L^* - x_{1e}(N^*) > 1$ ,

$$\Delta C_p(L^*, N^*) = \frac{3}{4} \Delta C_{p,a}(L^*, N^*) + \frac{1}{4} \Delta C_{p,b}(L^*, N^*) \quad (34)$$

In the evaluation of  $\Delta C_{p,b}(L^*, N^*)$ , the influence-function—pressure-coefficient summation may be separated into two parts. One part consists of all the spanwise

rows for which  $L^* - L \geq 2$ , and the second consists of only this  $L^* - L = 1$  row which is calculated with preliminary  $\Delta C_p$  values. The first part may be retained temporarily to avoid repetition in the subsequent calculation of  $\Delta C_p(L^*, N^*)$  for the following row.

For determination of the loading corresponding to a given camber surface, it is required that  $\Delta C_p$  be evaluated for all elements. Hence, there is little advantage in evaluation of forces and moments from section coefficients at selected span stations as was done in the design method.

The lift coefficient may be obtained from the following summation over all elements:

$$C_L = \frac{2}{\beta S} \sum_{N^*=0}^{N^*=N_{\max}} \sum_{L^*=L_{1e}}^{L^*=L_{te}} \left[ \frac{3}{4} \Delta C_p(L^*) + \frac{1}{4} \Delta C_p(L^* + 1) \right] A(L^*, N^*) B(L^*, N^*) C(L^*, N^*) \quad (35)$$

The pitching-moment coefficient about  $x = 0$  is

$$C_m = \frac{2}{\beta S \bar{c}} \sum_{N^*=0}^{N^*=N_{\max}} \sum_{L^*=L_{1e}}^{L^*=L_{te}} (L^*) \left[ \frac{3}{4} \Delta C_p(L^*) + \frac{1}{4} \Delta C_p(L^* + 1) \right] A(L^*, N^*) B(L^*, N^*) \times C(L^*, N^*) \quad (36)$$

The drag coefficient may be expressed as follows:

$$C_D = \frac{-2}{\beta S} \sum_{N^*=0}^{N^*=N_{\max}} \sum_{L^*=L_{1e}}^{L^*=L_{te}} \left[ \frac{3}{4} \Delta C_p(L^*) + \frac{1}{4} \Delta C_p(L^* + 1) \right] \left[ \frac{3}{4} \frac{\partial z_c}{\partial x}(L^*) + \frac{1}{4} \frac{\partial z_c}{\partial x}(L^* - 1) \right] A(L^*, N^*) B(L^*, N^*) C(L^*, N^*) \quad (37)$$

This relationship does not consider any contribution of the theoretical "leading-edge-suction" force or of any separated flow effects associated with its exclusion and accounts only for the inclination of the normal force to the relative wind.

The element weighting factors in equations (32) to (37) are defined in the description of the wing-design method. Figure 10 illustrates the element representation employed in wing-loading definition and in force and moment determination. The particular method of computing the total force and moment coefficients as described previously and illustrated in figure 10 was adopted to provide a more rapid convergence of total wing forces and to increase compatibility with the wing-design method.

The distribution of wing lift in the streamwise and spanwise direction may be obtained from summations, taken row by row, of grid-element forces in the L- and N-directions, respectively. These distributions are conveniently expressed as fractions of total wing lift as follows:

For the streamwise lift distribution,

$$\frac{(\text{Lift})_{L^*}}{\text{Total lift}} = \frac{2 \sum_{N^*=0}^{N^*=N_{\max}} \Delta C_p(L^*, N^*) A(L^*, N^*) B(L^*, N^*) C(L^*, N^*)}{\beta C_L S} \quad (38)$$

and for the spanwise lift distribution, at a selected  $N^*$  value on the right-hand wing panel only,

$$\frac{(\text{Lift})_{N^*}}{\text{Total lift}} = \frac{\sum_{L^*=L_{le}}^{L^*=L_{te}} \Delta C_p(L^*, N^*) A(L^*, N^*) B(L^*, N^*) C(L^*, N^*)}{\beta C_L S} \quad (39)$$

The method permits the evaluation of loadings for wings with an arbitrarily warped camber surface at zero angle of attack as specified by the element surface slopes  $\frac{\partial z}{\partial x} C(L^*, N^*)$  of equation (32). By repeating the solution for a flat wing of the same plan-form at unit angle of attack, and by calculating interference-drag coefficients, wing aerodynamic characteristics may be obtained over a range of angles of attack and lift coefficients. Lift and moment coefficients, respectively, may be found by a direct addition:

$$C_{L,T} = C_{L,C} + (C_{L,F})_{\alpha=1} \alpha \quad (40)$$

$$C_{m,T} = C_{m,C} + (C_{m,F})_{\alpha=1} \alpha \quad (41)$$

The drag coefficient, however, requires consideration of the drag of the warped wing, the drag variation with lift for the flat wing, and an interference drag defined by flat-wing pressures acting on the cambered wing surface and by cambered wing pressures acting on the flat-wing surface. By using the method shown in reference 7, the drag coefficient may be evaluated as

$$C_{D,T} = C_{D,C} + (C_{D,F-C} + C_{D,C-F}) \left[ \frac{C_L - C_{L,C}}{(C_{L,F})_{\alpha=1}} \right] + (C_{D,F})_{\alpha=1} \left[ \frac{C_L - C_{L,C}}{(C_{L,F})_{\alpha=1}} \right]^2 \quad (42)$$

The interference-drag terms employed in equation (42) are defined as follows:

For flat-wing pressures acting on the cambered wing surface,

$$C_{D, F-C} = \frac{-2}{\beta S} \sum_{N^*=0}^{N^*=N_{\max}} \sum_{L^*=L_{1e}}^{L^*=L_{te}} \left[ \frac{3}{4} (\Delta C_{p, F})_{\alpha=1}(L^*) + \frac{1}{4} (\Delta C_{p, F})_{\alpha=1}(L^* + 1) \right] \\ \times \left[ \frac{3}{4} \frac{\partial z_C}{\partial x_C}(L^*) + \frac{1}{4} \frac{\partial z_C}{\partial x_C}(L^* - 1) \right] A(L^*, N^*) B(L^*, N^*) C(L^*, N^*) \quad (43)$$

and for cambered wing pressures acting on the flat-wing surface,

$$C_{D, C-F} = -C_{L, C} \frac{\partial z_C}{(\partial x_F)_{\alpha=1}} = -C_{L, C}(-0.01746) \quad (44)$$

## ILLUSTRATIVE EXAMPLES

### Design Method

The effect of the design-program modifications on the definition of camber-surface slopes and ordinates is illustrated in figures 11 and 12, respectively. Program results for arrow wings with subsonic leading edges ( $\beta \cot \Lambda = 0.4, 0.6, \text{ and } 0.8$ ) designed to support a uniform load are compared with exact linearized-theory results from reference 12. Slopes and ordinates are shown as a function of chordwise position for three spanwise positions corresponding to adjacent element locations near the wing midsemi-span. Adjacent rather than widely separated stations are shown to illustrate better the highly localized irregularities which the newer method is designed to suppress. For highly swept wings (small values of  $\beta \cot \Lambda$ ) there are only minor improvements in camber-surface definition through use of the present method. Appreciable improvements, however, are noted for the largest value of  $\beta \cot \Lambda$  where the leading edge approaches the Mach line. Apparently, the reason for this behavior is that for highly swept wings the fore Mach cone region of integration is broad and can be adequately represented by straightforward numerical integration over rectangular elements; whereas for wing leading edges approaching the Mach line the region of integration is narrow and is poorly represented by a limited number of rectangular elements. The smoothing routine helps overcome the erratic behavior of the numerical integration techniques in this later case.

Application of the design method in the definition of camber surfaces designed to support representative component loadings and an optimum combination of those loadings is illustrated in figure 13. An arrow wing with a leading-edge sweep of  $70^\circ$  at  $M = 2.0$  is used as an example. Note the large local surface ordinates called for near the root

chord for all the loadings. Generally, these singularities occur whenever there is a discontinuity in leading-edge sweep (the apex in this case). Camber-surface severity in these regions can be minimized in a design problem by substitution of a smoothed leading edge so that the transition from one leading-edge sweep to another takes place over several leading-edge elements. A limitation may also be placed on the allowable ordinate at a specified location by exercising an available program option. There is no guarantee, however, that ordinates exceeding this limit will not then arise at some other location.

An illustration of the effect of the design-method number of component loadings on the optimum combination of loadings, on the camber surface, and on the drag-due-to-lift factor is given in figure 14 for an ogee wing at  $M = 2.0$ . The changes in optimized loadings appear to be relatively large compared to the resultant change in drag-due-to-lift factor (8.4 percent). Changes in the corresponding camber surface appear to be rather subtle. In spite of the predicted theoretical improvement with increasing component loadings, the use of more than three should be approached with caution. Much is yet to be learned concerning the degree to which linearized-theory methods can be implicitly followed. Certain restricted optimum-design approaches have, however, been shown to yield appreciable benefits. (See refs. 13, 14, and 15.)

#### Analysis Method

The present wing-evaluation method, through employment of the aft-element sensing technique, effectively eliminates the need for the powerful terminal smoothing operation of the previous method. This is shown in a set of examples for arrow wings for subsonic, sonic, and supersonic leading edges given in figure 15. Flat-wing lifting-pressure coefficients are shown as a function of chordwise position for one semispan section. Numerical-method results are compared with linearized theory (ref. 16). For the previous method (ref. 6), numerical results are shown with and without the nine-point smoothing operation.

The improvement afforded by the newer method may not be immediately apparent for the more highly swept wing leading-edge examples (low values of  $\beta \cot \Lambda$ ). The present-method results display a considerable amount of scatter about the theoretical curve, more than the previous-method results with application of the terminal smoothing technique. It will be noted, however, that, in spite of some initial oscillations near the leading edge, the present-method results approach rather closely the linearized-theory results. These oscillations appear to be mild enough for an uninformed manual fairing of the data to approximate closely the correct results. Such does not appear to be the case for the unsmoothed data from the previous method. Thus, a terminal smoothing procedure is essential to the success of the previous method but is not required for the present method. This elimination of the need for a final smoothing (and a corresponding

extension of the wing surface four elements behind the trailing edge) constitutes one of the prime advantages of the new system because, as will be demonstrated later, it permits consideration of subsonic trailing edges.

For wing subsonic leading-edge sweep angles in the range of much practical interest (values of  $\beta \cot \Lambda$  from 0.6 to 1.0), the present method is superior in predicting pressures. In general, unsmoothed pressures from the newer method give a better representation of exact linearized theory than do the smoothed pressures of the older system. The improvement for the sonic leading-edge case ( $\beta \cot \Lambda = 1.0$ ) is particularly impressive. With the previous method divergent oscillations could not be completely suppressed, and, thus, the exactly sonic leading-edge condition had to be avoided. Now, the sonic leading-edge condition seems to be handled as well as any other.

For wing supersonic leading-edge sweep angles there are only minor differences between the present and previous methods. Either appears to be adequate. In any case there appear to be no disadvantages associated with the newer method which overcome its obvious advantages at subsonic and near-sonic leading-edge conditions.

Another appraisal of the lifting-pressure-distribution representation of the present and the previous method is afforded in figure 16. Note that data from the present method is shown on the right-hand side of the figure and that data from the previous method is shown on the left. Spanwise pressure distributions are shown for stations at 25, 50, and 100 percent of the overall length of delta wings with values of  $\beta \cot \Lambda$  from 0.4 to 1.6. Wing program dimensions were chosen so that each wing contained approximately 2000 elements. Although there are instances where the present method gives a poor correlation, they are isolated and do not overcome the generally better handling of the problem with the present method. It might be pointed out that previous-method results cover only the smoothed pressures which require a trailing-edge extension and preclude consideration of subsonic trailing edges.

Correlation of numerical-method lift-curve slopes with linearized-theory values from reference 16 is shown in figure 17. There is seen to be very little difference between the two numerical methods, except for the particular case of  $\beta \cot \Lambda = 1.0$  where the newer method offers a distinct advantage. For other sweep angles, both methods agree reasonably well with the analytic results.

Correlation of numerical-method results with linearized theory for a more complex double-delta planform is given in figure 18. Theoretical results were obtained from reference 17. It is seen that pressure oscillations are more subdued in the present method, but that neither numerical method reproduces the pressure discontinuities. This discrepancy may be immaterial, however, because such discontinuities have not been observed in experimental investigations.

Application of the present numerical method to prediction of pressure distributions on a flat-plate wing with a subsonic trailing edge is illustrated in figure 19. Numerical-method results (new method only, previous method not applicable) are compared with theory from reference 18. The Kutta condition, vanishing  $\Delta C_p$  at the trailing edge, is seen to be met. However, again the pressure discontinuities are not properly represented. A better approximation may be obtained by increasing the number of elements and decreasing their size, but the jump will continue to be represented by a more gradual variation over a number of elements.

A final example of the application of the wing-evaluation method to flat-plate wings treats an arbitrary planform of the ogee type (fig. 20). The numerical methods were designed with application to just such arbitrary planforms as an objective; however, because theoretical solutions are not available for arbitrary planforms, verification of the methods was accomplished for the simpler planforms previously discussed. The data of figure 20 show a somewhat smaller degree of  $\Delta C_p$  oscillation for the present method; otherwise, the results are quite similar and appear to be in reasonable agreement.

#### Methods in Combination

In an airplane-design project it is often desirable to use the design method and the evaluation method in combination. Because design-method results can yield camber surfaces too severe for incorporation in practical airplanes, these surfaces are often modified and use is then made of the evaluation method to assess the effect of the modification. This procedure may be misleading, however, if there is not a sufficient degree of correspondence between the two methods. One test of this correspondence is to submit a design-method surface directly to the evaluation-method program and to compare drag-due-to-lift factors. In one instance reported in reference 11 a difference in drag-due-to-lift factor of as much as 7 percent was found. Use of the design-method smoothing procedure, the evaluation aft-element sensing technique, and appropriate treatment of numerical integrations has been found to reduce this discrepancy considerably. This improvement is illustrated in figure 21. The previously mentioned example from reference 11 has been used to make the comparison. At the left of the figure, data from reference 11 using the previous design and analysis methods have been repeated. Results for the same example when performed with the present methods are shown at the right. The results show an appreciable improvement for one of the most severe discrepancies encountered.

A more detailed comparison of design- and analysis-method results is shown in figures 22 and 23. Again, a camber surface from the design program has been submitted directly to the evaluation program. The first example is that of a clipped-tip delta wing with three component loadings at a Mach number of 2. A more complex ogee planform

and a seven-term loading is considered in the second example. The delta wing was represented by 2104 program elements and the ogee by 2387.

From figure 22 a comparison can be made of the design-method pressure distribution for an optimum combination of loadings and the pressure distribution evaluated for that surface by the analysis method. For both examples, evaluation-method pressures nearly duplicate the design pressures except in the immediate vicinity of the leading edge.

From figure 23 a comparison can be made of the design-method spanwise loading distribution and the loading distribution calculated by the analysis method. For the simpler case of three loadings on a delta wing, the loading distribution appears to be faithfully reproduced. For the seven-loading ogee example, discrepancies are more obvious. Much of the difficulty lies in drag-distribution peak in the vicinity of the root chord. Such peaks can occur wherever there are discontinuities in the wing leading-edge sweep. Thus, care must be exercised to provide closely spaced design-method computation stations in these regions. The integrated forces show the lack of a complete agreement between the design and analysis methods. Nevertheless, the discrepancies are relatively small and well within the ability of linearized-theory methods to account for real-world aerodynamic phenomena.

In order to illustrate convergence characteristics of the methods, the design-method—analysis-method correlation for the previous delta-wing example was repeated a number of times with various element arrays being used to represent the wing. In figure 24, force data and aerodynamic center are shown as a function of the number of elements. Inset sketches illustrate the planform representation for different numbers of elements. The dotted line simply indicates a constant level (for reference purposes) to which the results appear to be converging. Converged results consistent with the validity of linearized theory seem to be attained with about 300 to 1000 elements.

Although the correspondence of the design and analysis methods has been improved, essentially identical results are not obtained within reasonable computational times. Therefore, care must be taken in the conduct of trade or sensitivity studies in which the effects of relatively small changes in wing-design parameters are to be evaluated. Either method could be used in the prediction of trends (for example, the variation of drag-due-to-lift factors with sweep angle); however, any intermixing of results should be avoided.

An indication of the computational time requirements as well as of the convergence characteristics for typical applications of the present design and analysis methods is given in figure 25. The clipped-tip delta wing with  $\beta \cot \Lambda = 0.836$  was used for the examples. Drag-due-to-lift factor  $\Delta C_D / \beta C_L^2$  was taken as the quantity used to judge convergence. In the design of the camber surface and in the evaluation of the flat wing, these factors are applicable to the complete lift-drag polar. In the case of the evaluation

of a specified camber surface, lift and drag were evaluated for the condition corresponding to a specified design lift coefficient, and thus the factor is applicable for only one point on the lift-drag polar. The maximum number of wing elements employed was selected to give indications of a converged solution for all projects. Computational times shown here do not include the time required to place the program in core storage, a time which varies considerably from one system to another. These calculations were performed on the Control Data Corporation (CDC) 6600 computer.

Results shown herein indicate that, in instances where estimates of overall force characteristics are sufficient as in conceptual design projects, adequate results can be obtained in remarkably short times. Such a capability should be of use in the selection of candidate configurations from large numbers of possible combinations of geometric design variables. Detailed camber-surface descriptions and pressure distributions, of course, require a better planform representation and considerably greater computational times.

In the computer programs which now implement the numerical methods, emphasis was placed on the development of straight-forward logic closely associated with the physics and mathematics of the problem; little attention was given to advanced programming strategies.

#### CONCLUDING REMARKS

In rather extensive employment of numerical methods for the design and analysis of arbitrary-planform wings at supersonic speeds, certain deficiencies have been uncovered. Recently, means of overcoming the major part of these deficiencies have been devised and are now incorporated into the methods. In order to provide a self-contained description of the revised methods, the original development as well as the more recent revisions have been subjected to a thorough review in this report.

Revisions to the wing-design method have virtually eliminated irregularities that often arose in the definition of the camber surface in the immediate vicinity of the wing leading edge. An aft-element sensing technique has been incorporated into the analysis method to suppress pressure oscillations which formerly required application of a powerful nine-point smoothing formula. Elimination of the need for the smoothing formula and for the associated four-element trailing-edge extension now permits the handling of subsonic trailing edges. These improvements, in combination with more compatible summation methods in the design and analysis mode, have reduced small but disturbing discrepancies which sometimes arose between wing loadings and forces determined for an optimized wing and loadings and forces calculated for that same shape upon submittal to the evaluation program.

Examples have been presented to illustrate changes in program results brought about by the modifications and to show correlation with exact linearized-theory methods where applicable. Application of the methods to sample problems indicates that, in instances where estimates of overall force characteristics are sufficient, as in conceptual design projects, adequate results can be obtained in remarkably short times (Central Processing Unit CDC 6600 computer times measured in seconds). Detailed camber-surface descriptions and pressure distributions require considerably greater computational times.

Langley Research Center,  
National Aeronautics and Space Administration,  
Hampton, Va., August 12, 1974.

## APPENDIX

### COMPUTER-PROGRAM DESCRIPTIONS

#### Wing-Design Method

The numerical method for the definition of camber surfaces for given loadings and the method for the selection of an optimum combination of loadings have been combined and programmed for the CDC 6600 computer (Langley program A4411).

The wing-planform data may be submitted to the program in any convenient scale and/or units. Reduction to program scale is accomplished by built-in logic. For a given planform, the element arrangement is uniquely determined by selection of the number of semispan grid elements  $NON$  and by the choice of design Mach number. The number of both  $N$ 's and  $L$ 's is limited to 100. Thus,  $NON$  must be less than 100 or less than  $50\beta \text{ SPAN}/XMAX$ , whichever is smaller.

The user has the option of supplying wing leading- and trailing-edge coordinates as tabular entries for a full series of successive span stations corresponding to program-element locations ( $y = (b/2)N/NON$ ) or as tabular entries for a selected series of break or definition points. In the latter case, linear interpolation methods are exercised to provide the necessary full set of leading- and trailing-edge  $x$ -ordinates in program scale. The first option is appropriate for wings with continuous curvature as exemplified by the ogee type. The second option simplifies the handling of more conventional planforms composed of straight-line segments. A similar option is provided for the description of the specified area to which a linear chordwise loading is applied.

Surface slopes are not calculated for every wing element, but only at spanwise stations corresponding to selected integer values of  $N$  (JBYS). The number of spanwise stations selected may be as large as the number of  $N$ 's, but at the expense of increased computational time. A numerical trapezoidal-integration technique is used to obtain wing lift, drag, and pitching-moment coefficients from the spanwise-section data. This technique is simpler in application than the linked cubic formulation previously employed and is more directly comparable to the integration techniques used in the wing-evaluation program. When it is desirable to reduce computational time by employment of a relatively small number of spanwise stations, care must be exercised in their selection, especially for wings with complex leading-edge shapes. In the vicinity of leading-edge breakpoints or regions of rapid curvature it is necessary to have more closely spaced spanwise stations than for other locations because of the severe surface shapes that are often called for.

## APPENDIX – Continued

By employment of selector codes any combination of the eight loadings available may be considered in the optimization process. The user also has the option of applying the moment and/or the z-ordinate restraint. As a practical matter, it is believed that the first three loadings should be included in any optimization problem with at least one additional loading for each additional restraint.

The primary program results, the camber surface corresponding to an optimum combination of loadings subject to certain restraints, may be expressed in any desired scale and units by selection of the factor **RATIO**. Ordinates at the selected spanwise stations **JBYS** are given in terms of distance behind the wing leading edge and in terms of local chord fractions. Section aerodynamic characteristics as well as wing aerodynamic characteristics (lift, drag, and pitching moment) are given for the optimized wing design. Additional printout data include the set of interference-drag coefficients for all the loading-distribution—camber-surface pairings.

### Wing-Analysis Method

The numerical method for the determination of pressure loading for a given camber surface has been programed for the CDC 6600 computer (Langley program A4410).

Wing-planform data are submitted to the program in the same manner as described for the wing-design method. Again, the user has the option of defining the planform by a full set of leading- and trailing-edge ordinates or by a selected set of breakpoints.

The wing camber-surface definition is supplied as a set of ordinates at specified locations in percent of local chord for a set of selected span stations. A factor (**RATIO**) may be employed to convert nondimensionalized ordinates or ordinates in parametric form to the scale used in the wing-planform definition.

The numerical representation of the wing as an array of rectangular elements is controlled by selection of the number of desired semispan grid elements **NON**. This number may be very small (less than 10) or very large (greater than 50) depending on the purpose of the calculation as will be discussed later.

Additional input data for a reference area and a corresponding span allow the resultant aerodynamic coefficients to be expressed in terms of the arbitrary reference area as well as in program units.

Program results, the pressure coefficients for the camber surface and for a flat wing of the same planform, are tabulated for each of the program elements and are also given as a function of standard percent-chord stations for selected semispan stations if desired. Lift, drag, and pitching-moment coefficients for the program area and for a reference area are obtained for both the cambered and flat wing from program summations.

## APPENDIX – Concluded

Interference-drag coefficients between the flat and cambered wing surfaces and pressures are used in the definition of tabulated lift-drag polar data. Streamwise and spanwise lift-distribution data are also provided.

## REFERENCES

1. Baals, Donald D.; Robins, A. Warner; and Harris, Roy V., Jr.: Aerodynamic Design Integration of Supersonic Aircraft. *J. Aircraft*, vol. 7, no. 5, Sept.-Oct. 1970, pp. 385-394.
2. Carlson, Harry W.; and Harris, Roy V., Jr.: A Unified System of Supersonic Aerodynamic Analysis. *Analytic Methods in Aircraft Aerodynamics*, NASA SP-228, 1970, pp. 639-658.
3. Bonner, E.: Expanding Role of Potential Theory in Supersonic Aircraft Design. *J. Aircraft*, vol. 8, no. 5, May 1971, pp. 347-353.
4. Woodward, F. A.: An Improved Method for the Aerodynamic Analysis of Wing-Body-Tail Configurations in Subsonic and Supersonic Flow. Pt. I - Theory and Application. NASA CR-2228, Pt. I, 1973.
5. Carlson, Harry W.; and Middleton, Wilbur D.: A Numerical Method for the Design of Camber Surfaces of Supersonic Wings With Arbitrary Planforms. NASA TN D-2341, 1964.
6. Middleton, Wilbur D.; and Carlson, Harry W.: A Numerical Method for Calculating the Flat-Plate Pressure Distributions on Supersonic Wings of Arbitrary Planform. NASA TN D-2570, 1965.
7. Middleton, Wilbur D.; and Carlson, Harry W.: Numerical Method of Estimating and Optimizing Supersonic Aerodynamic Characteristics of Arbitrary Planform Wings. *J. Aircraft*, vol. 2, no. 4, July-Aug. 1965, pp. 261-265.
8. Lomax, Harvard; Heaslet, Max. A.; and Fuller, Franklyn B.: Integrals and Integral Equations in Linearized Wing Theory. NACA Rep. 1054, 1951. (Supersedes NACA TN 2252.)
9. Mangler, K. W.: Improper Integrals in Theoretical Aerodynamics. Rep. No. Aero. 2424, British R.A.E., June 1951.
10. Grant, Frederick C.: The Proper Combination of Lift Loadings for Least Drag on a Supersonic Wing. NACA Rep. 1275, 1956. (Supersedes NACA TN 3533.)
11. Sorrells, Russell B.; and Miller, David S.: Numerical Method for Design of Minimum-Drag Supersonic Wing Camber With Constraints on Pitching Moment and Surface Deformation. NASA TN D-7097, 1972.
12. Tucker, Warren A.: A Method for the Design of Sweptback Wings Warped To Produce Specified Flight Characteristics at Supersonic Speeds. NACA Rep. 1226, 1955. (Supersedes NACA RM L51F08.)

13. Carlson, Harry W.: Aerodynamic Characteristics at Mach Number 2.05 of a Series of Highly Swept Arrow Wings Employing Various Degrees of Twist and Camber. NASA TM X-332, 1960.
14. Robins, A. Warner; Morris, Odell A.; and Harris, Roy V., Jr.: Recent Research Results in the Aerodynamics of Supersonic Vehicles. *J. Aircraft*, vol. 3, no. 6, Nov.-Dec. 1966, pp. 573-577.
15. McLean, Francis E.; and Carlson, Harry W.: Application of Wing Warp and Aerodynamic Interference To Improve Supersonic Performance. Proceedings of NASA Conference on Supersonic-Transport Feasibility Studies and Supporting Research -- September 17-19, 1963, NASA TM X-905, 1963, pp. 165-176.
16. Puckett, A. E.; and Stewart, H. J.: Aerodynamic Performance of Delta Wings at Supersonic Speeds. *J. Aeronaut. Sci.*, vol. 14, no. 10, Oct. 1947, pp. 567-578.
17. Cohen, Doris; and Friedman, Morris D.: Theoretical Investigation of the Supersonic Lift and Drag of Thin, Sweptback Wings With Increased Sweep Near the Root. NACA TN 2959, 1953.
18. Cohen, Doris: Formulas for the Supersonic Loading, Lift and Drag of Flat Swept-Back Wings With Leading Edges Behind the Mach Lines. NACA Rep. 1050, 1951.

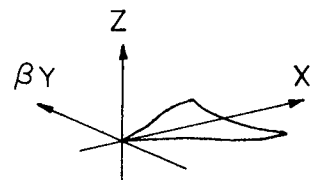
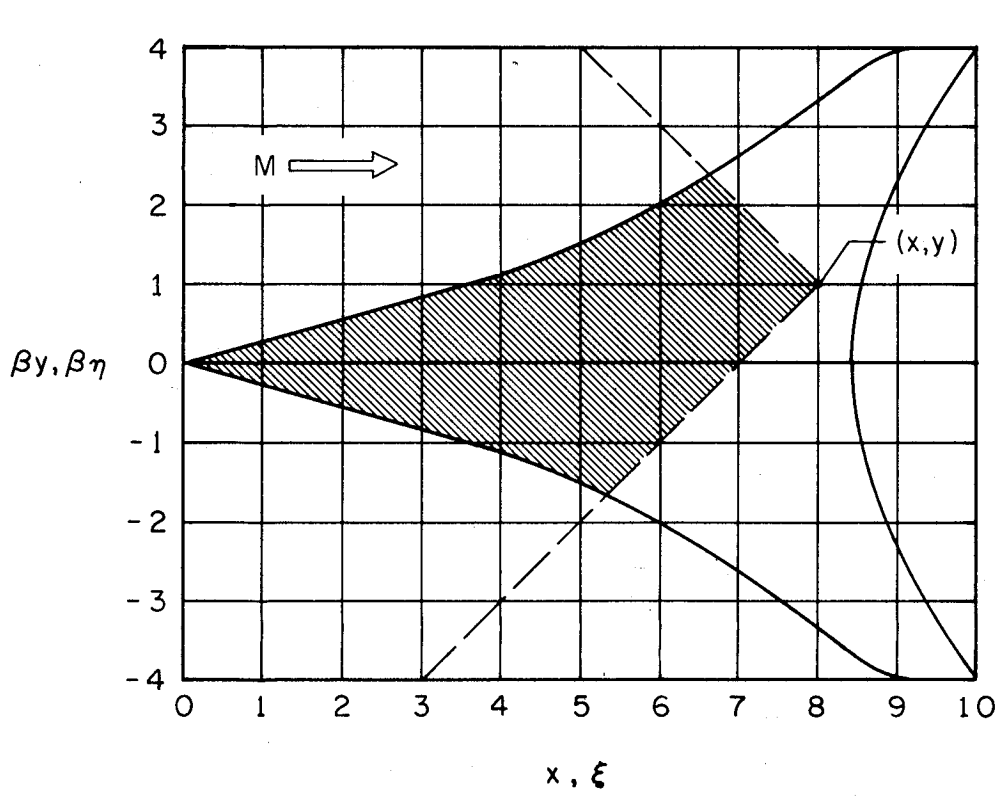


Figure 1.- Cartesian coordinate system.

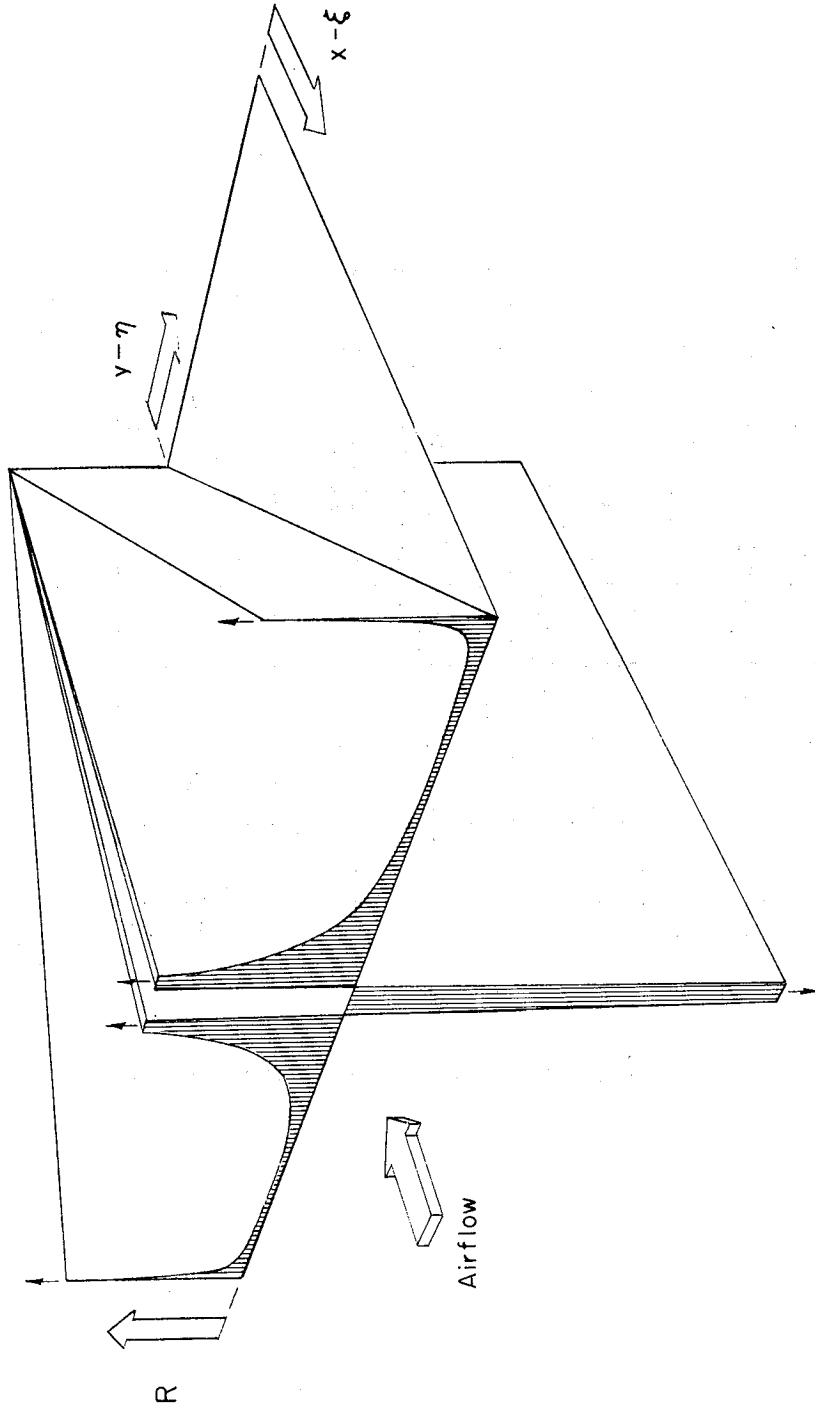


Figure 2.- Graphical representation of the influence factor R.

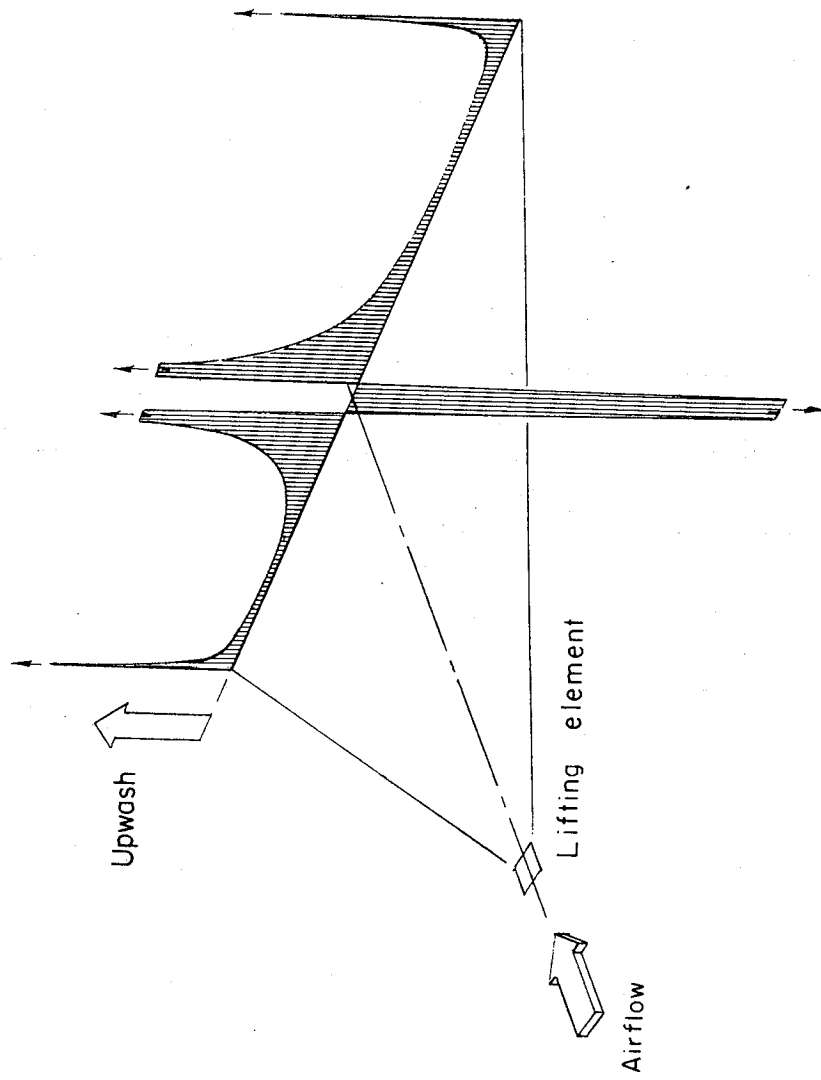


Figure 3.- Graphical representation of the upwash produced by a lifting element.

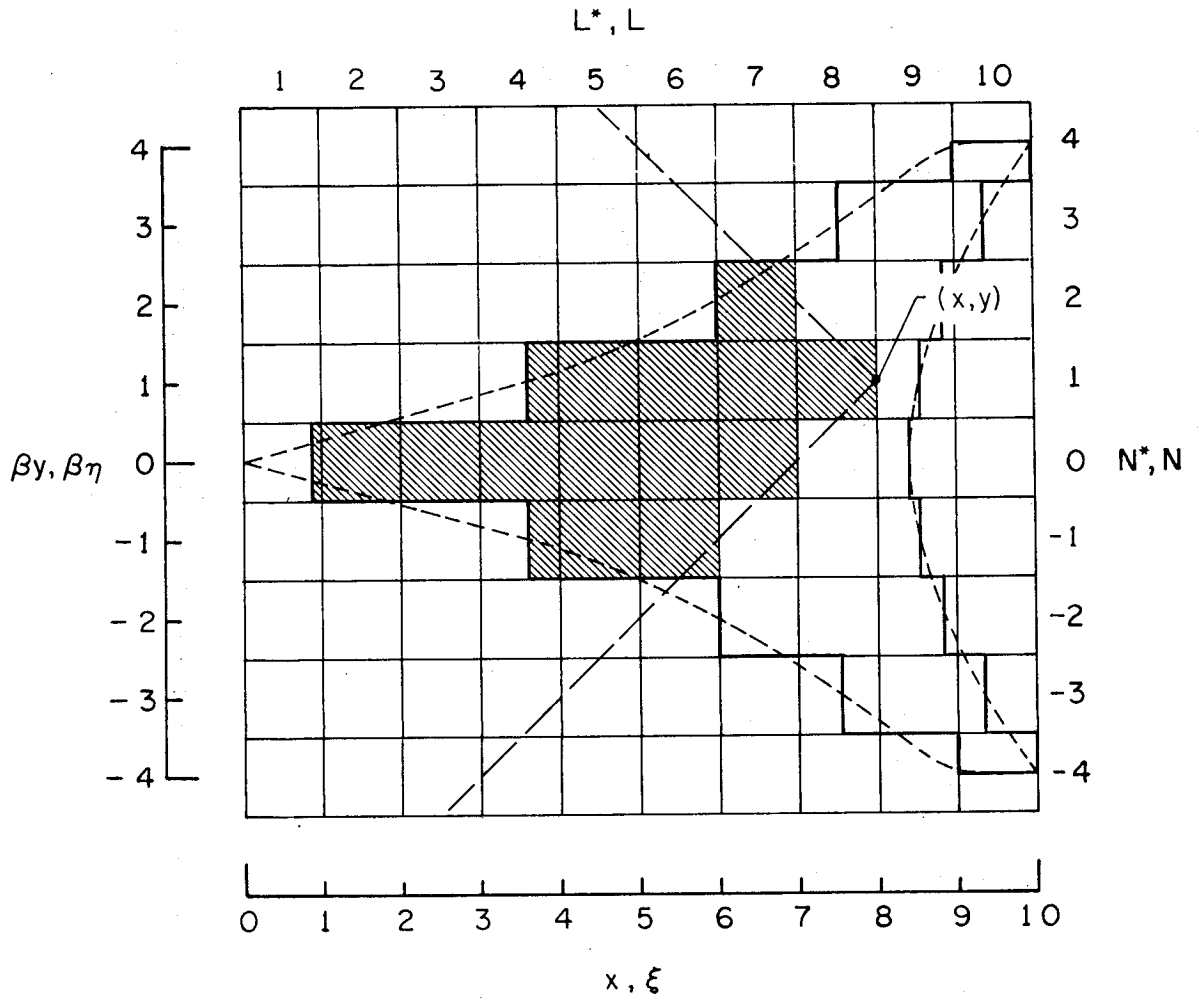


Figure 4.- Grid system used in numerical solution.

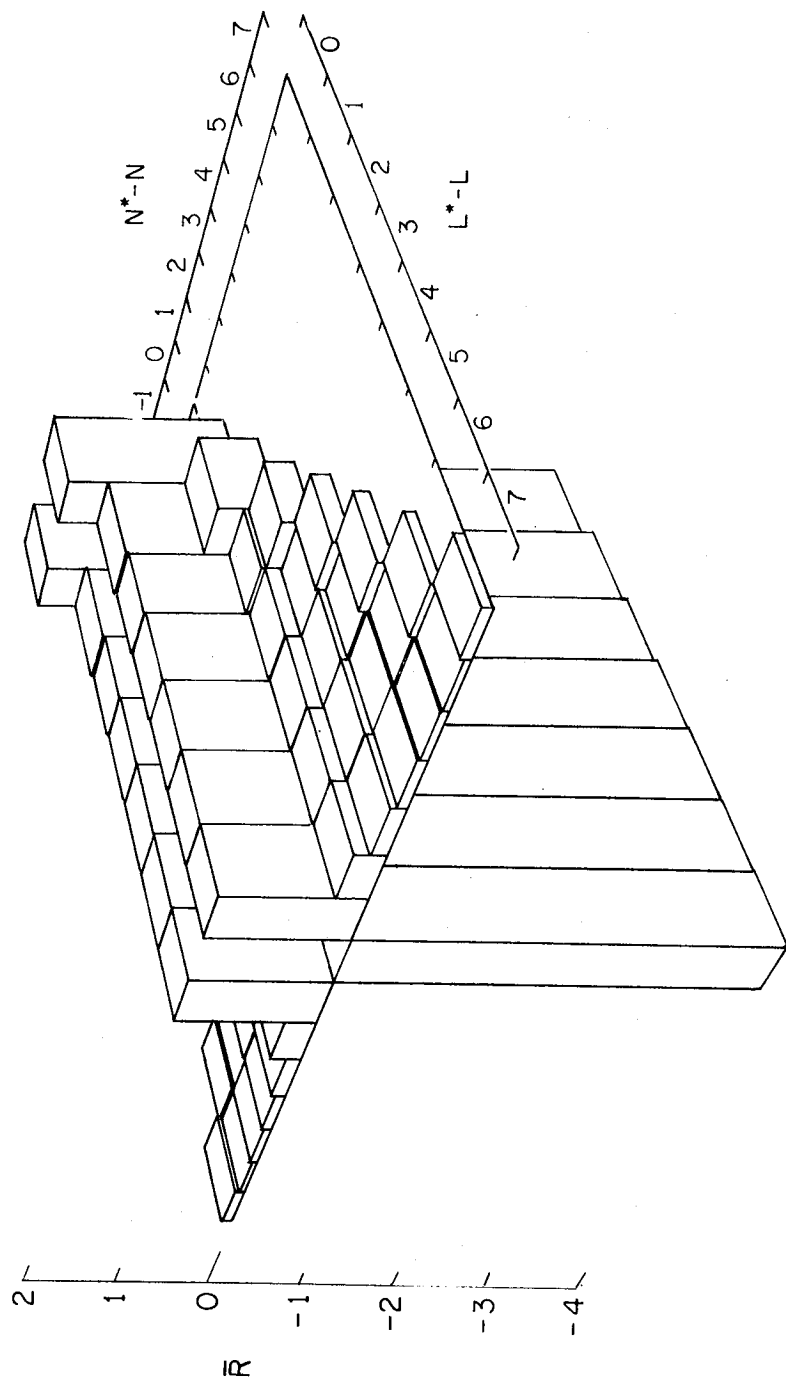


Figure 5.- Numerical representation of the influence factor  $R$  (the  $\bar{R}$  function).

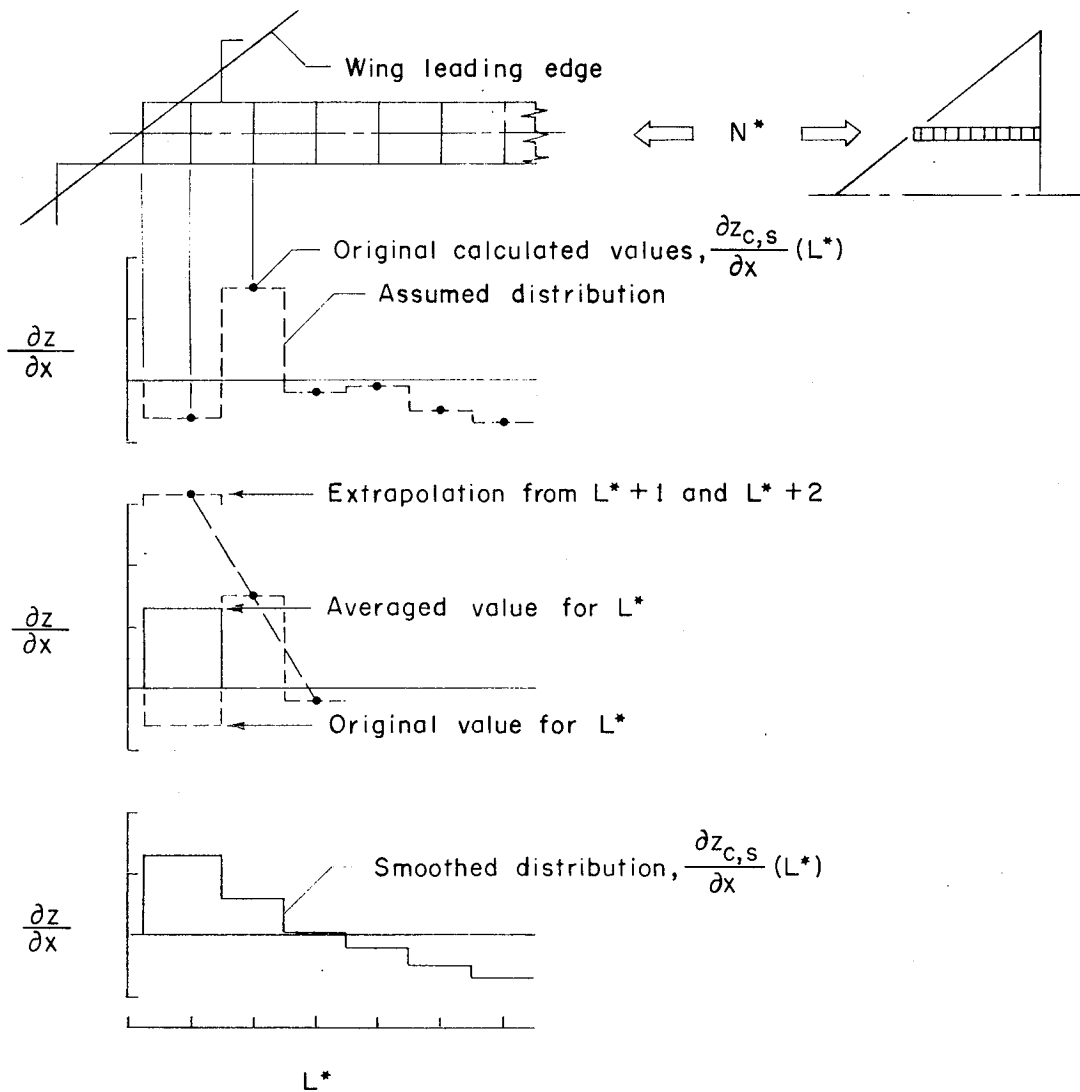


Figure 6.- Illustration of the application of the surface-slope smoothing technique in the wing-design method.

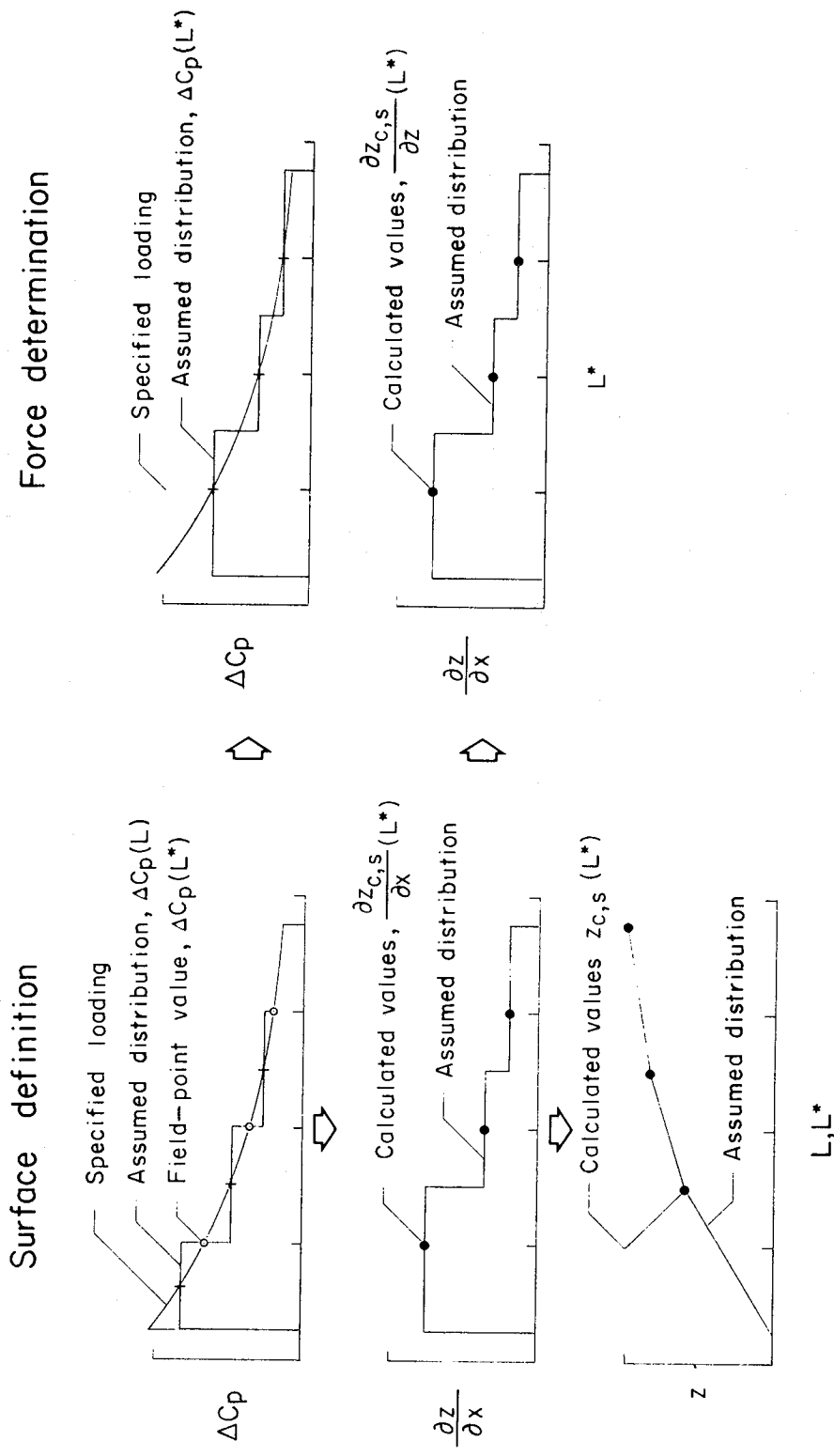


Figure 7.- Illustration of element pressure coefficient and surface slope representation for the wing-design method.

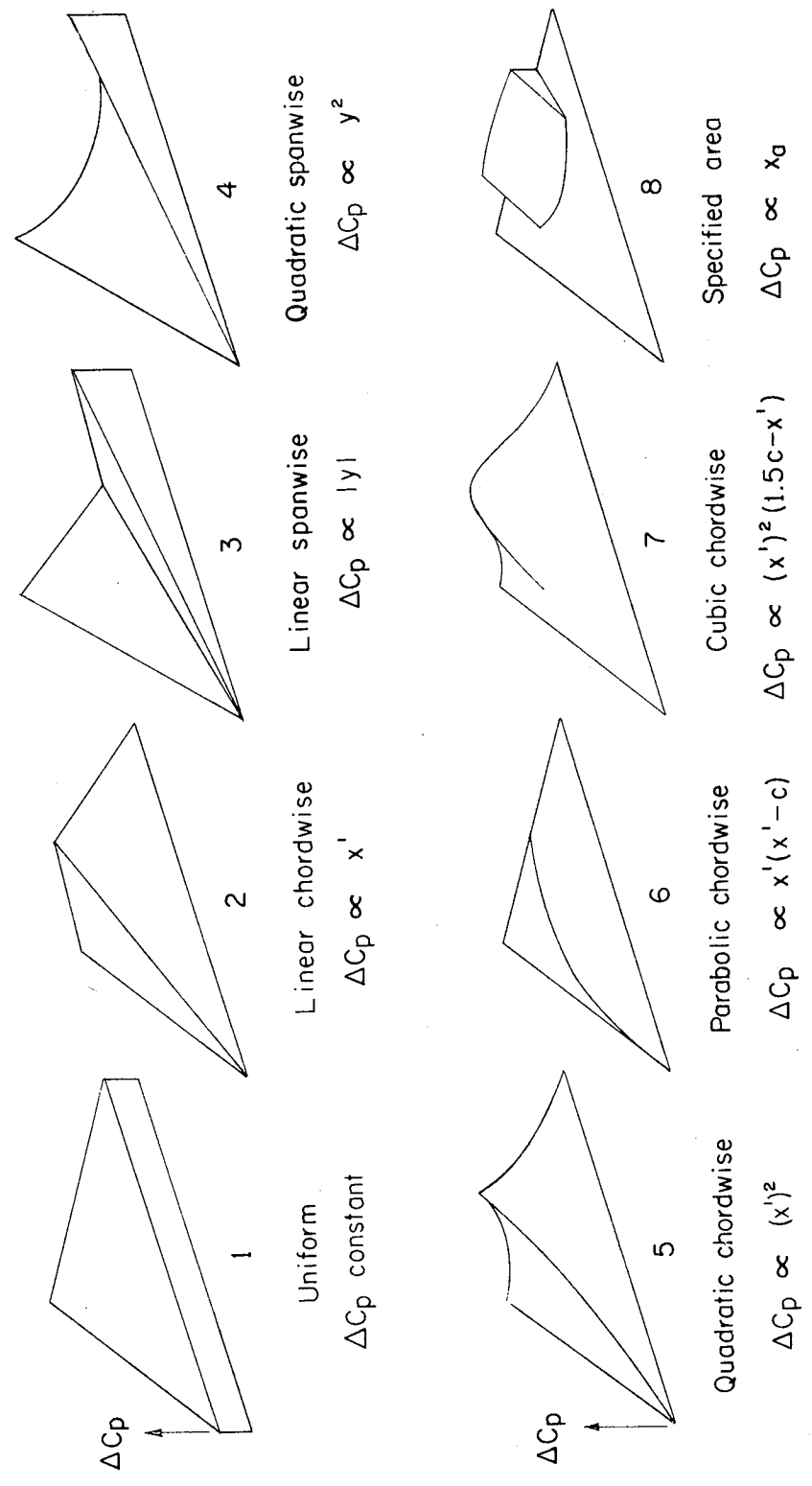
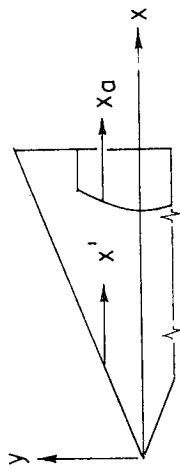


Figure 8.- Illustration of component loadings for the design of wing camber surfaces.

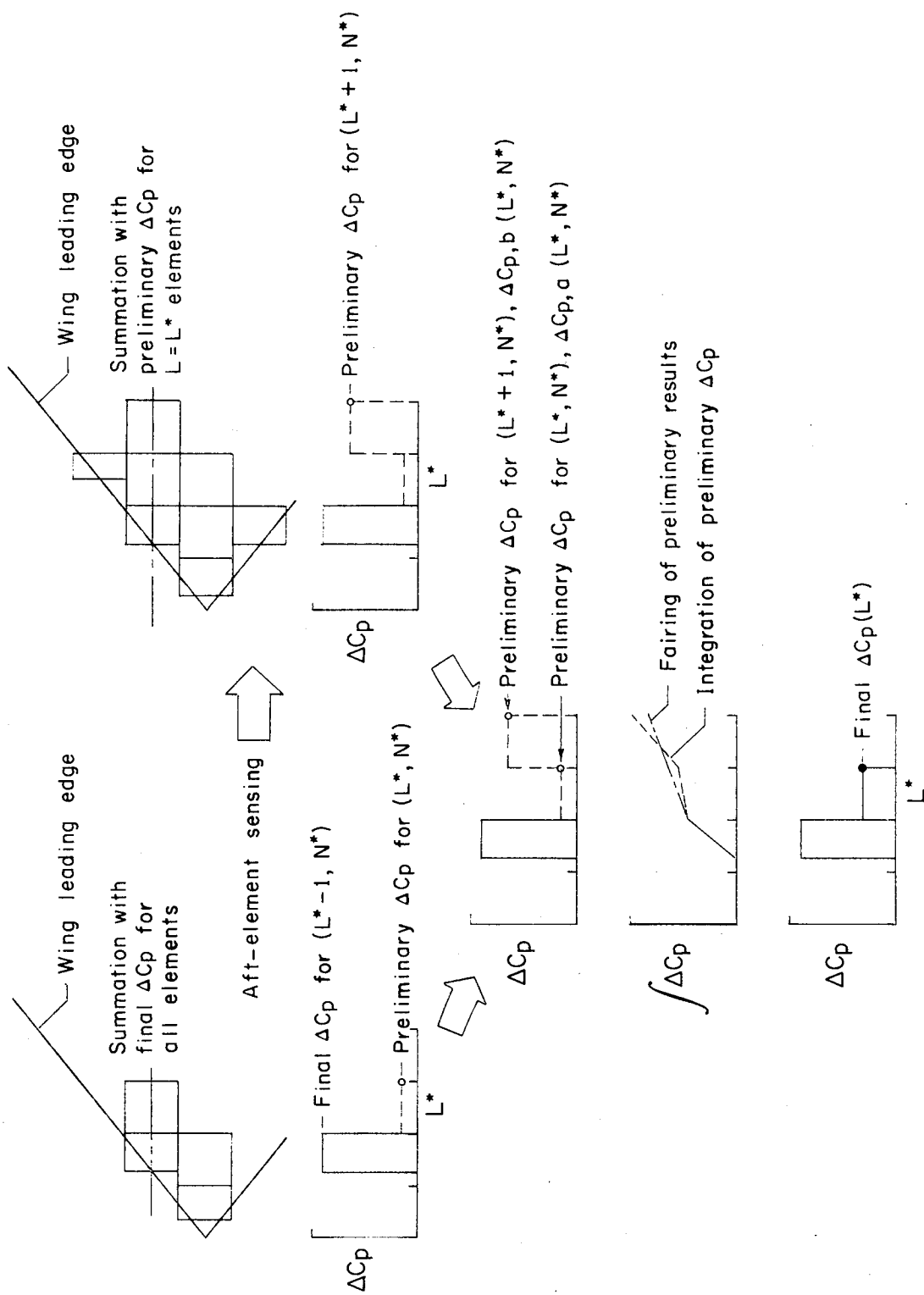


Figure 9.- Illustration of the application of the aft-element sensing technique in the wing-evaluation method.

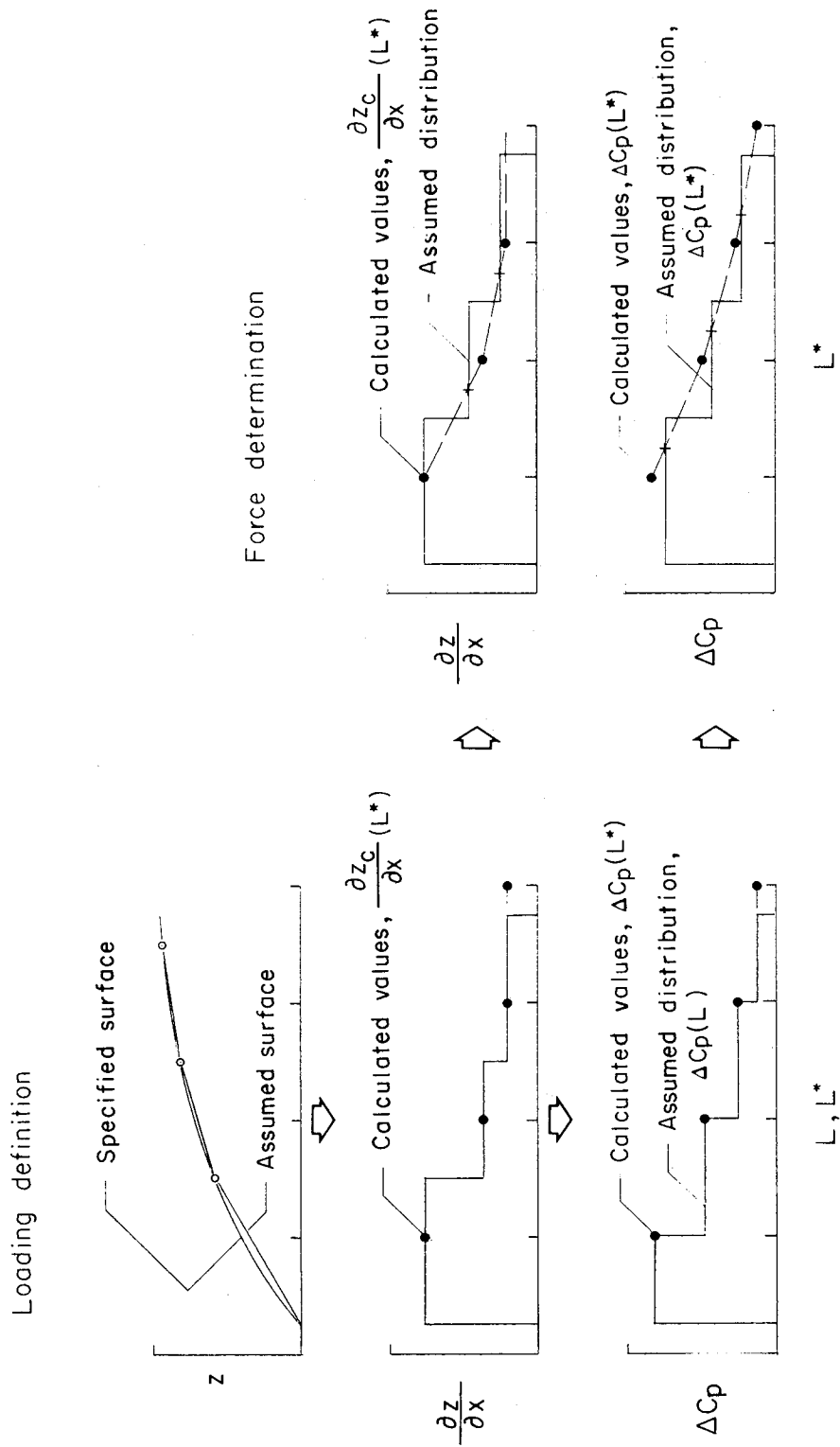
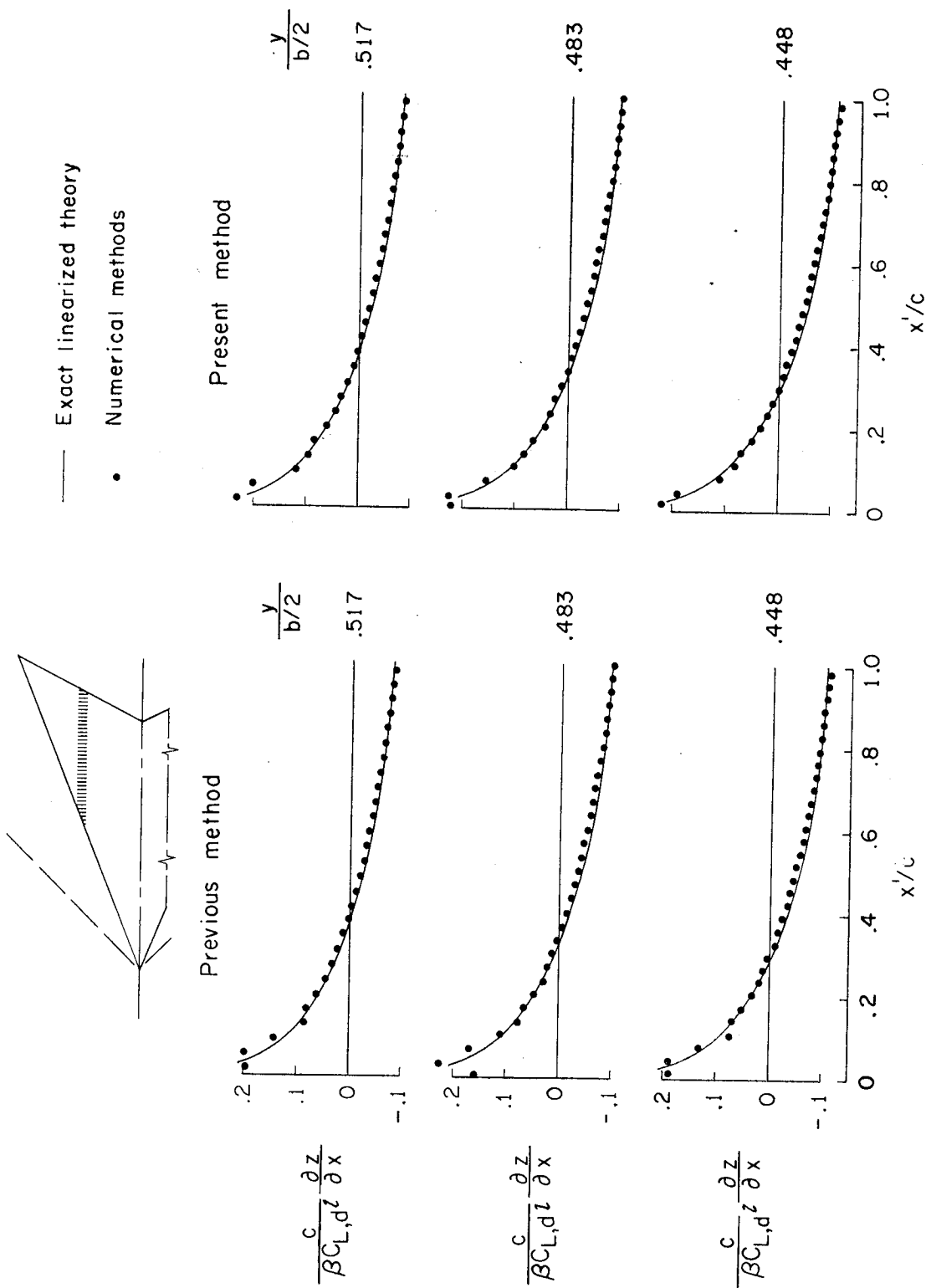
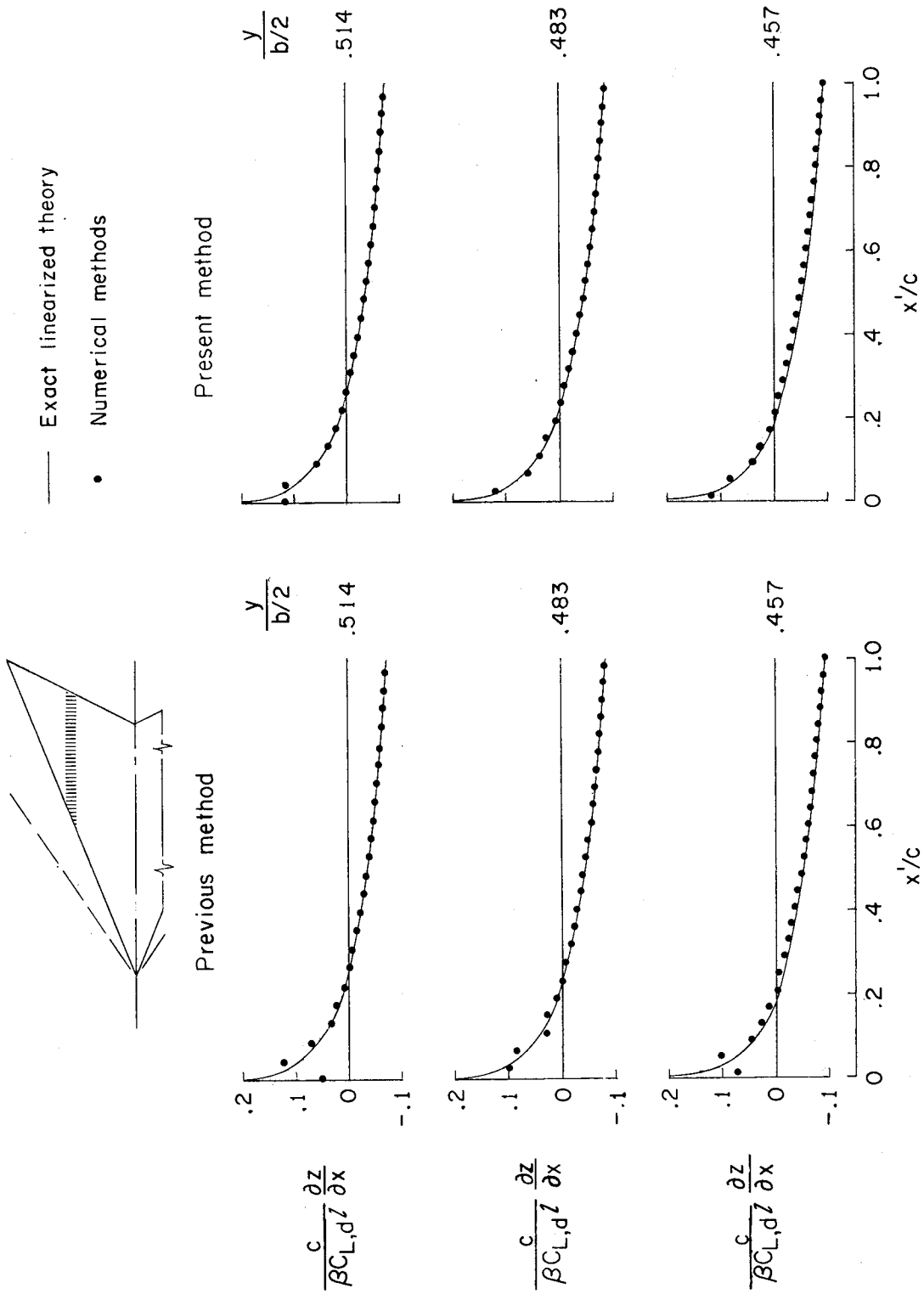


Figure 10.- Illustration of element surface slope and pressure-coefficient representation for the wing-evaluation method.



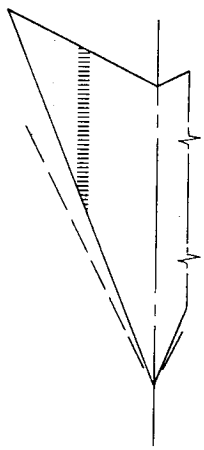
(a)  $\beta \cot \Lambda = 0.4$ .

Figure 11.- Present and previous design-method results for the definition of camber-surface slopes required to support a uniform load.



(b)  $\beta \cot \Lambda = 0.6$ .

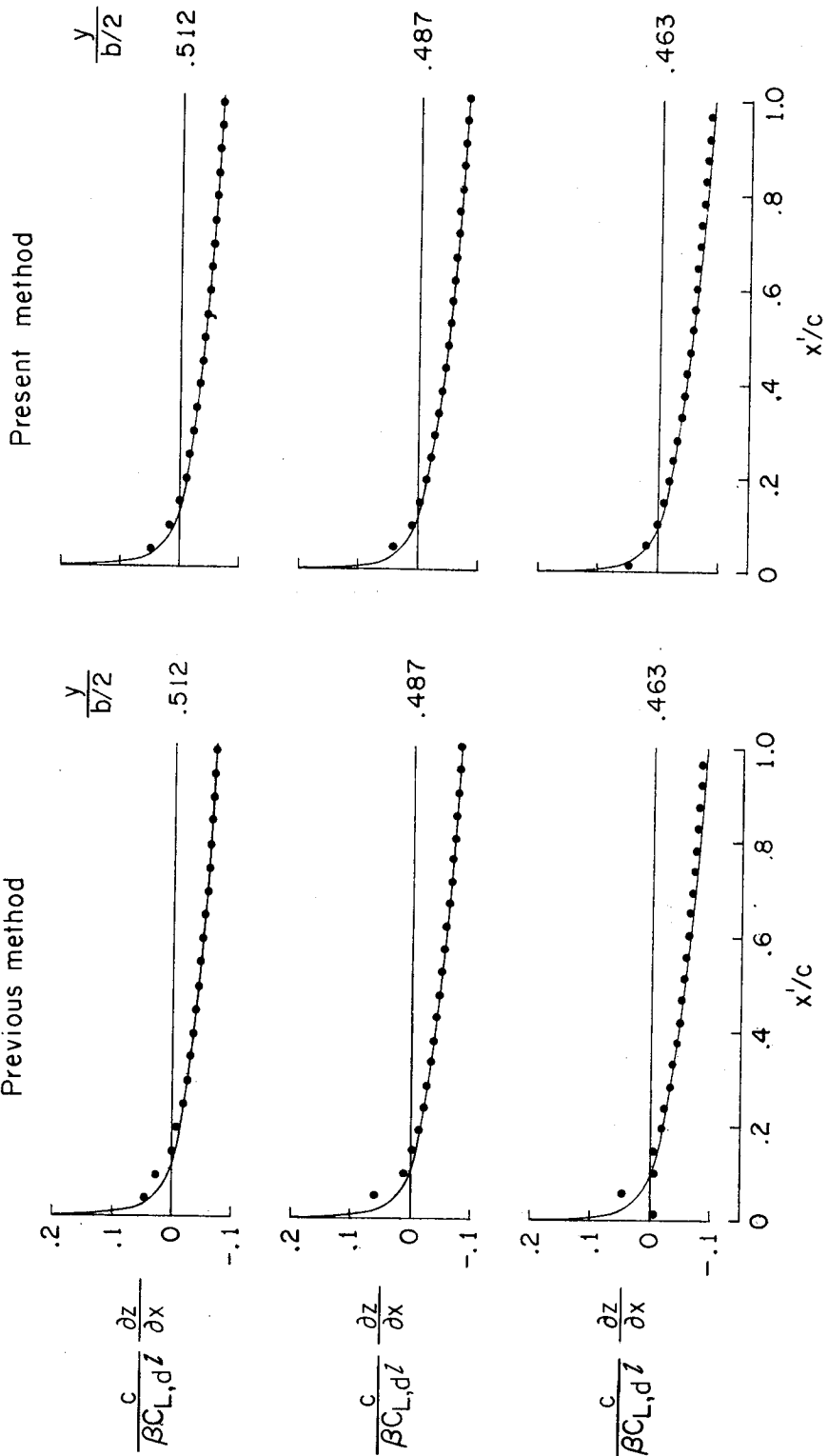
Figure 11.- Continued.



— Exact linearized theory

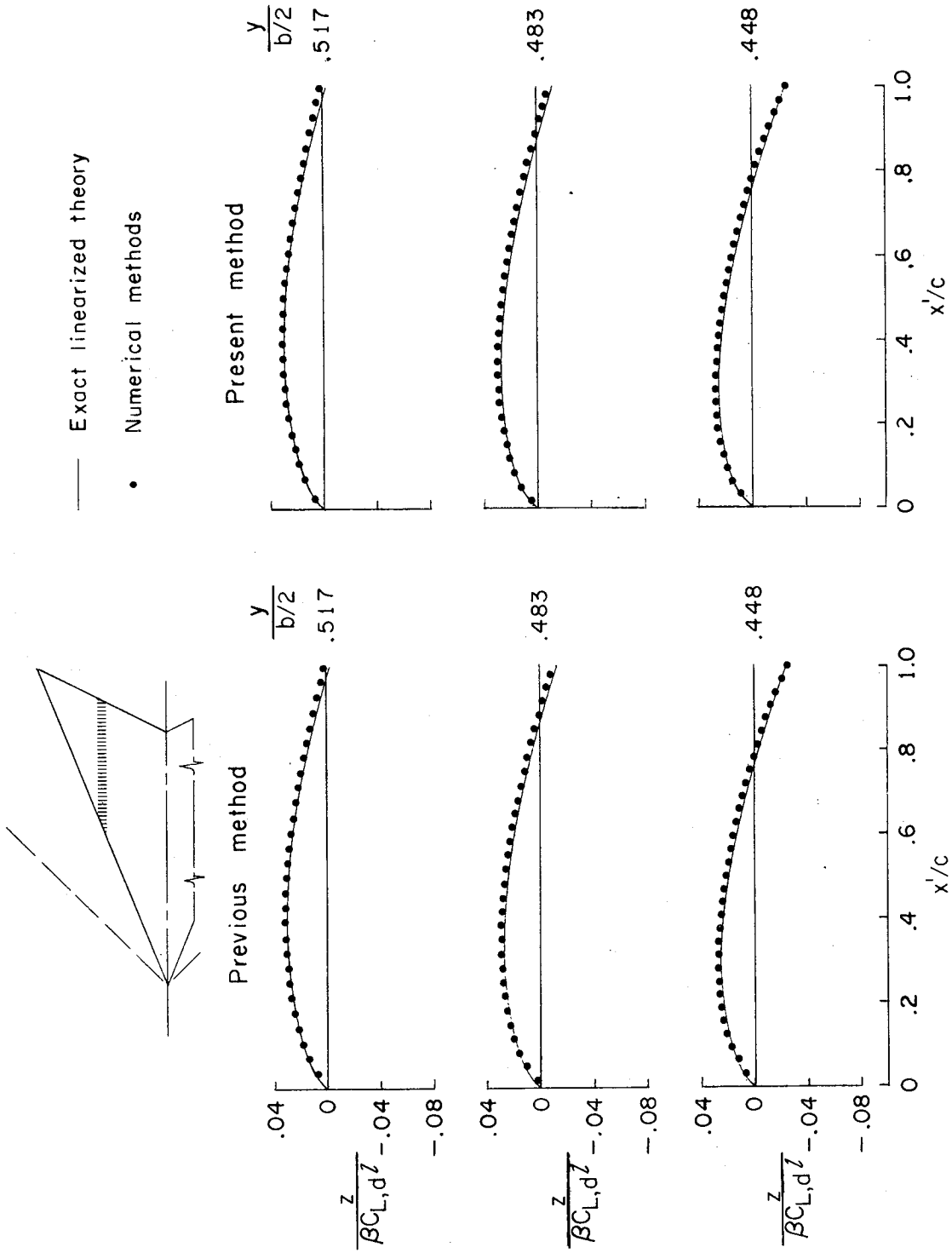
• Numerical methods

Previous method



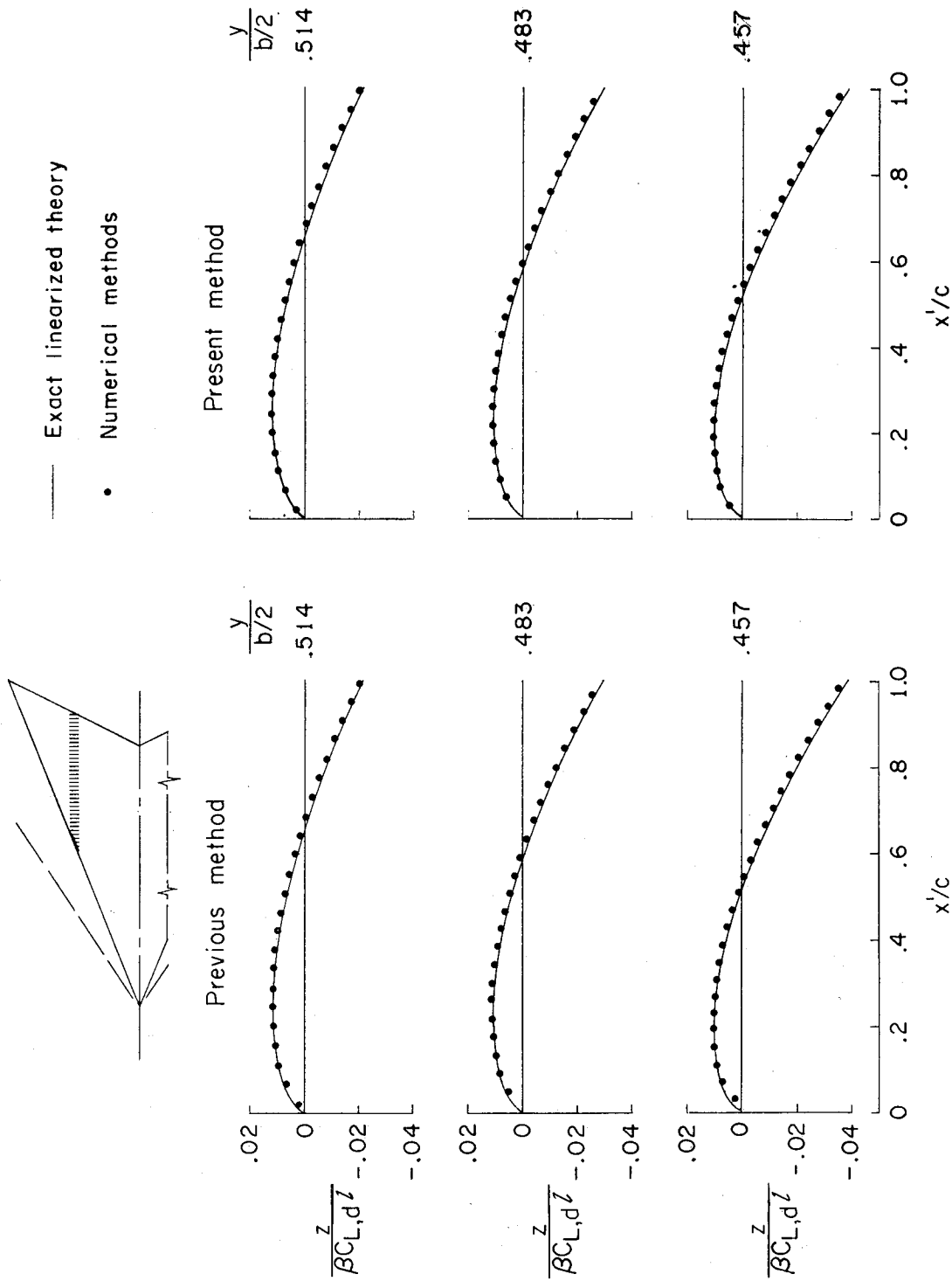
(c)  $\beta \cot \Lambda = 0.8$ .

Figure 11.- Concluded.

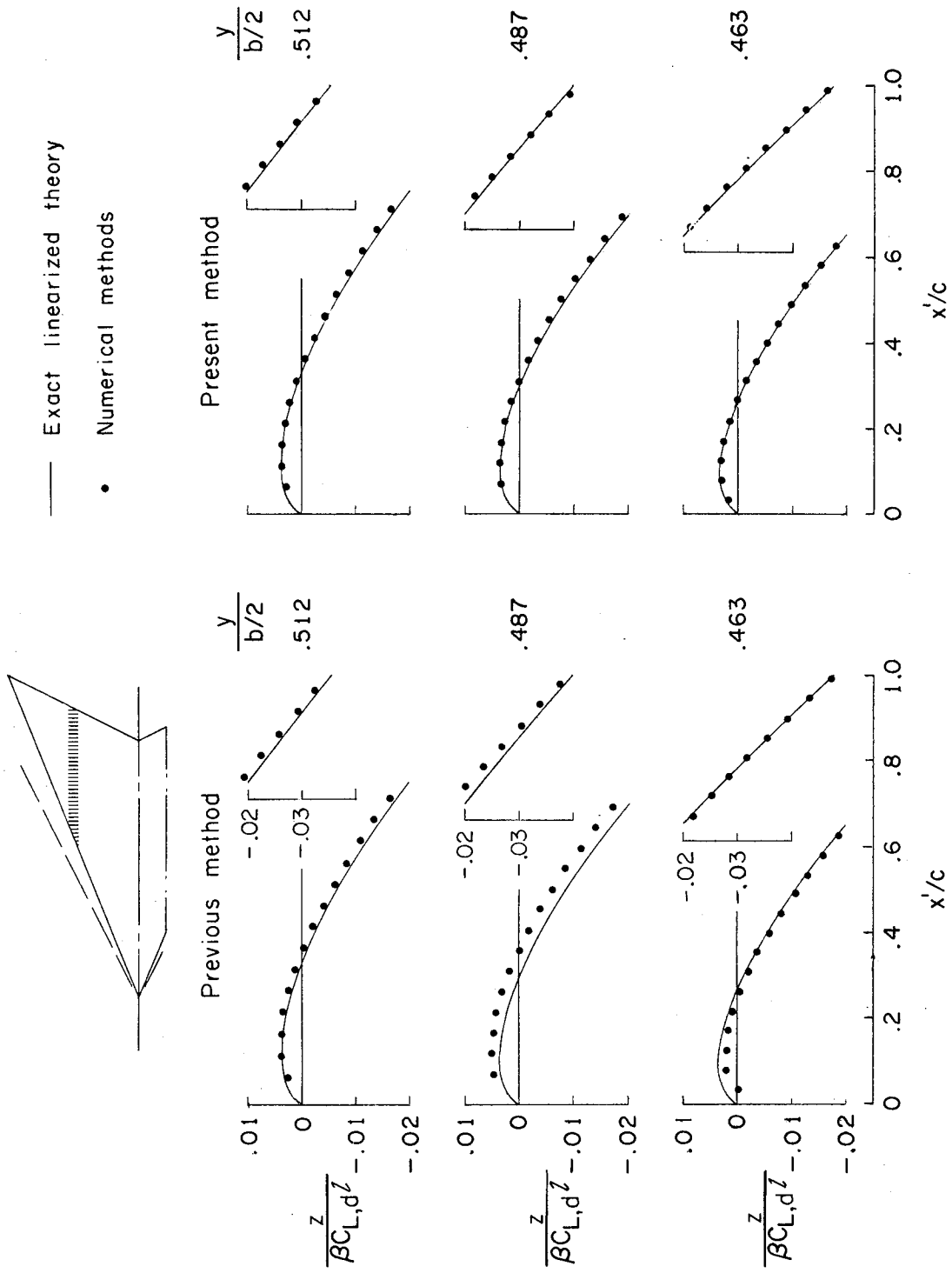


(a)  $\beta \cot \Lambda = 0.4$ .

Figure 12.- Present and previous design-method results for the definition of camber-surface ordinates required to support a uniform load.



(b)  $\beta \cot \Lambda = 0.6$ .  
 Figure 12.- Continued.



(c)  $\beta \cot \Lambda = 0.8$ .

Figure 12.- Concluded.

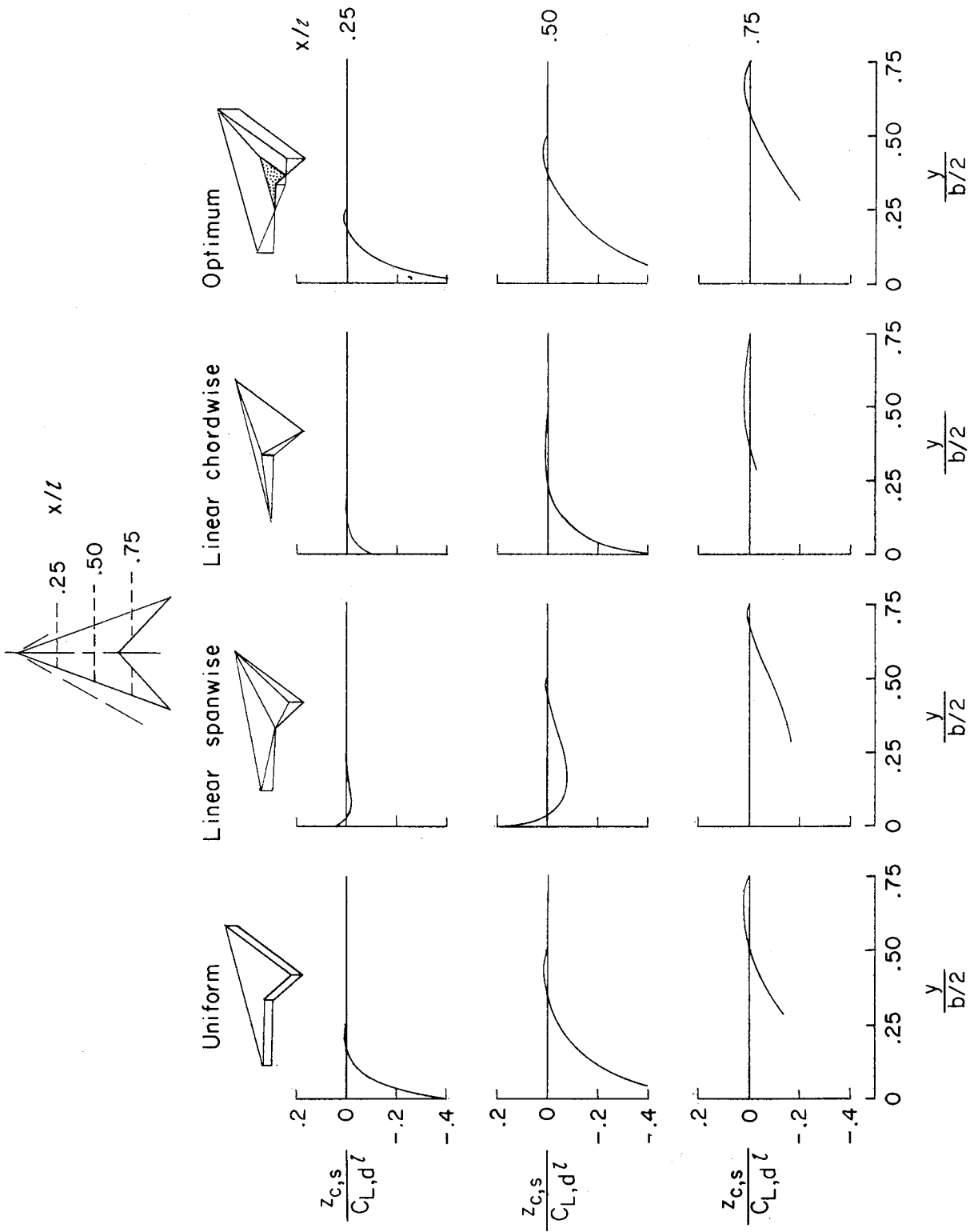


Figure 13.- Numerical-method solutions for camber surfaces to support various loadings on an arrow wing with  $\Lambda = 70^\circ$ .  $M = 2.0$ .

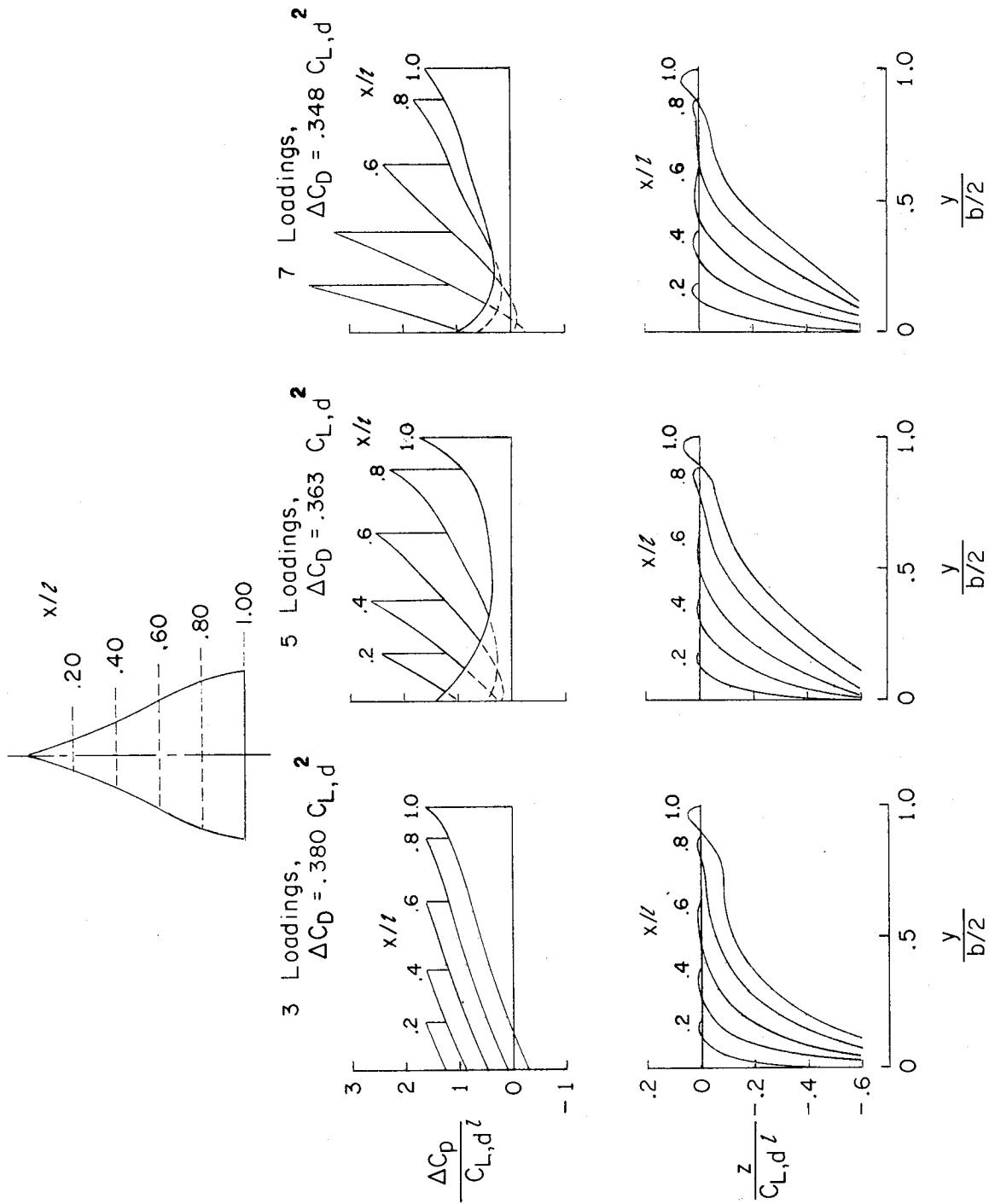
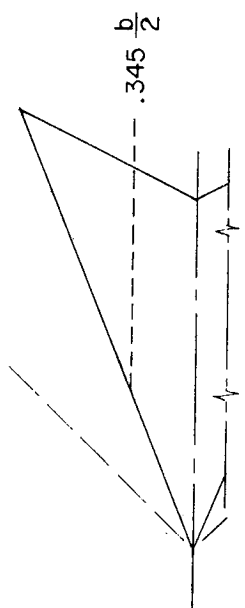
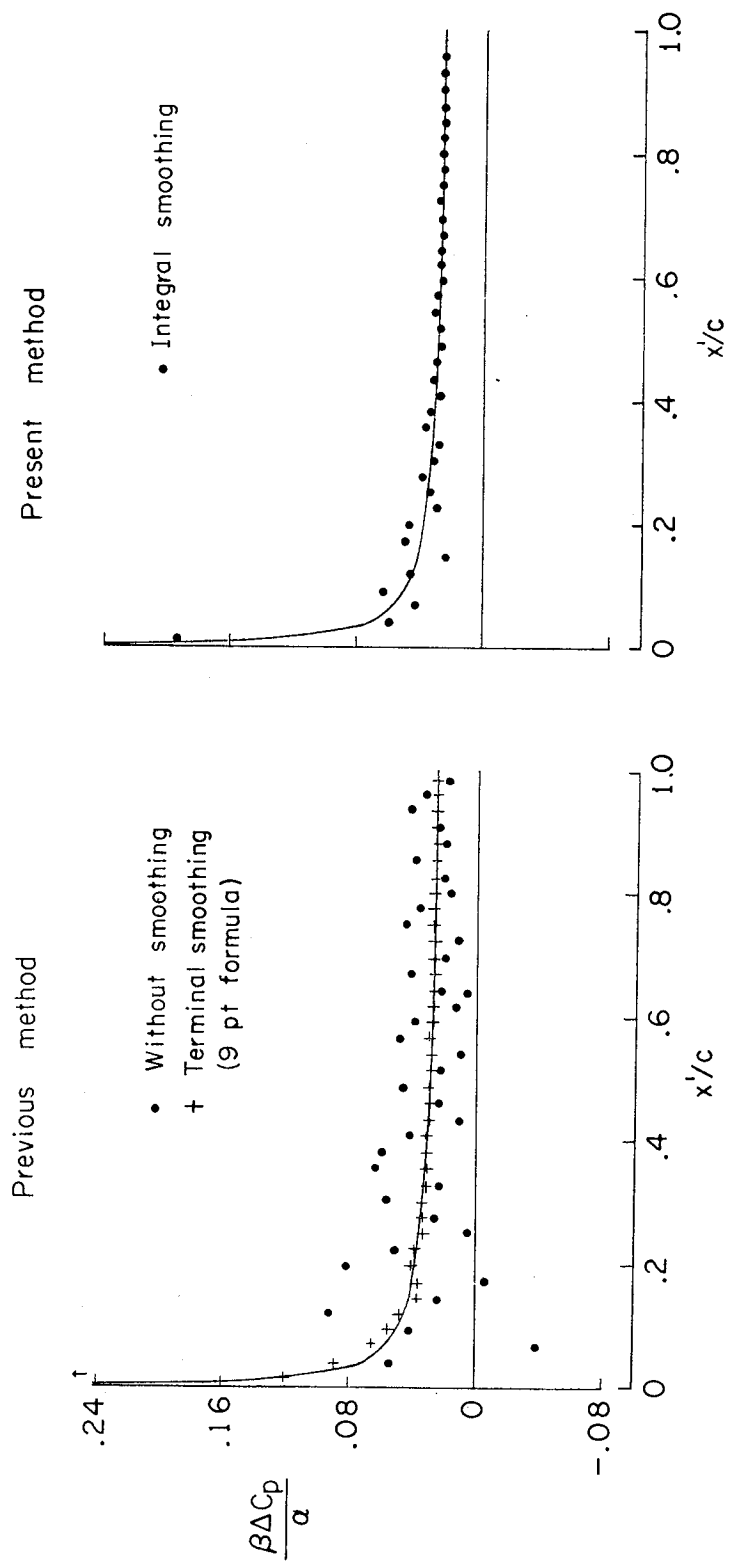


Figure 14.- Numerical-method solutions for camber surfaces to support optimum combinations of loadings for an ogee wing.  $M = 2.0$ .

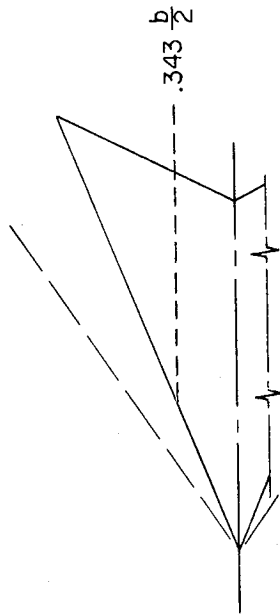


— Exact linearized theory  
 •, + Numerical methods



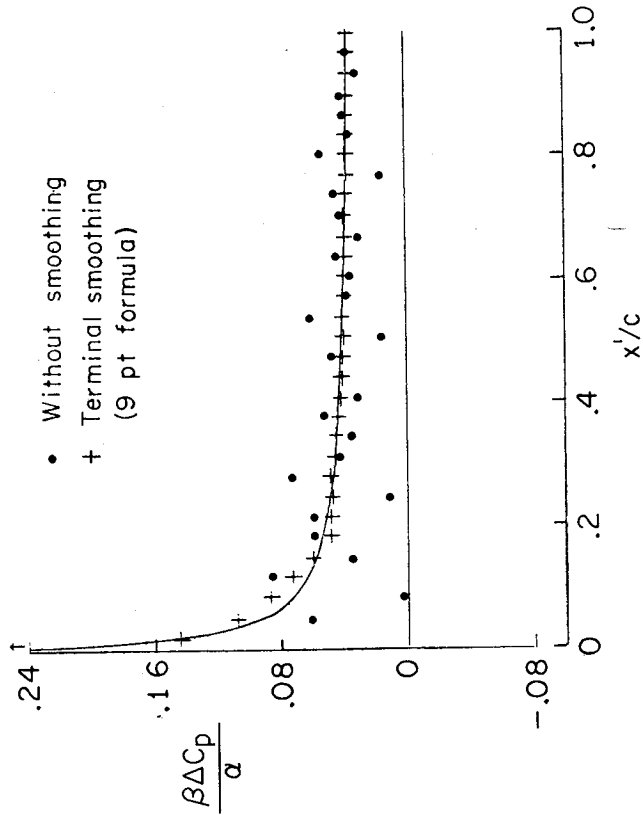
(a)  $\cot \Lambda = 0.4$ .

Figure 15.- Pressure-smoothing characteristics of present and previous evaluation methods. Flat-arrow wings.

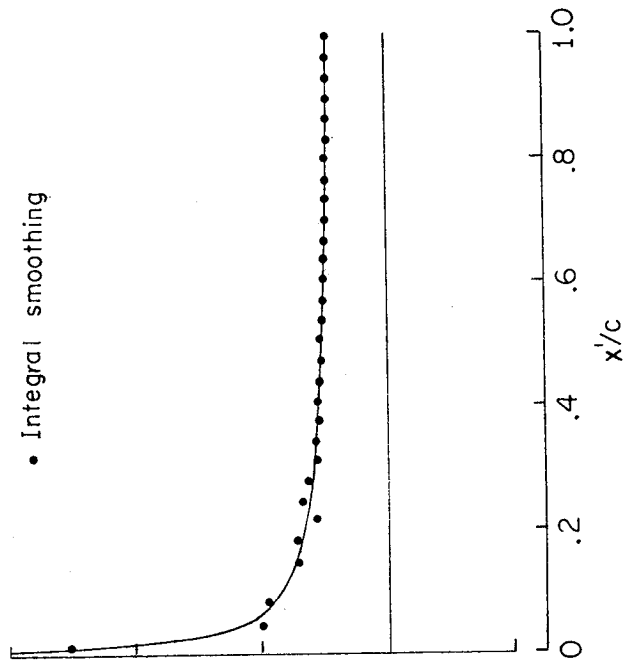


— Exact linearized theory  
 •, + Numerical methods

Previous method

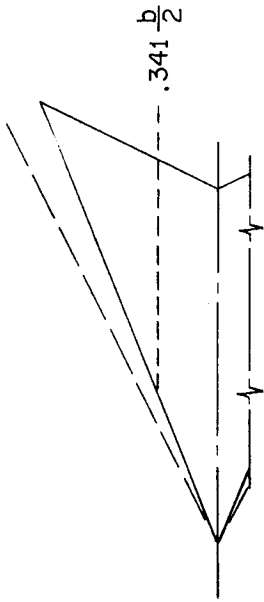


Present method



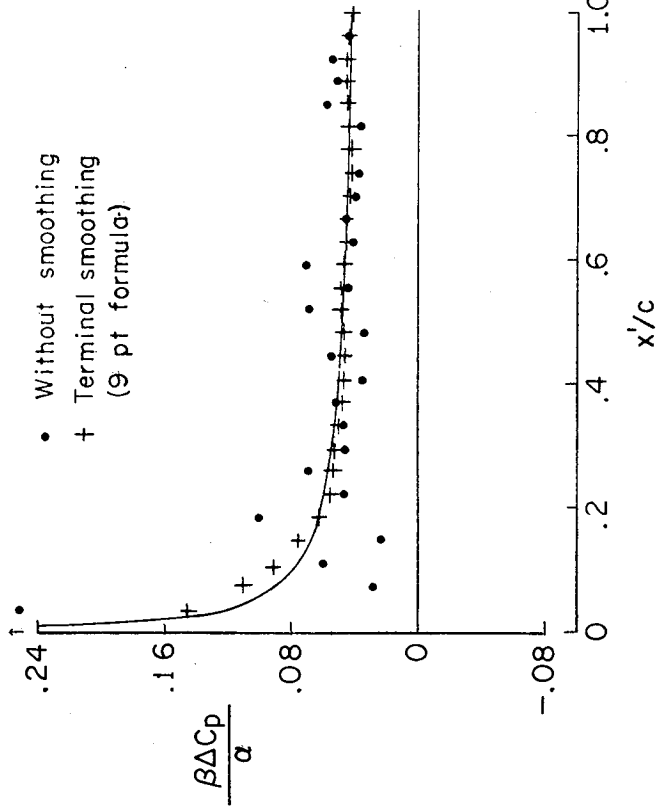
(b)  $\beta \cot \Lambda = 0.6$ .

Figure 15.- Continued.

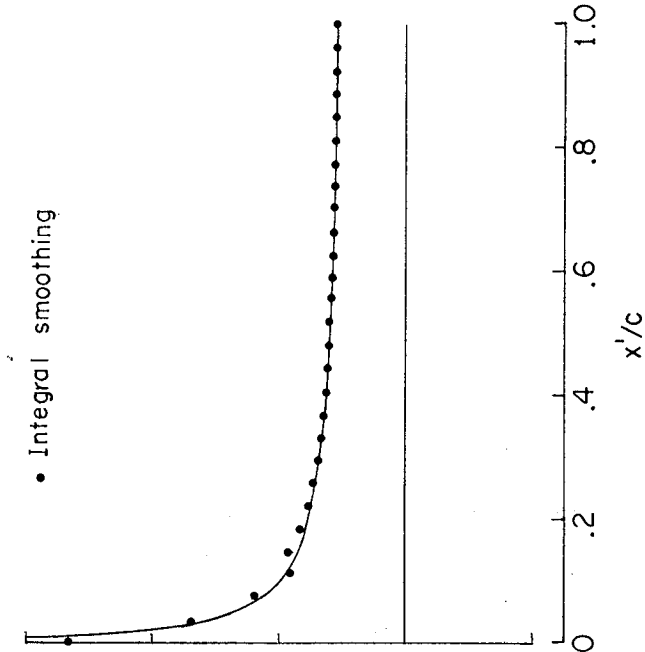


- 
- Exact linearized theory
- ,+ Numerical methods

Previous method

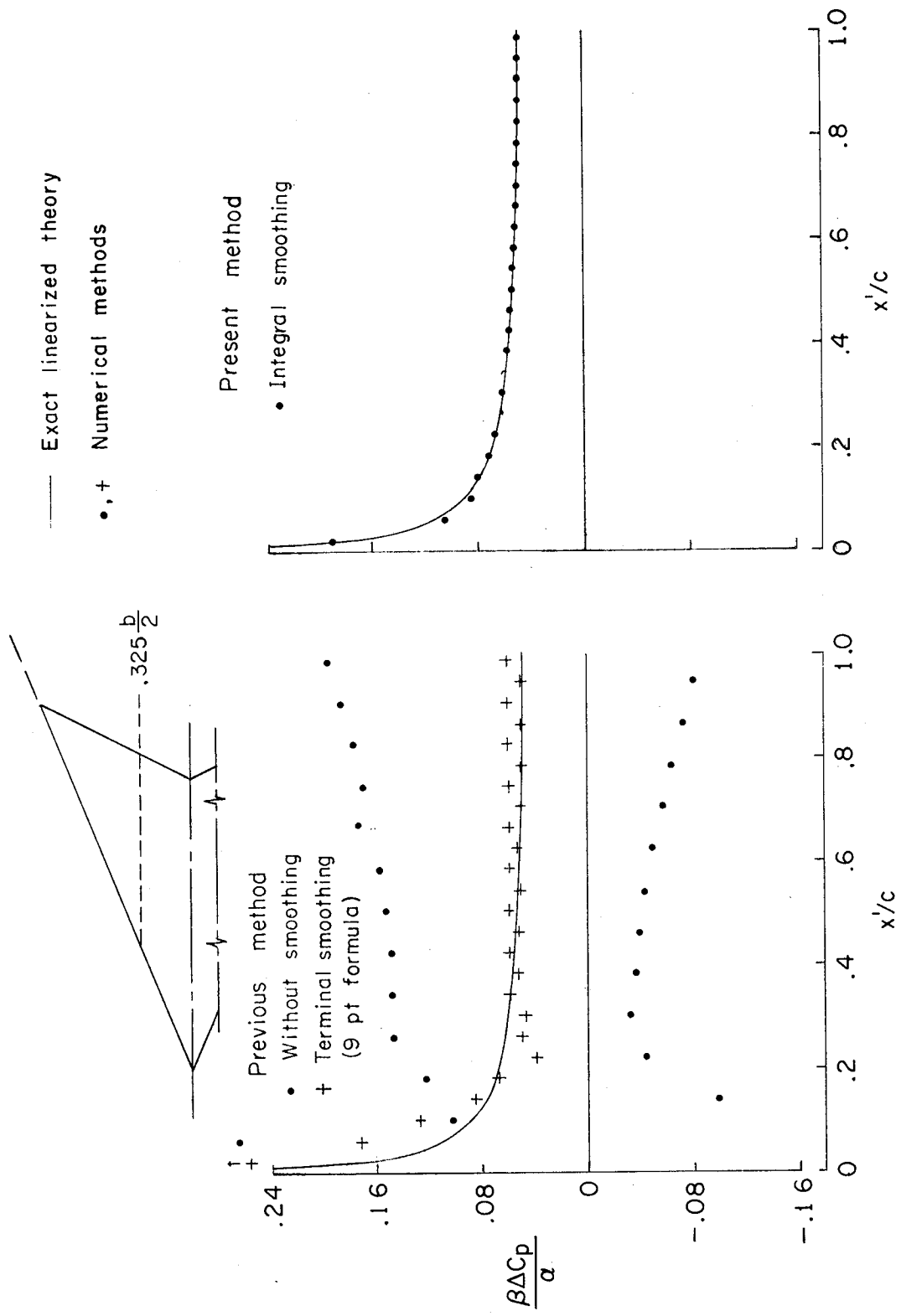


Present method



(c)  $\beta \cot \Lambda = 0.8$ .

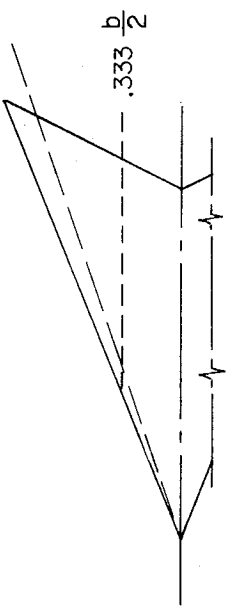
Figure 15.- Continued.



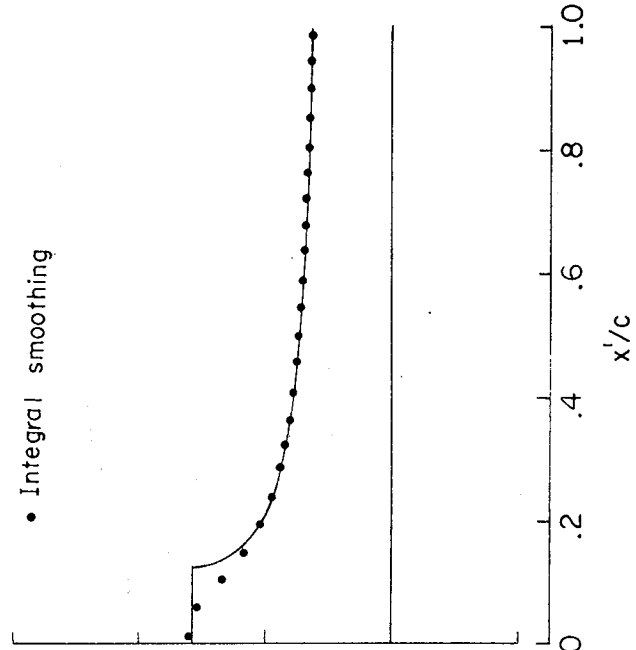
(d)  $\beta \cot \Lambda = 1.0$ .

Figure 15.- Continued.

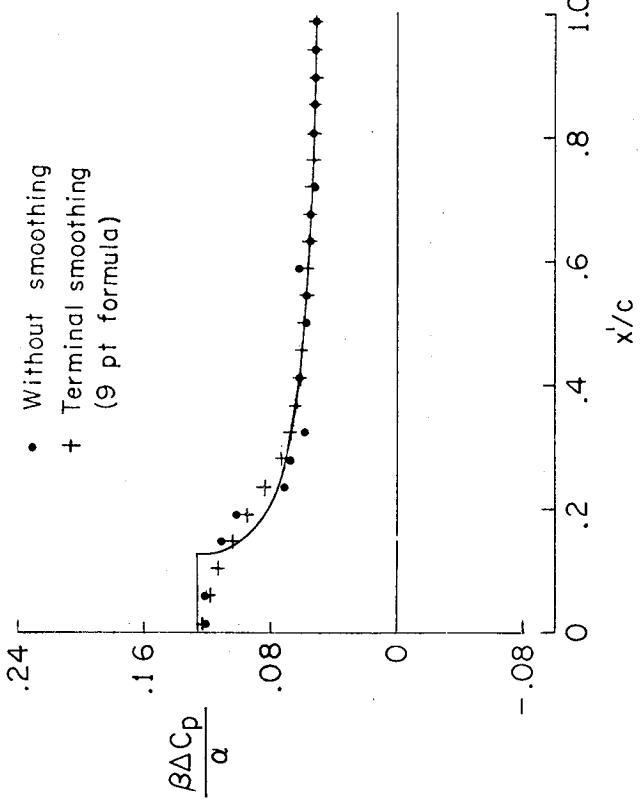
— Exact linearized theory  
 •, + Numerical methods



Present method

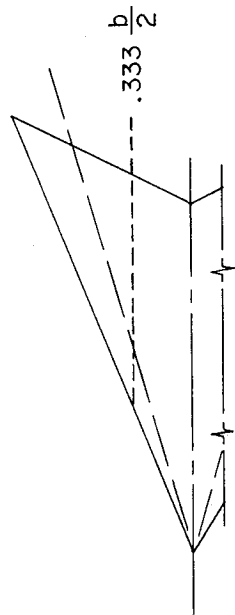


Previous method



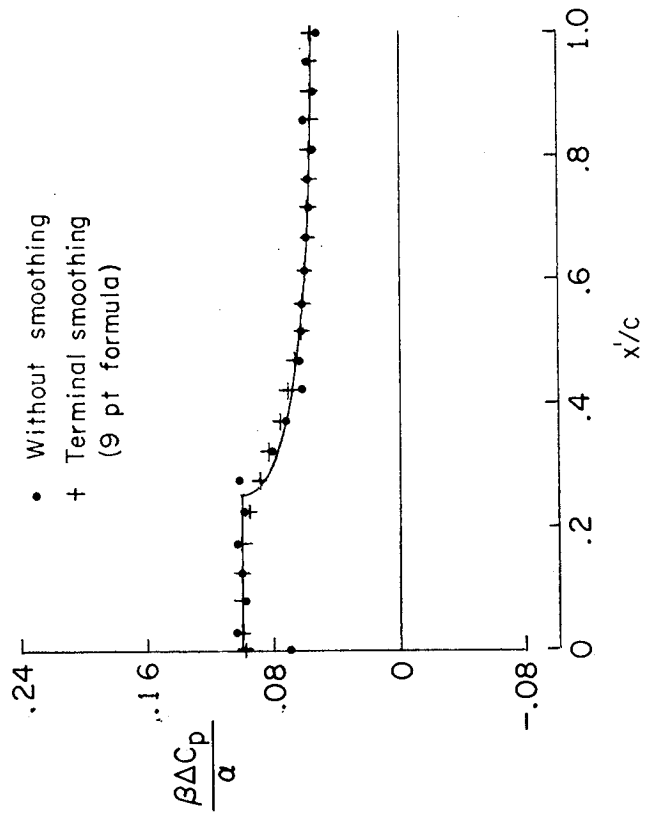
(e)  $\beta \cot \Lambda = 1.2.$

Figure 15.- Continued.

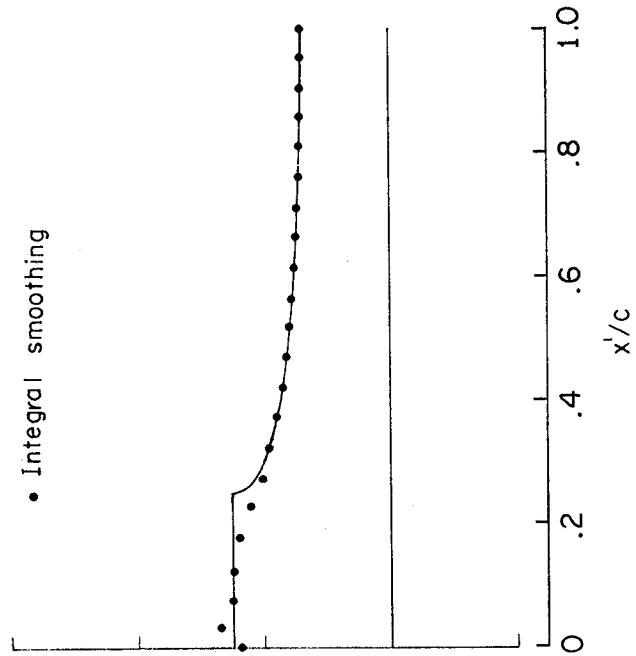


— Exact linearized theory  
 •, + Numerical methods

Previous method



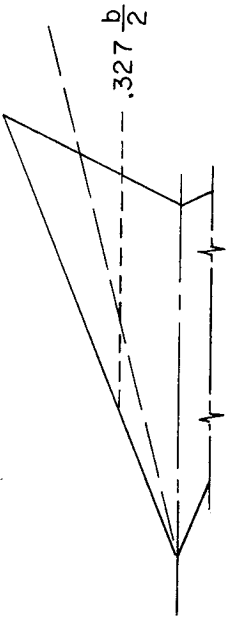
Present method



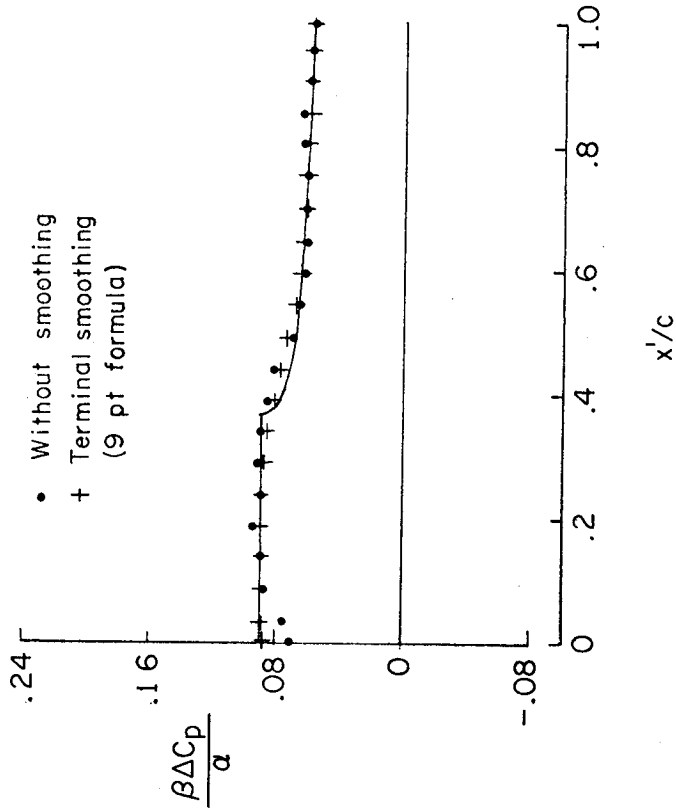
(f)  $\beta \cot \Lambda = 1.4$ .

Figure 15.- Continued.

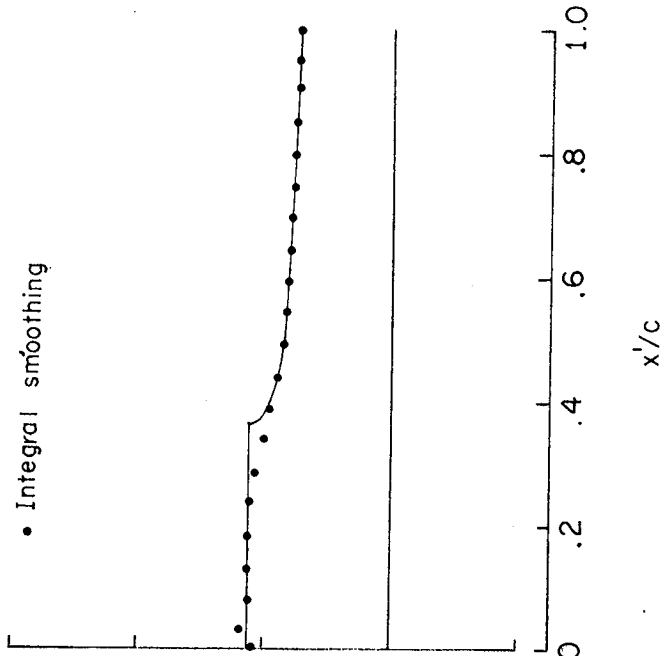
— Exact linearized theory  
 •, + Numerical methods



Previous method

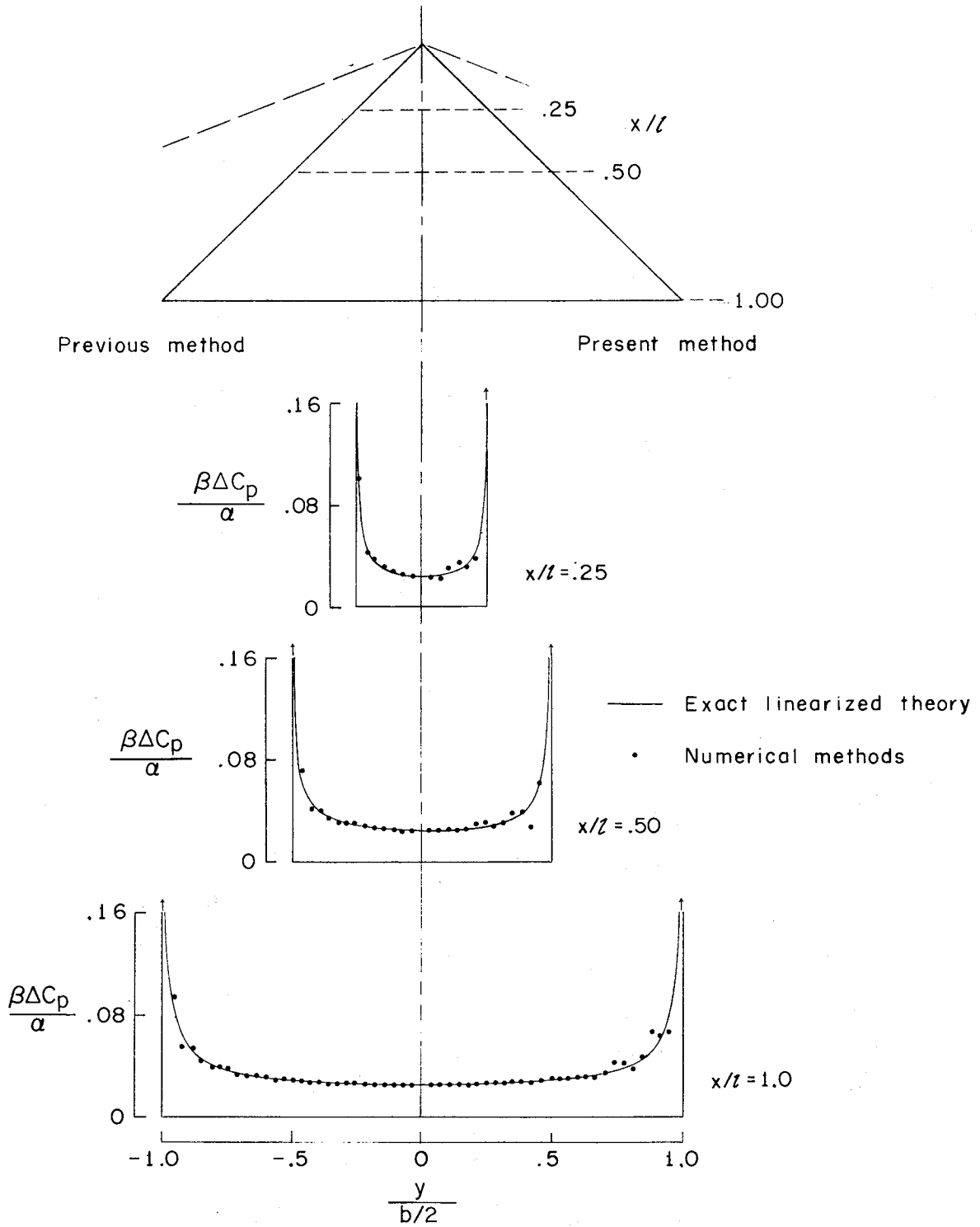


Present method



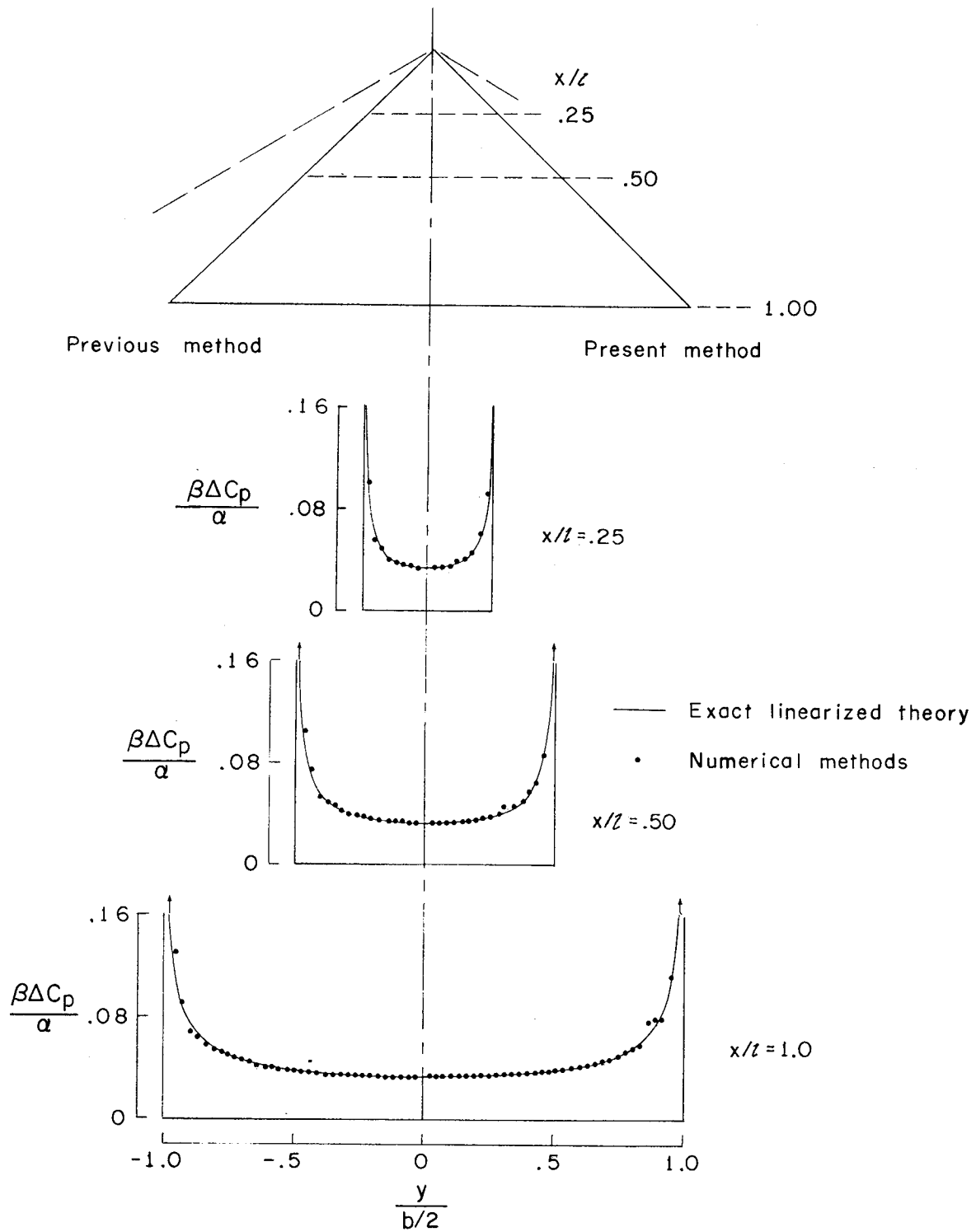
(g)  $\beta \cot \Lambda = 1.6$ .

Figure 15.- Concluded.



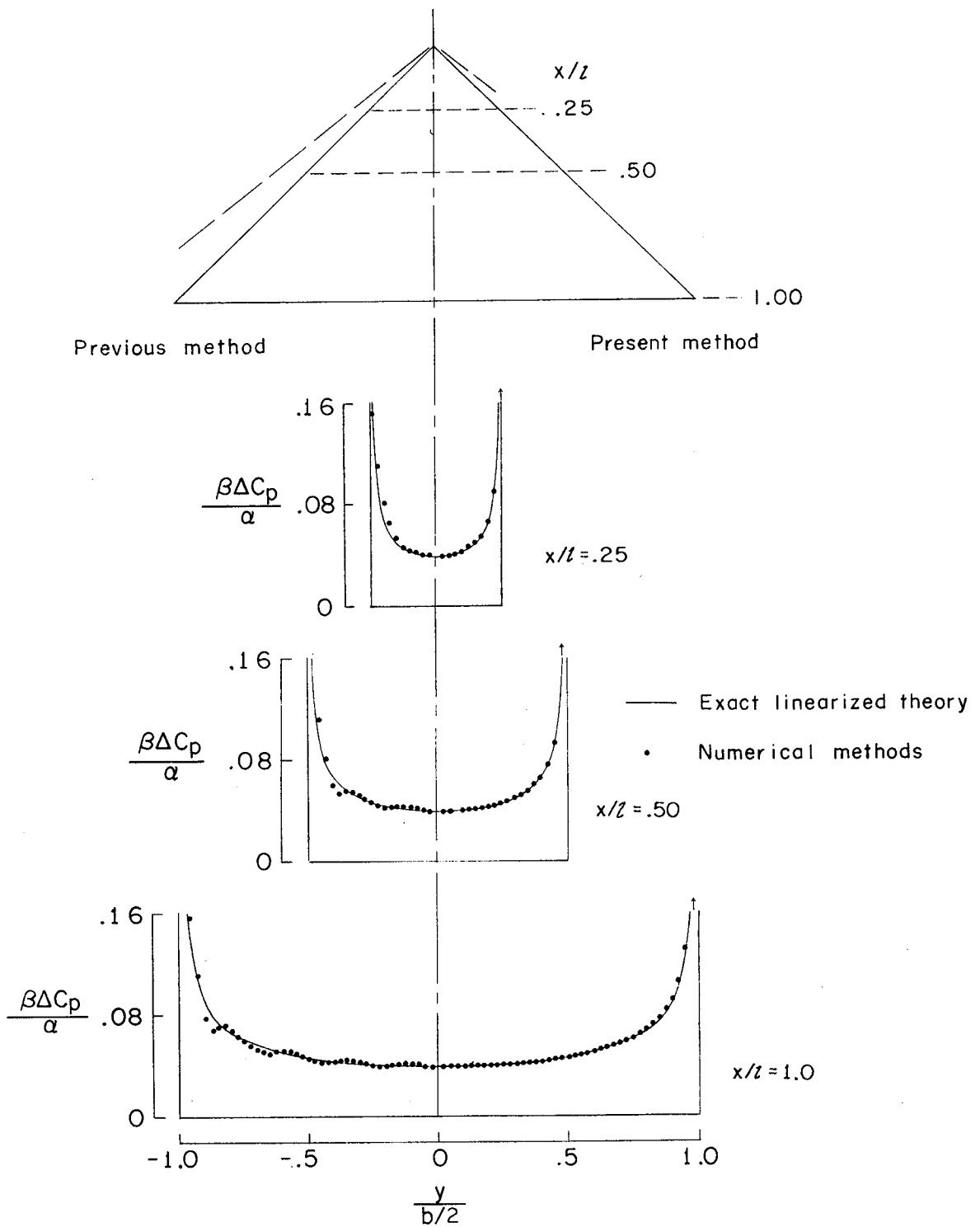
(a)  $\beta \cot \Lambda = 0.4$ .

Figure 16.- Present and previous evaluation-method results for pressure distributions on flat delta wings. Present method shown for right-hand wing panel; previous method, for left-hand panel.



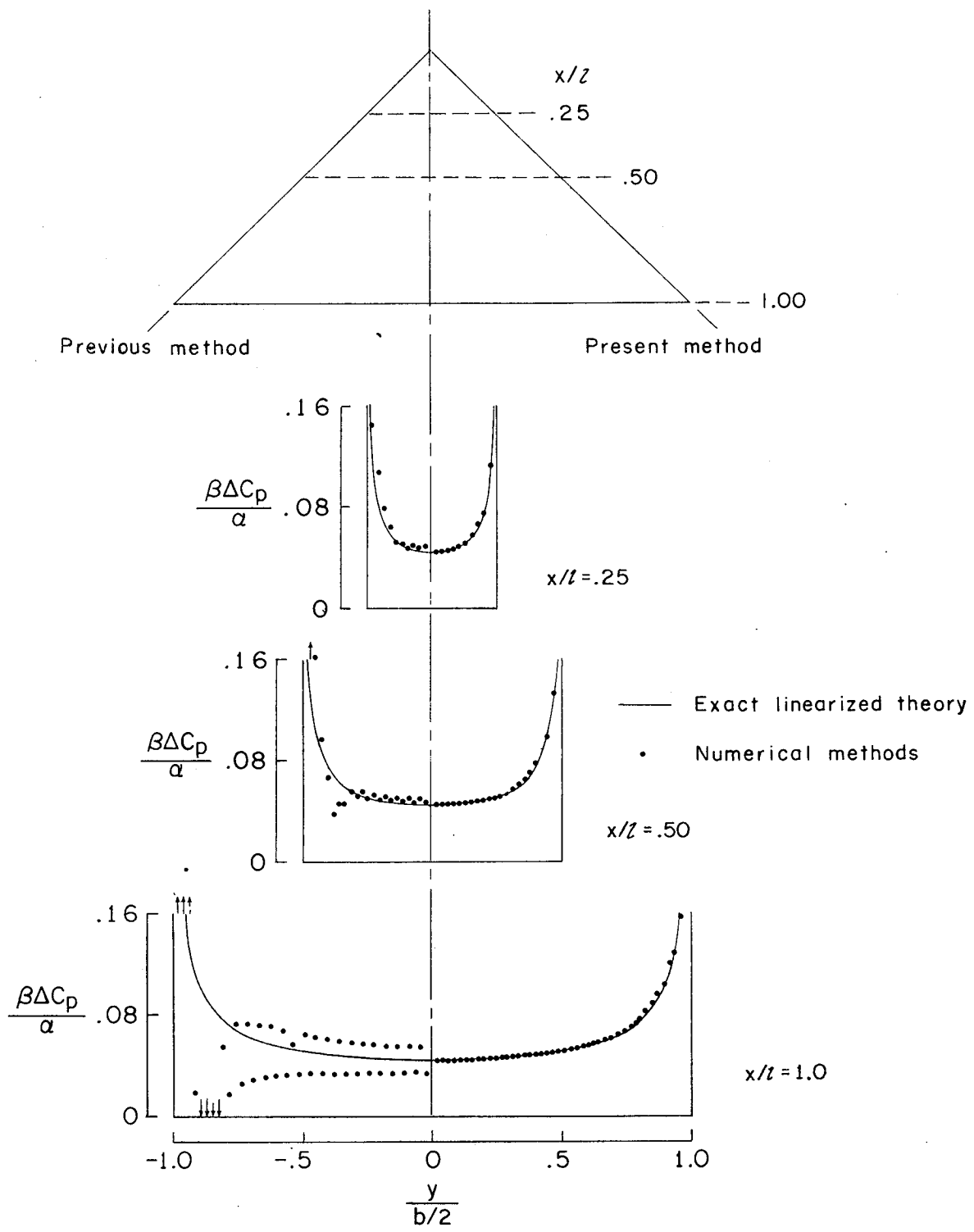
(b)  $\beta \cot \Lambda = 0.6$ .

Figure 16.- Continued.



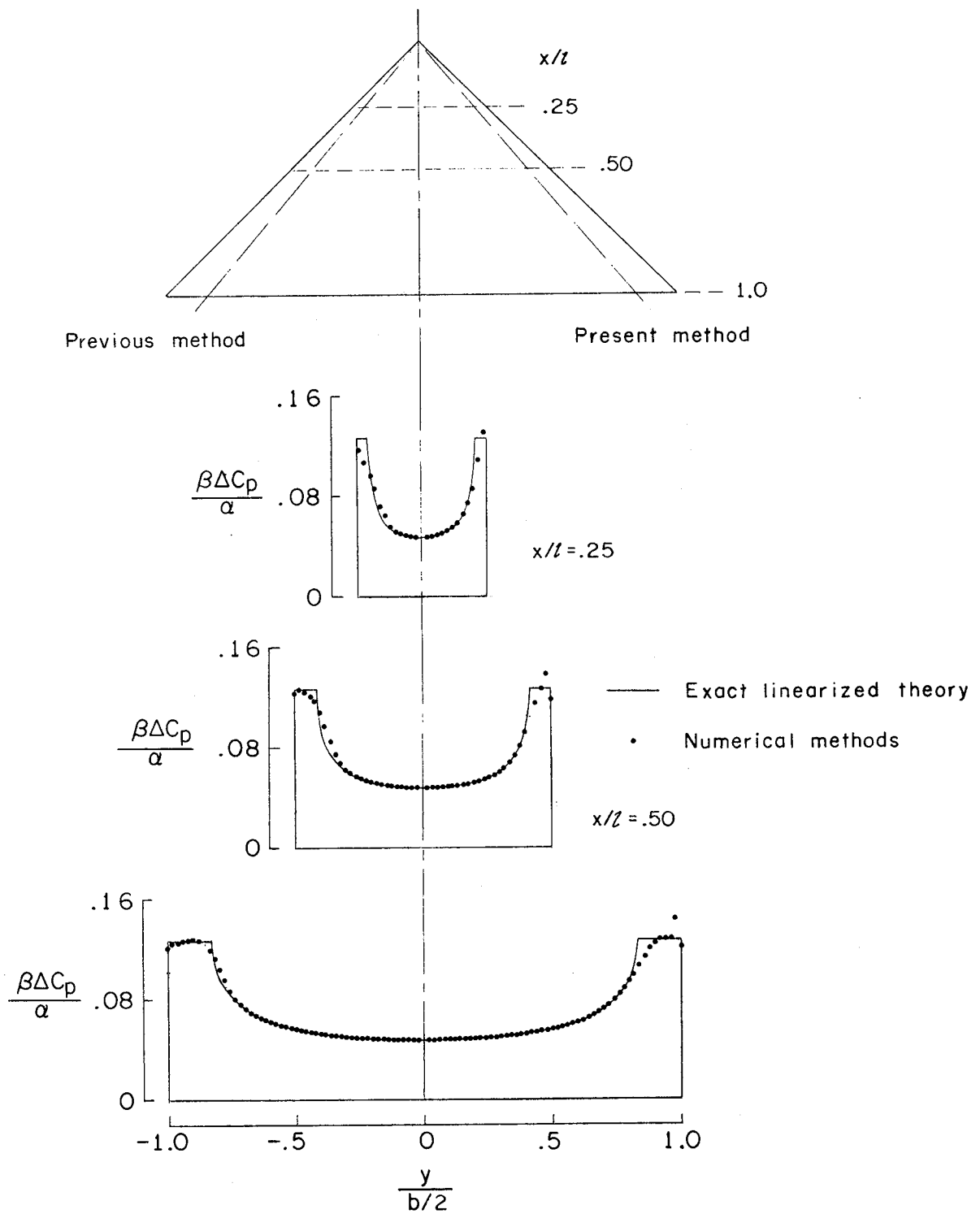
(c)  $\beta \cot \Lambda = 0.8$ .

Figure 16.- Continued.



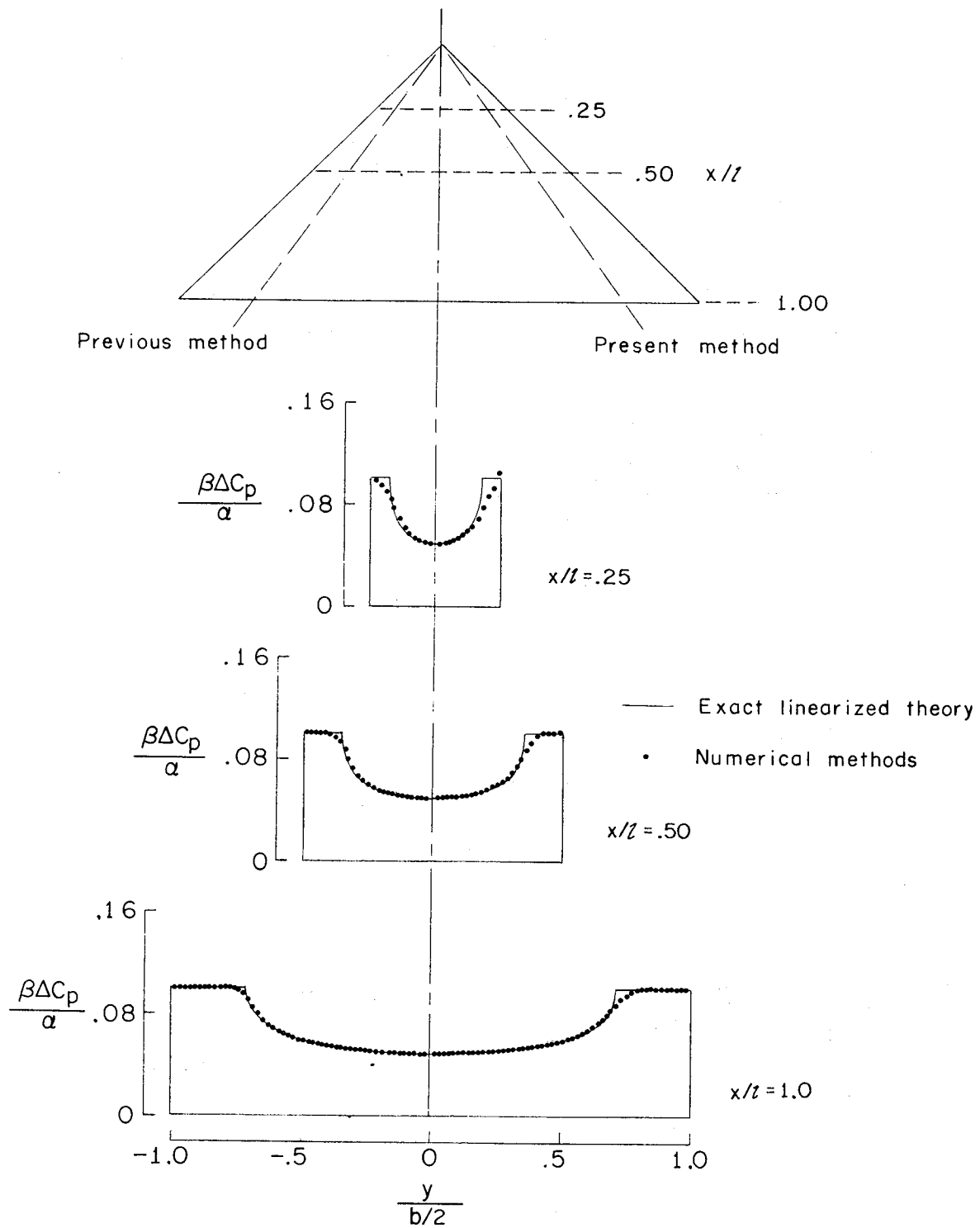
(d)  $\beta \cot \Lambda = 1.0$ .

Figure 16.- Continued.



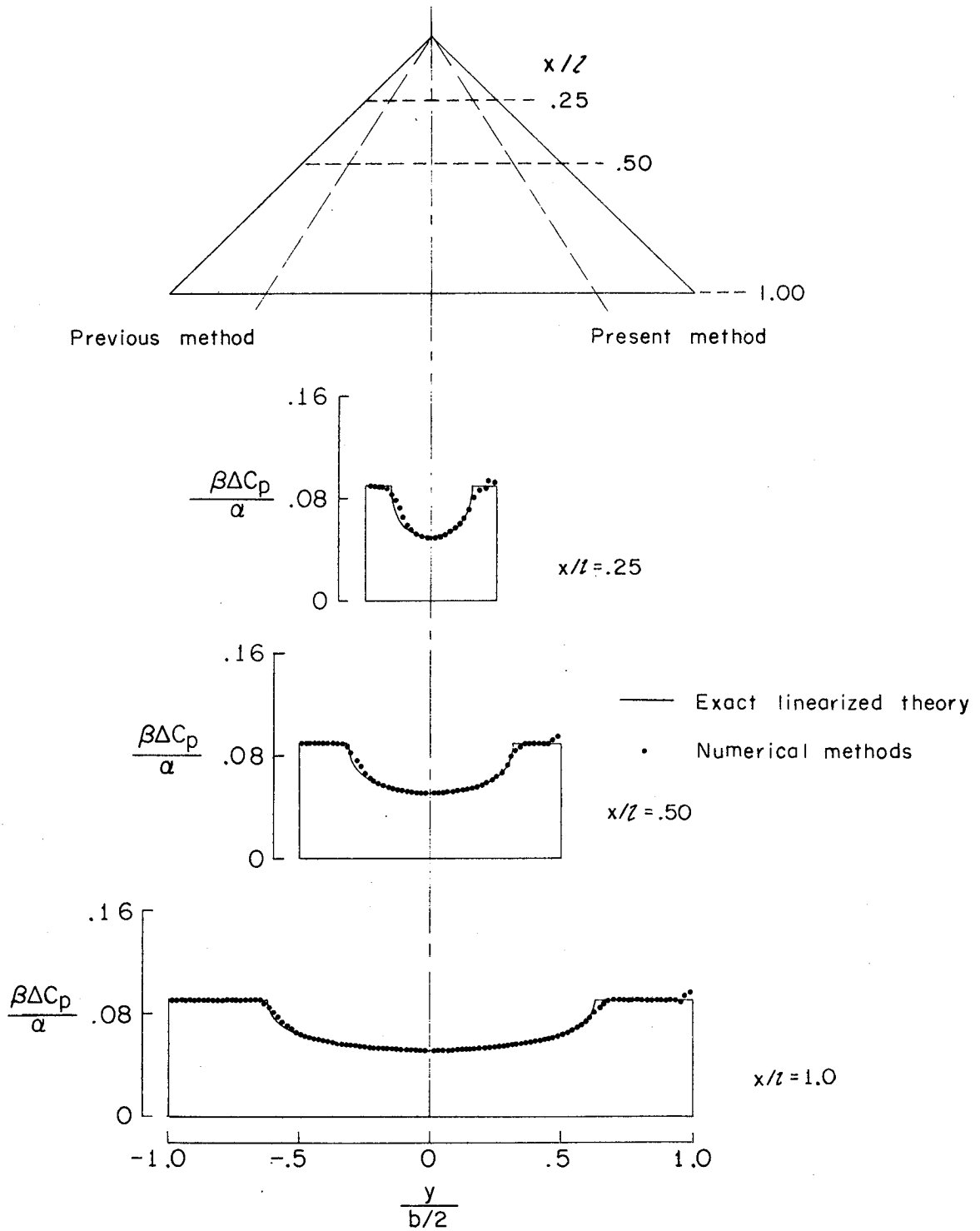
(e)  $\beta \cot \Lambda = 1.2$ .

Figure 16.- Continued.



(f)  $\beta \cot \Lambda = 1.4$ .

Figure 16.- Continued.



(g)  $\beta \cot \Lambda = 1.6$ .

Figure 16.- Concluded.

— Exact linearized theory

• Numerical methods

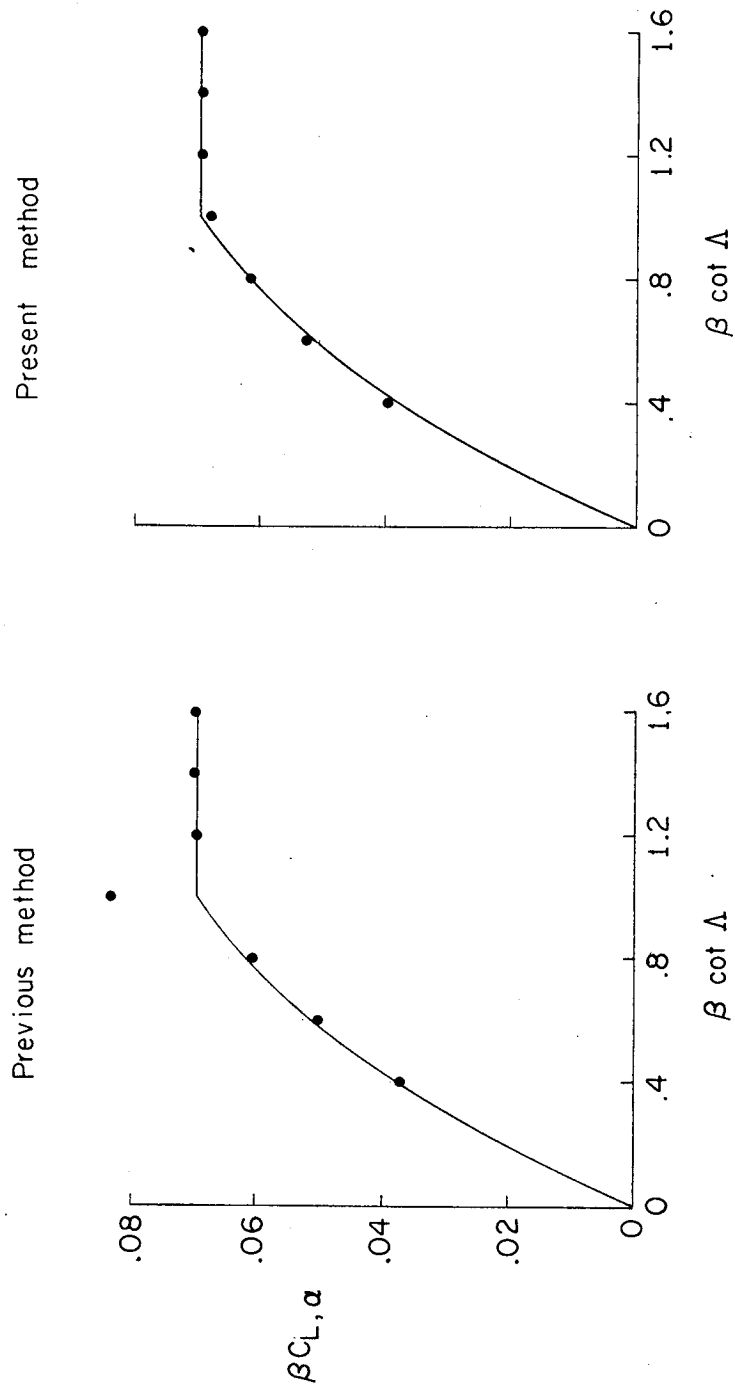
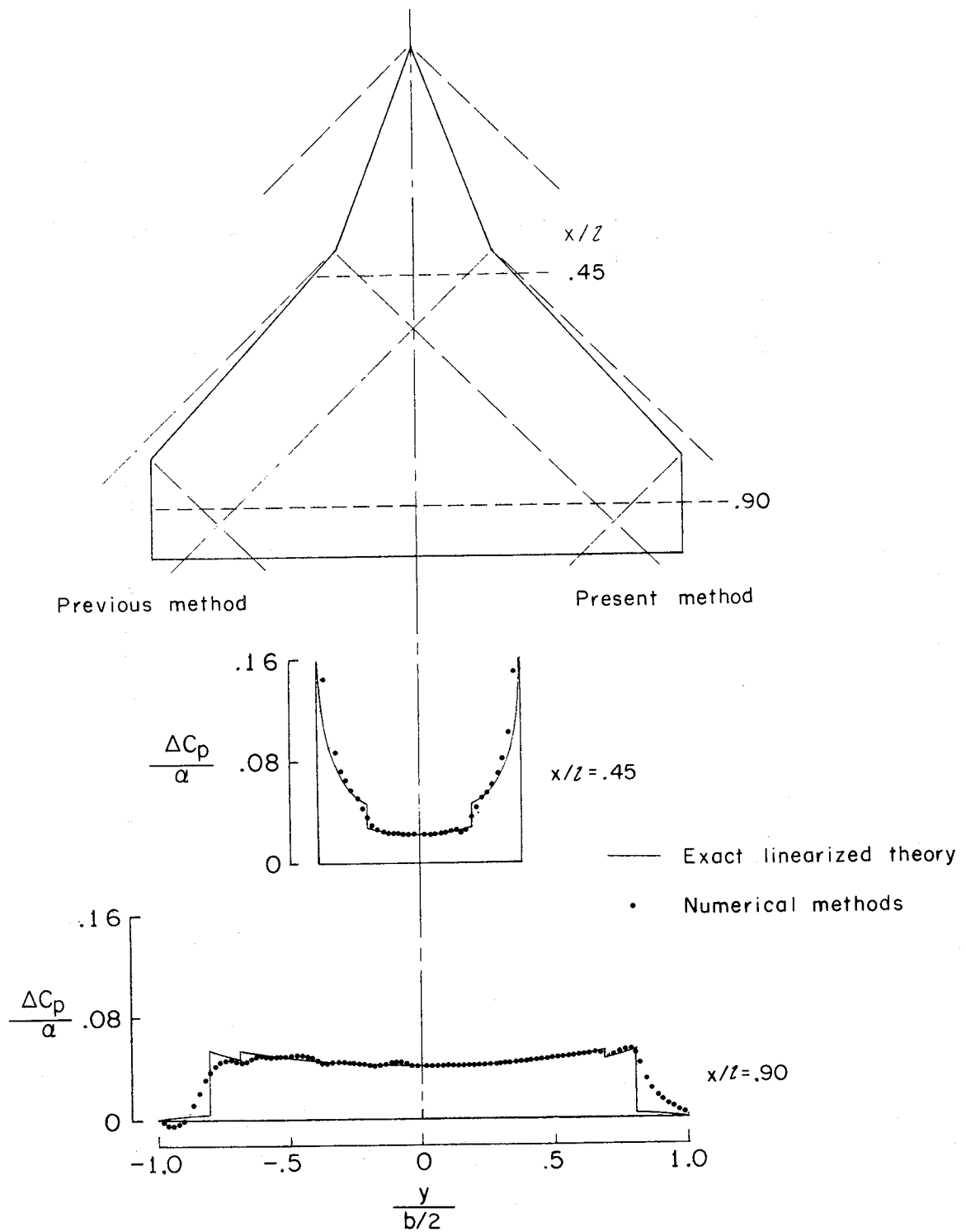
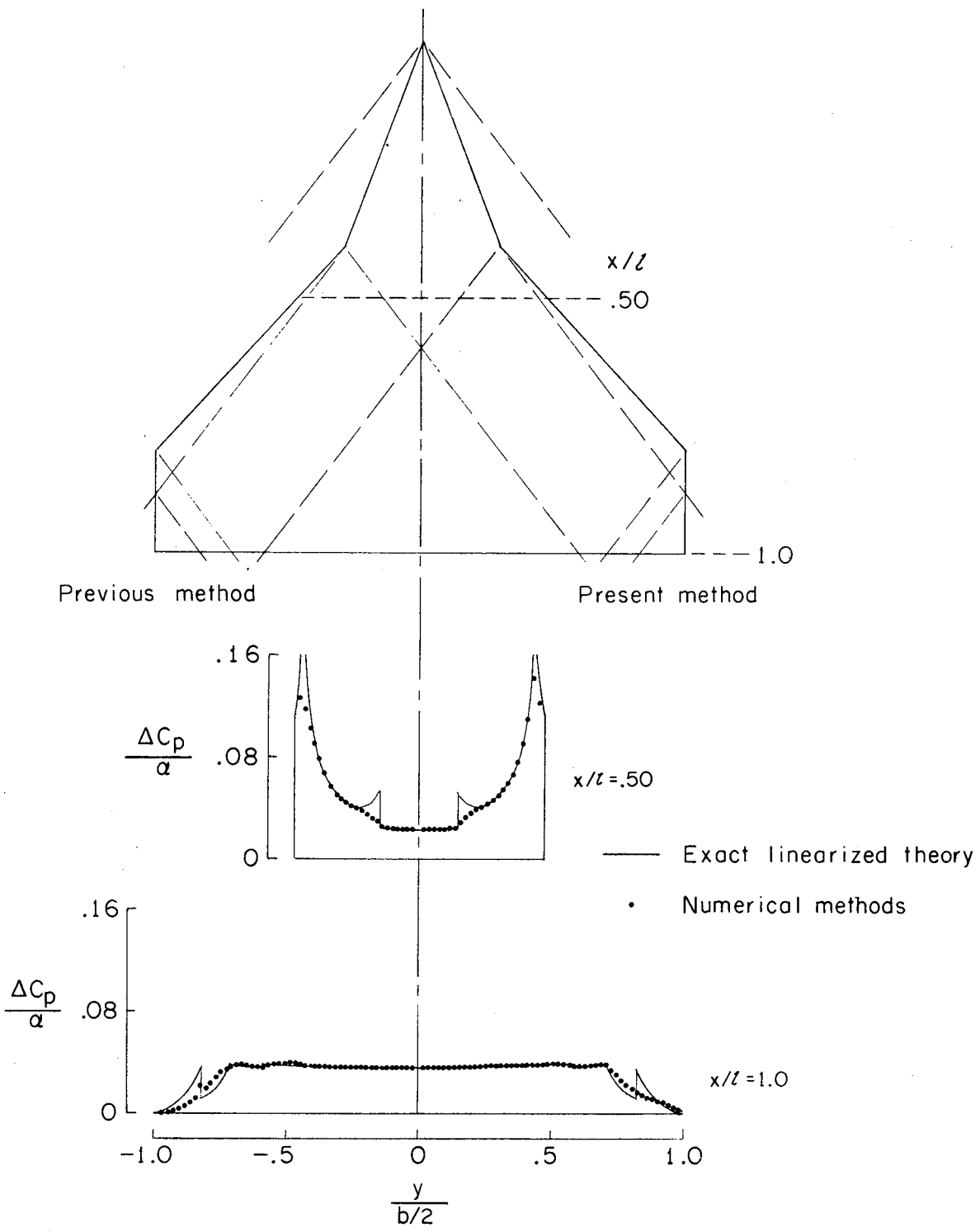


Figure 17.- Present and previous evaluation-method results for lift-curve slopes of flat delta wings.



(a)  $M = \sqrt{2}$ .

Figure 18.- Present and previous evaluation-method results for pressure distributions on flat double-delta wings. Present method shown for right-hand wing panel; previous method, for left-hand panel.



(b)  $M = 1.667$ .

Figure 18.- Concluded.

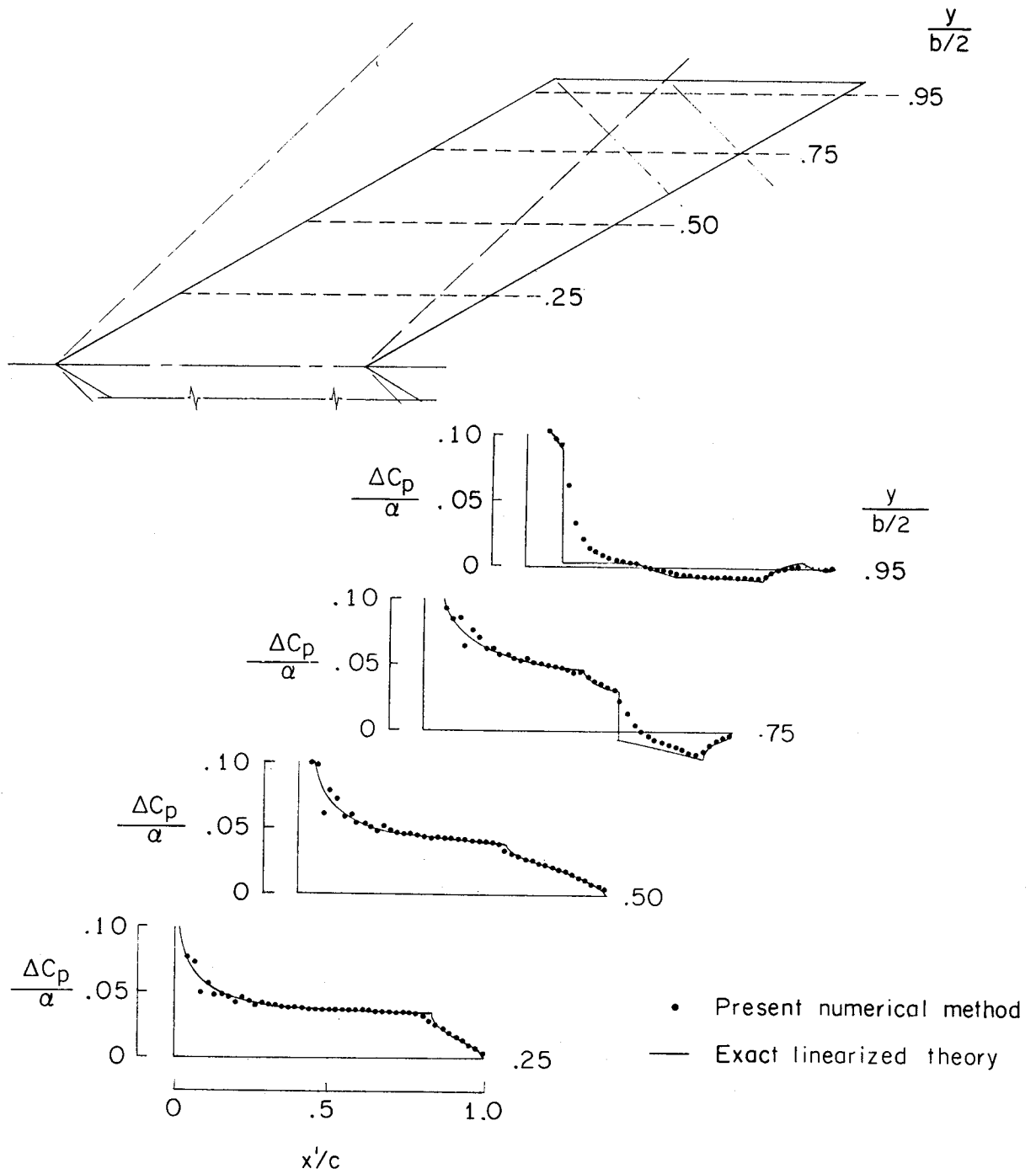


Figure 19.- Present evaluation-method results and linearized-theory—lift-cancellation-method results for pressure distributions on a flat untapered wing with subsonic leading and trailing edges.  $M = \sqrt{2}$ .

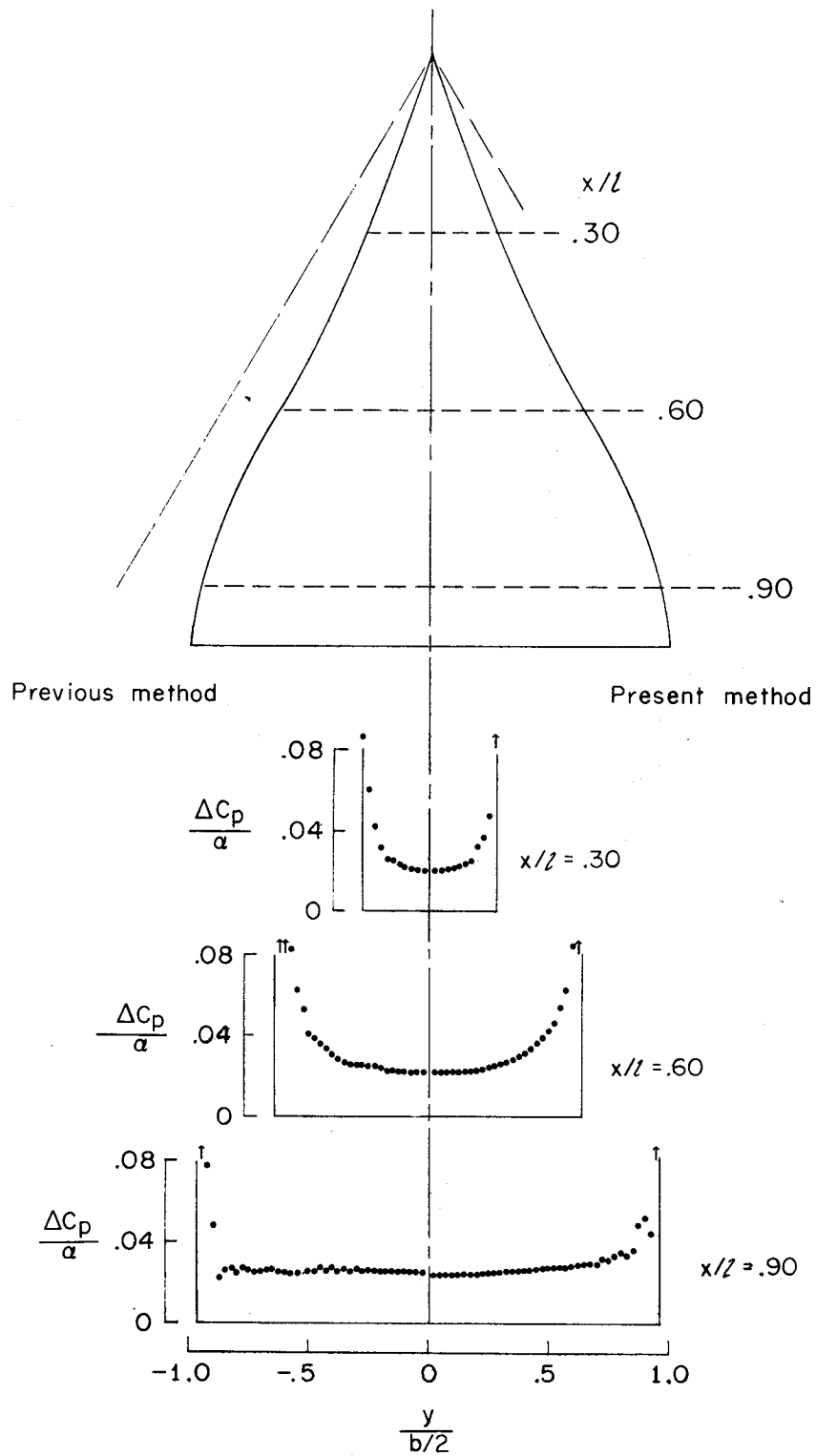


Figure 20.- Present and previous evaluation-method results for pressure distributions on a flat ogee wing.  $M = 2.0$ . Present method shown for right-hand wing panel; previous method, for left-hand panel.

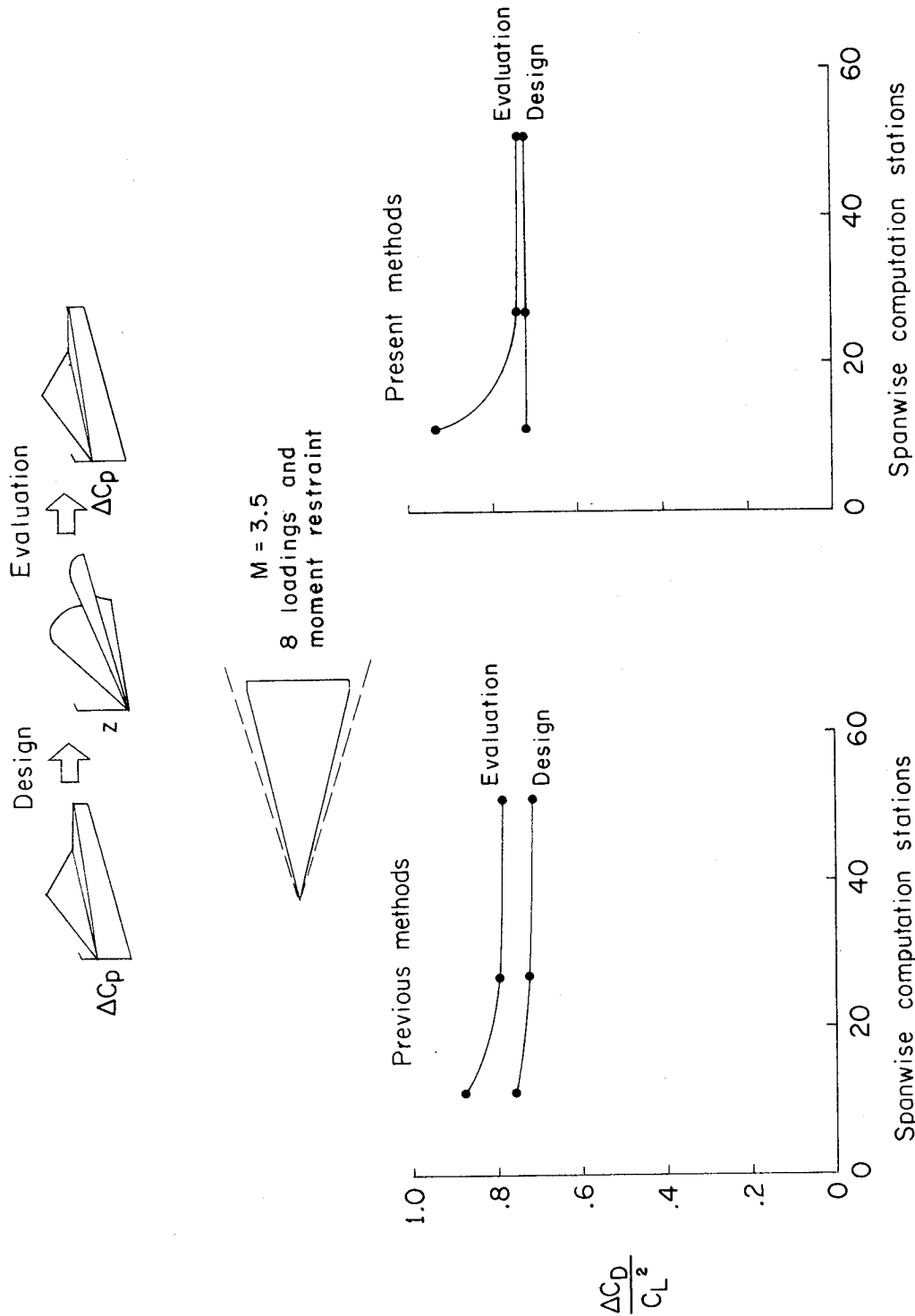
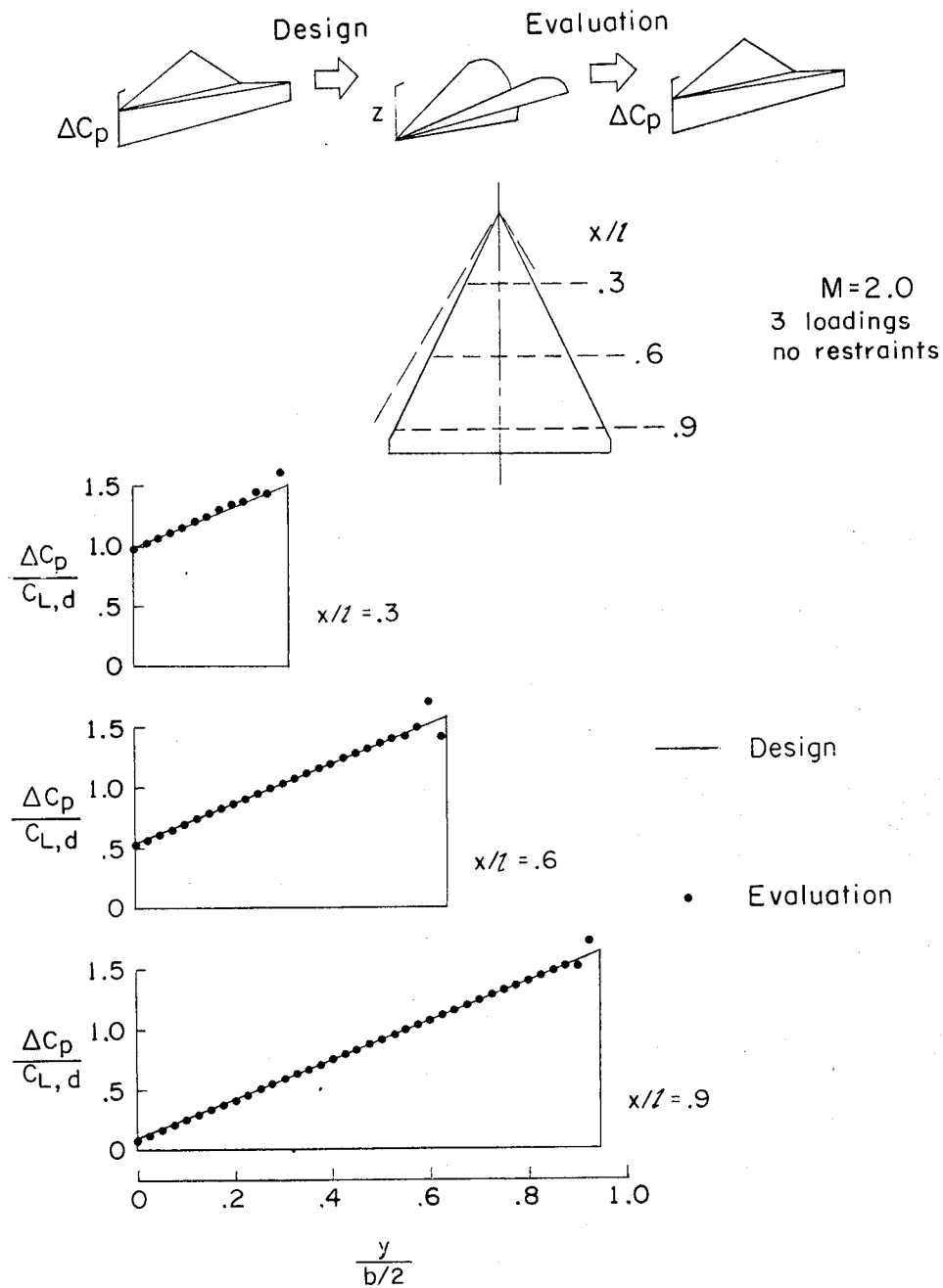
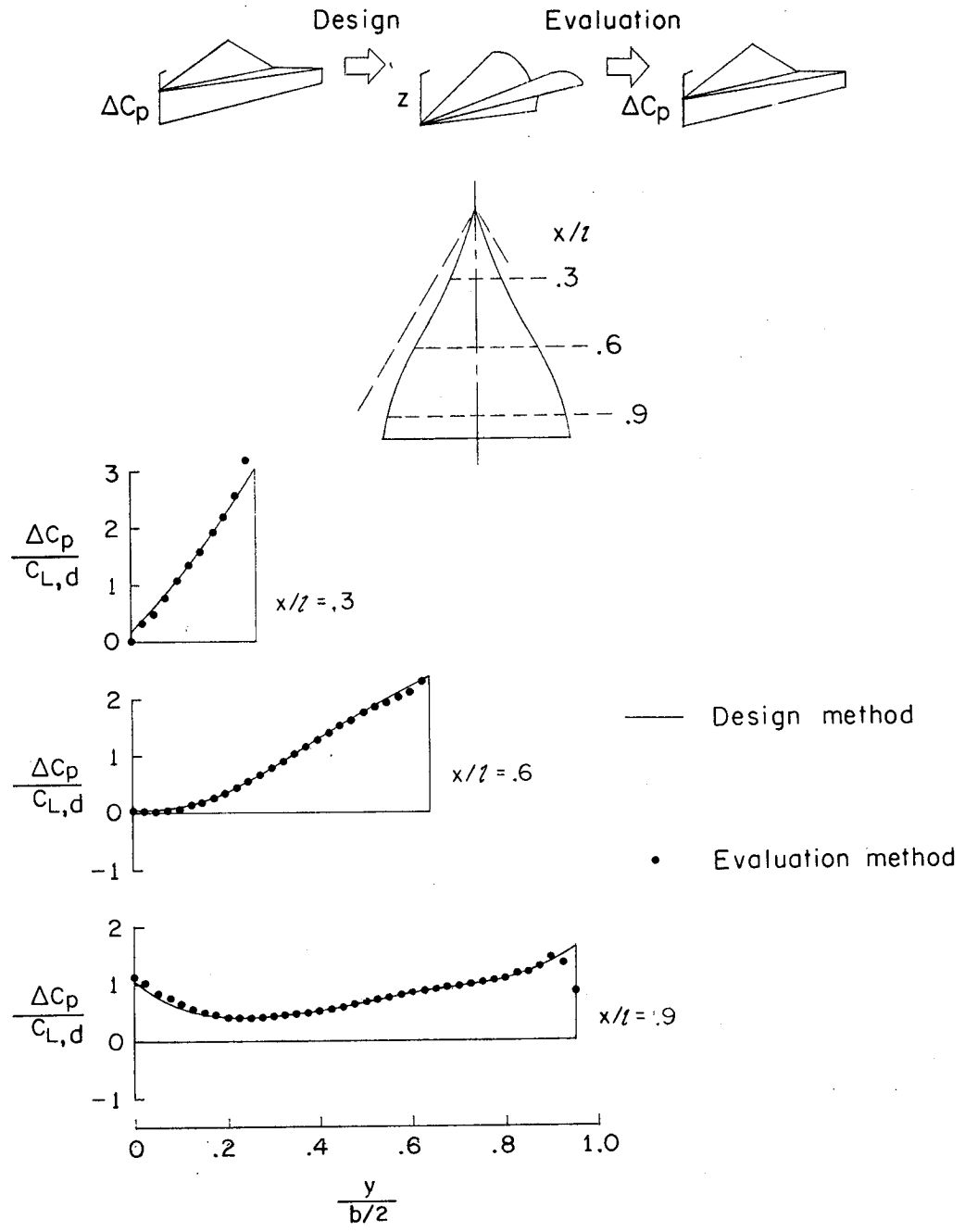


Figure 21.- Correlation of design-method drag-to-lift factors with evaluation-method results for the same wing surface. Example from reference 11 treated with both present and previous methods.



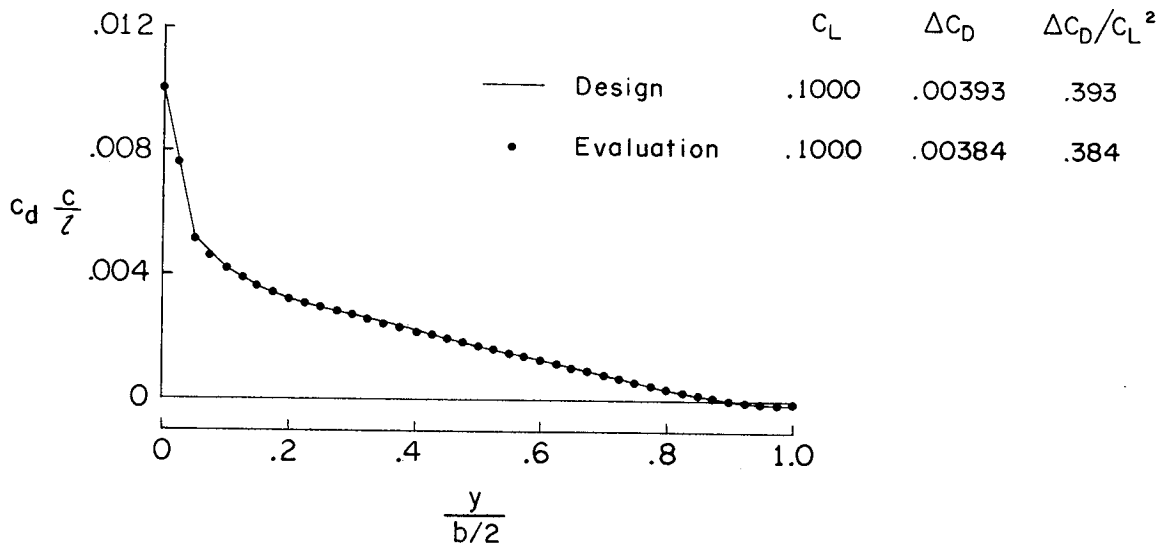
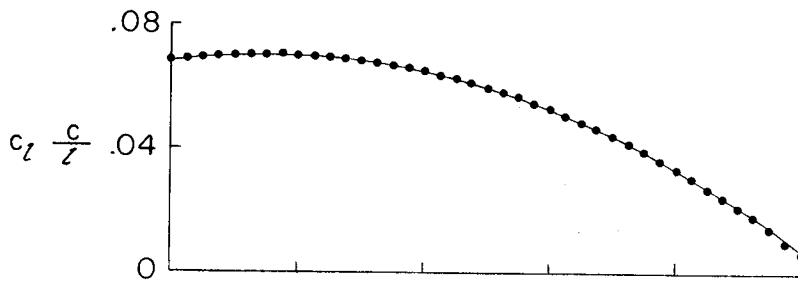
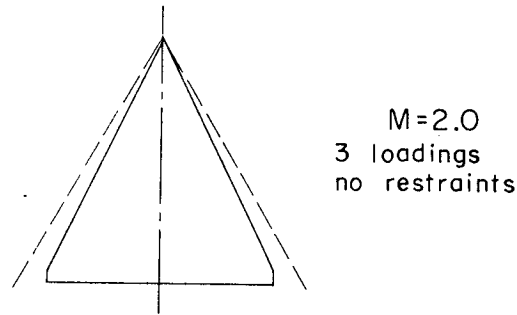
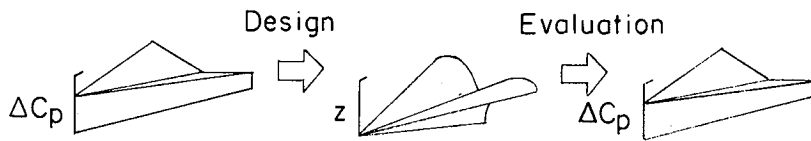
(a) Delta wing; three loadings; M = 2.0.

Figure 22.- Correlation of design-method specified pressure distribution with evaluation-method results for the same wing surface.



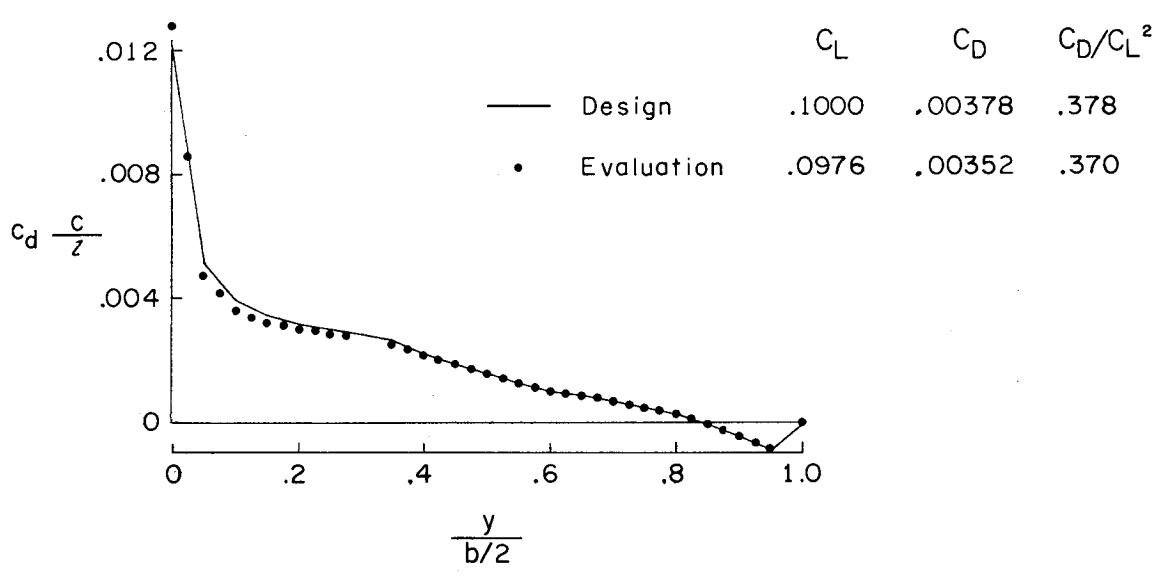
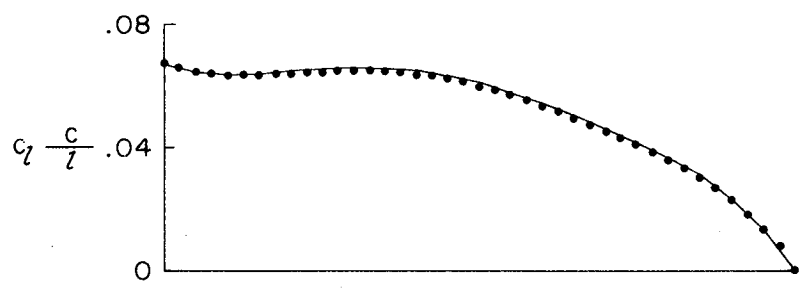
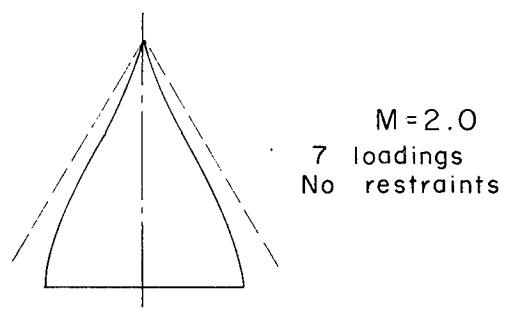
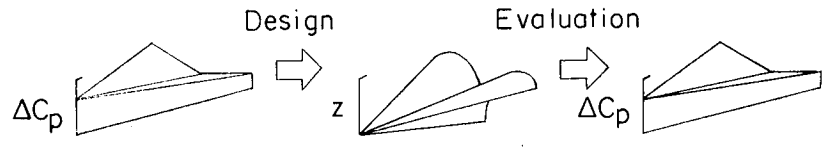
(b) Ogee wing; seven loadings;  $M = 2.0$ .

Figure 22.- Concluded.



(a) Delta wing; three loadings;  $M = 2.0$ .

Figure 23.- Correlation of design-method spanwise loading distributions with evaluation-method results for the same surface.



(b) Ogee wing; seven loadings;  $M = 2.0$ .

Figure 23.- Concluded.

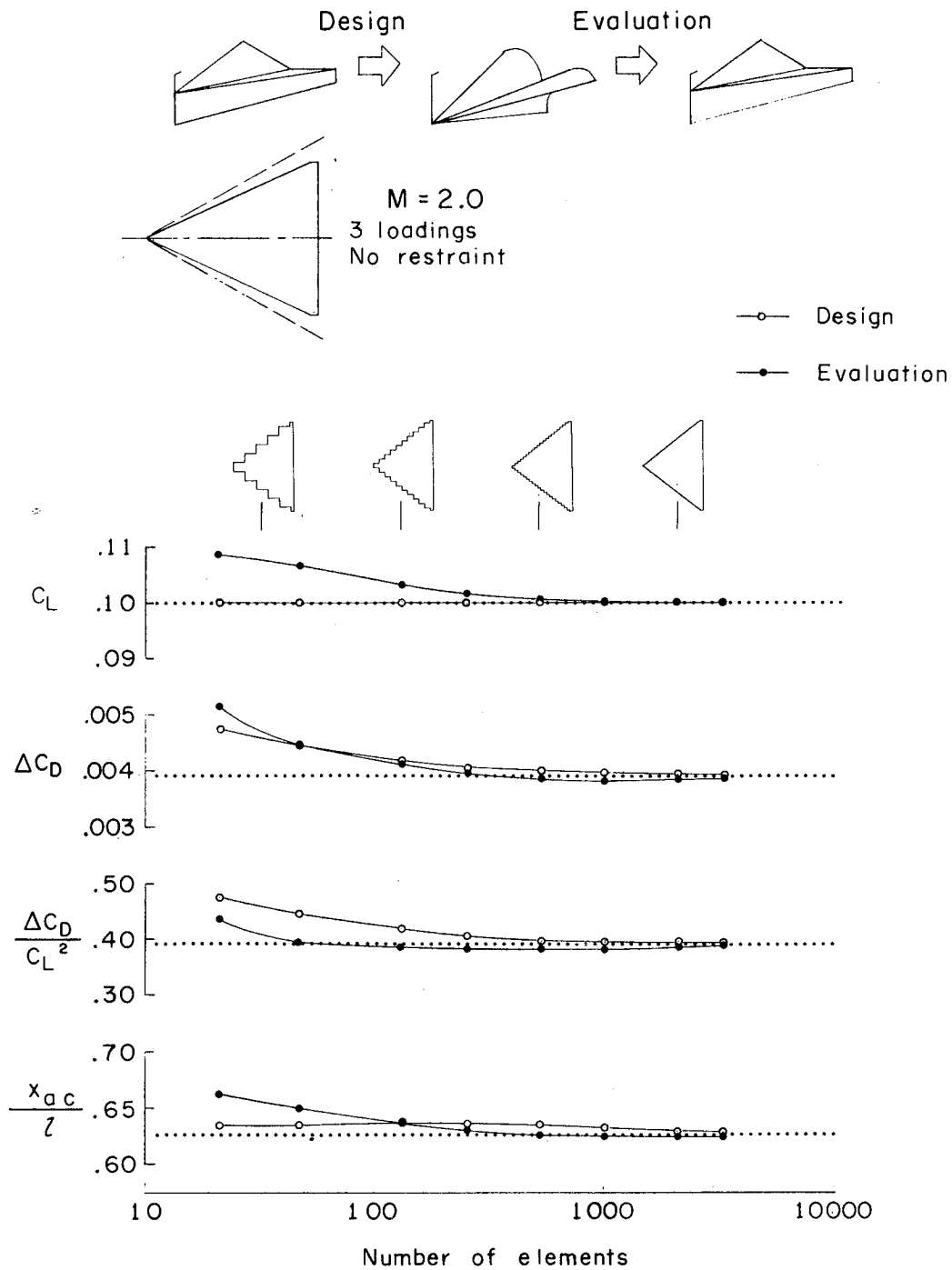


Figure 24.- Correlation of design- and evaluation-method aerodynamic coefficients for the same wing surface. Modified delta wing; M = 2.0; three loadings.

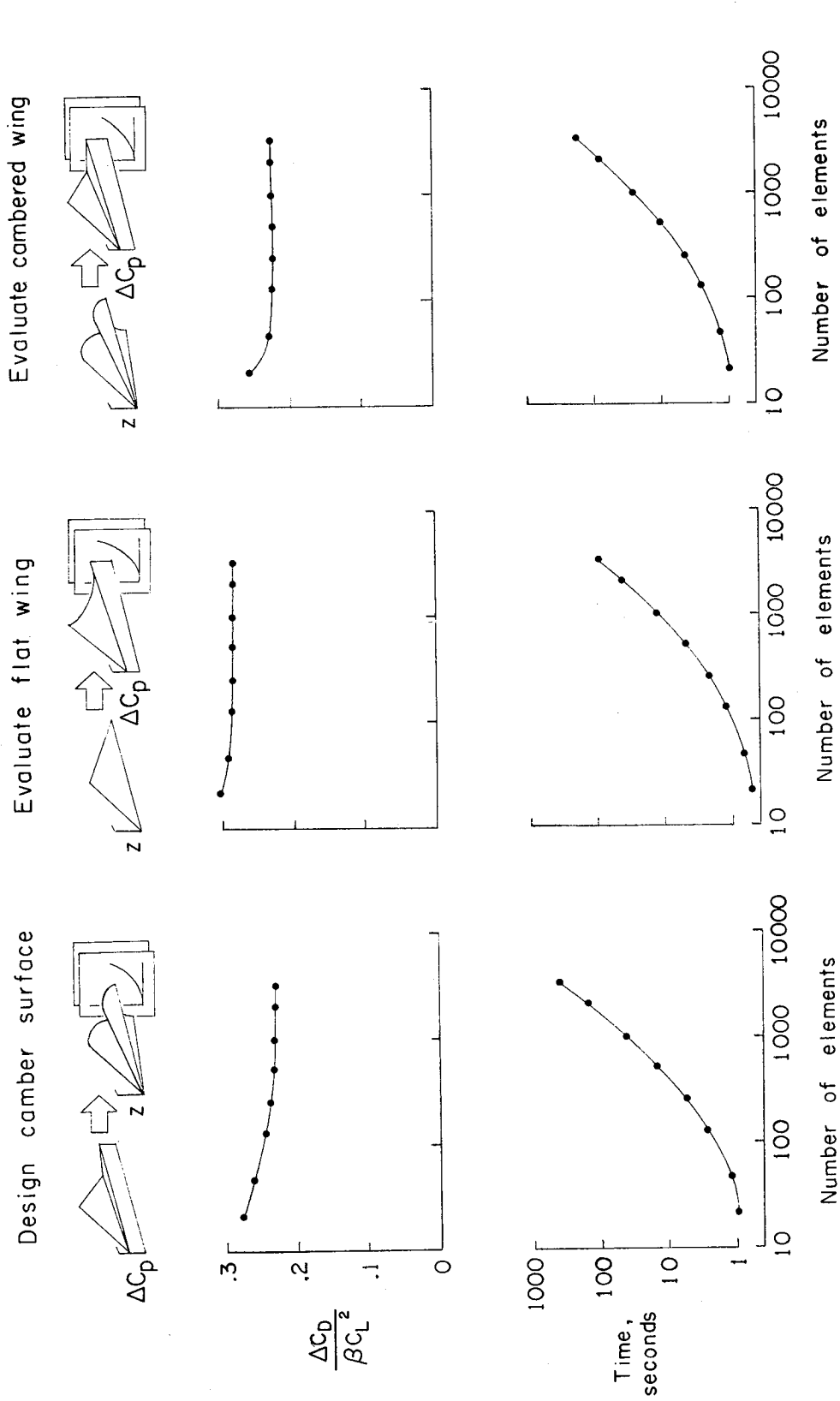


Figure 25.- Convergence characteristics and computational time requirements (Central Processing Unit CDC 6600 computer) for typical applications of the present design and analysis methods.